

**DEVELOPMENT AND OPTIMIZATION OF WIRELESS CHARGING
SYSTEM FOR ELECTRIC VEHICLE (EV)**

CHONG WEI YOU


**A project report submitted in partial fulfilment of the
requirements for the award of Bachelor of Engineering
(Honours) Electrical and Electronic Engineering**

**Lee Kong Chian Faculty of Engineering and Science
Universiti Tunku Abdul Rahman**

April 2020

DECLARATION

I hereby declare that this project report is based on my original work except for citations and quotations which have been duly acknowledged. I also declare that it has not been previously and concurrently submitted for any other degree or award at UTAR or other institutions.

Signature : 

Name : CHONG WEI YOU

ID No. : 15UEB01822

Date : 14/4/2020

APPROVAL FOR SUBMISSION

I certify that this project report entitled “**DEVELOPMENT AND OPTIMIZATION OF WIRELESS CHARGING SYSTEM FOR ELECTRIC VEHICLE (EV)**” was prepared by **CHONG WEI YOU** has met the required standard for submission in partial fulfilment of the requirements for the award of Bachelor of Engineering (Honours) Electrical and Electronic Engineering at Universiti Tunku Abdul Rahman.

Approved by,

Signature : 

Supervisor : Ts. Dr. CHEW KUEW WAI

Date : 17/4/2020

Signature : _____

Co-Supervisor : _____

Date : _____

The copyright of this report belongs to the author under the terms of the copyright Act 1987 as qualified by Intellectual Property Policy of Universiti Tunku Abdul Rahman. Due acknowledgement shall always be made of the use of any material contained in, or derived from, this report.

© Year, Name of candidate. All right reserved.

ACKNOWLEDGEMENTS

I would like to thank everyone who had contributed to the successful completion of this project. I would like to express my gratitude to my research supervisor, Ts. Dr. Chew Kuew Wai for his invaluable advice, guidance and his enormous patience throughout the development of the research.

In addition, I would also like to express my gratitude to my loving parents and friends who had helped and given me encouragement in order to make the project successful. When conducting this research, there was a problem which was the lack of resources faced by me. I feel very thankful for those who contribute the resources for me to make this project successful.

ABSTRACT

Wireless charging for electric vehicle (EV) was an innovative invention as it did not need a direct connection or contact between vehicle and the charging cable. The owner of the wireless charging electric vehicle just have to park their vehicles just above the transmitter charging pad within the acceptable lateral range between the transmitter and receiver pad beneath the electric vehicle. The objectives of this project were to study the wireless charging system of electric vehicle, design and optimize the system in terms of coil alignment, compensation circuit and coil design to solve the issues of power loss and improving charging rate when charging the electric car. The methodology was the power source is direct from wall socket that provides $240V_{ac}$ with 50Hz. The AC current was rectified and inverted back to produce higher frequency AC current up to 20kHz. The coil design was in spiral flat circular shape to ensure the magnetic field produced was evenly distributed. For the alignment system, mechanical aligner was constructed and communicate with mobile phone with the concept of Internet of Things (IoT). The results shown that the greater the misalignment, the lower the power efficiency, mutual inductance, and coupling coefficient verified using simulation software called Ansys Maxwell and SIMULINK. In conclusion, the project was conducted successfully as the results from simulation matched with the experimental results.

TABLE OF CONTENTS

DECLARATION		i
APPROVAL FOR SUBMISSION		ii
ACKNOWLEDGEMENTS		iv
ABSTRACT		v
TABLE OF CONTENTS		vi
LIST OF TABLES		ix
LIST OF FIGURES		xi
LIST OF EQUATIONS		xvi
LIST OF SYMBOLS / ABBREVIATIONS		xviii
LIST OF APPENDICES		xix
CHAPTER		
1	INTRODUCTION	
1.1	General Introduction	1
1.2	Importance of the Study	1
1.3	Problem Statement	2
1.4	Aim and Objectives	3
1.5	Scope and Limitation of the Study	3
1.6	Contribution of the Study	3
2	LITERATURE REVIEW	
2.1	Introduction	5
2.2	Literature Review	6
2.2.1	Battery Chargers Error! Bookmark not defined.	
2.2.2	Basics of Wirelss Power Transmission	8
2.2.2.1	Coupling Methods	8
2.2.2.2	Coil Designs with Power Efficiency	11
2.2.2.3	Efficiency versus Misalignment of Coil of Wireless Power Transmission	13
2.2.3	Basics of Electronics Circuit Designs	15

	2.2.3.1 Inverter	16
	2.2.3.2 Compensation Network	19
	2.2.3.3 Converter	23
	2.2.3.4 Internet of Things (IoT)	25
2.3	Summary	26
3	METHODOLOGY AND WORK PLAN	
3.1	Introduction	28
3.2	System Design	29
	3.2.1 Electrical Circuit Design	29
	3.2.2 Mechanical Aligner Design	35
	3.2.2.1 Transmitter Side	35
	3.2.2.2 Receiver Side	41
	3.2.2.3 Internet of Things (IoT)	43
3.3	Hardware Requirements, Costs, and Work Schedule	46
3.4	Summary	47
4	RESULTS AND DISCUSSION	
4.1	Introduction	49
4.2	Results	49
	4.2.1 Effect of Coil Distance, Lateral Misalignemtn,and Angle Difference (Experimental)	49
	4.2.2 Effect of Coil Turns and Inner Radius (Experimental)	52
	4.2.3 Effect of Coil Turns and Outer Radius (Experimental)	54
	4.2.4 Battery Charging Behaviour (Experimental)	56
	4.2.5 Simulation using MATLAB (SIMULINK)	57
	4.2.6 Simulation using Ansys Maxwell	59
4.3	Discussion	65
	4.3.1 Effect of Coil Distance, Lateral Misalignment,and Angle Difference (Experimental)	65

4.3.2	Effect of Coil Turns, Inner Radius and Outer Radius (Experimental)	68
4.3.3	Battery Charging Behaviour (Experimental)	70
4.3.4	Simulation using MATLAB (SIMULINK)	72
4.3.5	Simulation using Ansys Maxwell	72
4.4	Summary	73
5	CONCLUSIONS AND RECOMMENDATIONS	
5.1	Conclusions	74
5.2	Recommendations for future work	74
6	ADDITIONAL STUDY FROM PROJECT	
6.1	Ohmic Loss Analysis	77
6.2	Temperature Analysis	79
	REFERENCES	81
	APPENDICES	85

LIST OF TABLES

Table 2.2.2.2.1 Electrical Resistivity, Thermal Conductivity, Relative Electrical Conductivity and Relative Thermal Conductivity of Metals	11
Table 2.2.2.2.2 Comparison of Different Shape of Coils	13
Table 2.2.3.1.1 Truth Table of Full-Bridge Inverter Error! Bookmark not defined.	7
Table 2.2.3.2.1 Resonance Frequencies with Different Conditions in SS Topology	22
Table 2.2.3.2.2 Qualitative Comparisons of Four Topologies	22
Table 3.2.1.1 Current Carrying Capacity of Copper Cable	34
Table 3.3.1 Cost of Hardware for Project	47
Table 3.3.2 Gantt Chart of Project Work Schedule	47
Table 4.2.1.1 Results of Power Efficiency against Distance between Transmitter Coil and Receiver Coil	50
Table 4.2.1.2 Results of Power Efficiency against Lateral Misalignment between Transmitter Coil and Receiver Coils	51
Table 4.2.1.3 Results of Power Efficiency against Tilting Angle Difference between Transmitter Coil and Receiver Coil	51
Table 4.2.2.1 Compensation Capacitance needed for Different Number of Coil Turns with Fixed Outer Radius	52
Table 4.2.2.2 Power Efficiency against Coil Turns with Fixed Outer Radius	53
Table 4.2.3.1 Compensation Capacitance needed for Different Number of Coil Turns with Fixed Inner Radius	54
Table 4.2.3.2 Power Efficiency against Coil Turns with Fixed Inner Radius	55

Table 4.2.4.1 Charging Current and Voltage of Battery (1.2Ah, 12V Lead Acid Dead Battery with Initial Voltage 3.35V)	56
Table 4.2.6.1 Simulation of Self-Inductance against Coil Turns with Fixed Outer Radius	59
Table 4.2.6.2 Simulation of Self-Inductance against Coil Turns with Fixed Inner Radius	60
Table 4.2.6.3 Simulated Coupling Coefficient and Mutual Inductance against Misalignment Coordinate relative to Origin of Transmitter Coil (Distance, d)	63
Table 4.2.6.4 Simulated Coupling Coefficient and Mutual Inductance against Misalignment Coordinate relative to Origin of Transmitter Coil (Lateral Distance, L)	63

LIST OF FIGURES

Figure 1.2.1 Thevenin's Equivalent Circuit	2
Figure 2.2.1.1 Graph of CC/CV Charging Method	6
Figure 2.2.1.2 Waveform of Pulsed Charging Method	7
Figure 2.2.2.1.1 Resonant Inductive Coupling	9
Figure 2.2.2.1.2 Capacitive Coupling	Error! Bookmark not defined.
Figure 2.2.2.1.3 Structure of Conventional Magnetron	10
Figure 2.2.2.1.4 Flow of Electrons in Interact Space using Left Hand Rule	10
Figure 2.2.2.1.5 Resonant Cavity Magnetron	10
Figure 2.2.2.2.1 Single-Coil Circular Rectangular Pad (CRP)	12
Figure 2.2.2.2.2 Single-Coil Circular Non-Polarized Pad (CP)	12
Figure 2.2.2.2.3 Multiple-Coil Homogeneous Pad (HP)	12
Figure 2.2.2.2.4 Double-D Polarized Pad (DDP)	12
Figure 2.2.2.2.5 Multiple-Coil Double-D Quadrature Polarized Pad (DDQP)	13
Figure 2.2.2.2.6 Multiple-Coil Bipolar Polarized Pad (BPP)	13
Figure 2.2.2.3.1 Lateral, Angular Misalignment and Coil Distance	14
Figure 2.2.2.3.2 Graph of Inductance versus Lateral Misalignment of Coils	14
Figure 2.2.2.3.3 Graph of Mutual Inductance versus Distance of Coils	15
Figure 2.2.2.3.4 Graph of Mutual Inductance versus Angular Misalignment of Coils	15
Figure 2.2.3.1 Block Diagram of Inductive Wireless Vehicle Charging	16
Figure 2.2.3.1.1 Half-Bridge Inverter	16
Figure 2.2.3.1.2 Full-Bridge Inverter	16
Figure 2.2.3.1.3 Full-Bridge Inverter (Ideal Switch)	17
Figure 2.2.3.1.4 Waveform of Four MOSFET and Output Voltage	18

Figure 2.2.3.2.1 Series-Series Circuit (SS)	19
Figure 2.2.3.2.2 Series-Parallel Circuit (SP)	19
Figure 2.2.3.2.3 Parallel-Series Circuit (PS)	19
Figure 2.2.3.2.4 Parallel-Parallel Circuit (PP)	20
Figure 2.2.3.2.5 Frequency Splitting	21
Figure 2.2.3.3.1 Half-Wave Rectifier	24
Figure 2.2.3.3.2 Full-Wave Rectifier (Center Tapped Rectifier)	24
Figure 2.2.3.3.3 Full-Wave Rectifier (Bridge Rectifier)	24
Figure 2.2.3.3.4 Output Waveform of Half-Wave and Full-Wave Rectifier	25
Figure 2.2.3.4.1 Internet of Things	26
Figure 2.3.1 Parallel Angular Misalignment of Rectangular Pad	27
Figure 3.1.1 Overall Block Diagram of the Project	28
Figure 3.2.1.1 Overall Connection of the Hardware	29
Figure 3.2.1.2 Six-Pin Center-Tapped Transformer (0-115-230 to 12-0-12V, 4A.50VA)	30
Figure 3.2.1.3 Bridge Rectifier (1000V, 10A)	30
Figure 3.2.1.4 High Frequency Inverter (20kHz)	30
Figure 3.2.1.5 Power Resistor (100W, 1 Ω)	31
Figure 3.2.1.6 Illustration of SP Topology with Calculated Value of Resonance Capacitance and Inductance in 20 kHz	32
Figure 3.2.1.7 Verifying Inductance Value with LCR Meter	32
Figure 3.2.1.8 DC Buck-Boost Converter (Input: 5-30V, Output: 1.5-35C, Max Current: 4A)	33
Figure 3.2.1.9 DC Battery Charging Controller (6-60 VDC)	33
Figure 3.2.1.10 DC 12V, 1.2Ah Battery (GPP1212)	34
Figure 3.2.2.1.1 Transmitter Aligner (Top Level, Top View)	36
Figure 3.2.2.1.2 Transmitter Aligner (Front View)	36

Figure 3.2.2.1.3 Transmitter Aligner (Side View)	37
Figure 3.2.2.1.4 Transmitter Aligner (Rear View)	37
Figure 3.2.2.1.5 Transmitter Aligner (Level 1, Bottom View)	37
Figure 3.2.2.1.6 Transmitter Aligner (Level 2, Top View)	38
Figure 3.2.2.1.7 Combination of Movement of Servo Motor (Level 1) and Servo Motor (Level2) (Top View)	38
Figure 3.2.2.1.8 Illustration of Infrared Sensor Behaviour when Encounter White and Black Surface	38
Figure 3.2.2.1.9 Transmitter Pad (Level 3, Side View)	39
Figure 3.2.2.1.10 Behaviour of Ultrasonic Sensor	39
Figure 3.2.2.1.11 Circuit Diagram of Transmitter Aligner	40
Figure 3.2.2.2.1 Receiver Aligner (Top View)	41
Figure 3.2.2.2.2 Receiver Aligner (Front View)	41
Figure 3.2.2.2.3 Receiver Aligner (Side View)	42
Figure 3.2.2.2.4 Circuit Diagram of Receiver Aligner	42
Figure 3.2.2.3.1 Layout of “Blynk” Mobile Application	43
Figure 3.2.2.3.2 Flow Chart for Program Flow (Transmitter Aligner)	44
Figure 3.2.2.3.3 Flow Chart for Program Flow (Receiver Aligner)	45
Figure 4.2.1.1 Graph of Power Efficiency against Coil Distance between Transmitter Coil and Receiver Coil	50
Figure 4.2.1.2 Graph of Power Efficiency against Lateral Misalignment between Transmitter Coil and Receiver Coil	51
Figure 4.2.1.3 Graph of Power Efficiency against Tiling Angle Difference between Transmitter Coil and Receiver Coil	52
Figure 4.2.2.1 Graph of Self-Inductance against Coil Turns with Fixed Outer Radius	53
Figure 4.2.2.2 Graph of Power Efficiency against Coil Turns with Fixed Outer Radius	54

Figure 4.2.3.1 Graph of Self-Inductance against Coil Turns with Fixed Inner Radius	55
Figure 4.2.3.2 Graph of Power Efficiency against Coil Turns with Fixed Inner Radius	56
Figure 4.2.4.1 Graph of Charging Behaviour for Lead Acid Battery	57
Figure 4.2.5.1 Simulation Circuit of Wireless Power Transfer Circuit (SIMULINK)	57
Figure 4.2.5.2 Simulation Results at Step Down Transformer (1)Primary Voltage, (2)Secondary Voltage, (3)Rectified Voltage	58
Figure 4.2.5.3 Simulation Results of (4)High Frequency Inverted Voltage (Transmitter), (5)Received Voltage (Receiver), (6)Rectified Voltage	58
Figure 4.2.5.4 Simulation Results of (7)Transmitter Current, (8)Receiver Current	59
Figure 4.2.6.1 Simulated Self-Inductance against Coil Turns	60
Figure 4.2.6.2 Magnetic Field Intensity of Coil (N=5, Fixed Outer Radius=150mm)	61
Figure 4.2.6.3 Magnetic Field Intensity of Coil (N=14, Fixed Outer Radius=150mm)	61
Figure 4.2.6.4 Magnetic Field Intensity of Coil (N=5, Fixed Inner Radius=62.5mm)	61
Figure 4.2.6.5 Magnetic Field Intensity of Coil (N=14, Fixed Inner Radius=62.5mm)	62
Figure 4.2.6.6 Setting of Coils in Simulation	62
Figure 4.2.6.7 Simulated Mutual Inductance and Coupling Coefficient against Misalignment in Distance, d and Lateral Distance, L	64
Figure 4.2.6.8 Magnetic Field Intensity of Coils with Misalignment Coordinate (0, 0, 10)	64
Figure 4.2.6.9 Magnetic Field Intensity of Coils with Misalignment Coordinate (0, 0, 100)	65
Figure 4.2.6.10 Magnetic Field Intensity of Coils with Misalignment Coordinate (0, 100, 10)	65
Figure 4.3.1.1 Graph of Power Efficiency against Distance, Lateral Misalignment, and Angle Difference	66

Figure 4.3.1.2 Two Coils Connected in Series with Magnetic Fields in One Direction	66
Figure 4.3.2.1 Section View of a Circular Flat Spiral Coil	68
Figure 4.3.3.1 Analysis of CC/CV Curve of Charging Battery	71
Figure 5.2.1 PVC Covered Copper Wire	74
Figure 5.2.2 Insulated Bare Copper Wire	75
Figure 5.2.3 Ansys Logo	76
Figure 5.2.4 Detail of Curve Line Built Up with Multiple Straight Line (Ansys Maxwell)	76
Figure 5.2.5 Detail of 3-Dimensional View of Simulation (Ansys Discovery Aim)	76
Figure 6.1.1 Simulation of Ohmic Loss of Coil	77
Figure 6.1.2 Compress and Tensile Stress of Bending Conductor	78
Figure 6.1.3 Stress of Conductor	78
Figure 6.1.4 Strain of Conductor	78
Figure 6.1.5 Relationship of Stress and Strain	79
Figure 6.1.6 Simulation of Temperature of Coil	79
Figure 6.1.7 Graph of Resistance against Temperature	80

LIST OF EQUATION

Equation 1.1 Reflection Coefficient	1
Equation 2.1 Electromotive Force	8
Equation 2.2 Resistance of Conductor	12
Equation 2.3 Equivalent Impedance at Secondary Side (SS)	20
Equation 2.4 Equivalent Impedance at Secondary Side (SP)	20
Equation 2.5 Equivalent Input Impedance (PP)	20
Equation 2.6 Imaginary Part of Input Impedance (PP)	21
Equation 2.7 Resonance Frequency (PP)	21
Equation 2.8 Time Constant	23
Equation 2.9 Charging Voltage at Specific Time	23
Equation 2.10 Discharging Voltage at Specific Time	23
Equation 3.1 Inductive Reactance	32
Equation 3.2 Resonant Condition	32
Equation 4.1 Total Voltage Drop across two Inductive Coils	66
Equation 4.2 Derived Total Voltage Drop across two Inductive Coils	67
Equation 4.3 Mutual Inductance	67
Equation 4.4 Coupling Coefficient	67
Equation 4.5 Quality Factor of Primary Inductive Coil	67
Equation 4.6 Quality Factor of Secondary Inductive Coil	67
Equation 4.7 Self-Inductance of Circular Flat Spiral Coil	68
Equation 4.8 Percentage Error	68
Equation 4.9 Resonance Condition	69
Equation 4.10 Total Impedance	69
Equation 4.11 Electromotive Force	70

Equation 4.12 Ampere Hour	71
Equation 6.1 Ohmic Loss	77
Equation 6.2 Stress of Conductor	78
Equation 6.3 Strain of Conductor	78
Equation 6.4 Young Modulus of Conductor	79
Equation 6.5 Resistance of Conductor against Change of Temperature	80

LIST OF SYMBOLS / ABBREVIATIONS

Γ	reflective coefficient
\mathcal{E}	electromotive force, V
ρ	resistivity, Ω m
ℓ	length, m
ω	resonant frequency, Hz
τ	time constant
k	coupling coefficient
α	temperature coefficient of resistance
T	temperature
Z_L	load impedance, Ω
Z_S	source impedance, Ω
R	resistance, Ω
A	cross sectional area, mm^2
d	distance, mm
L	lateral distance, mm
θ	tilting angle, $^\circ$
X_L	inductive reactance, Ω
X_C	capacitive reactance, Ω
N	coil turns
Q	quality factor
M	mutual inductance, μH

LIST OF APPENDICES

APPENDIX A: KBPC 1010 Datasheet	85
APPENDIX B: Arduino UNO R3 Datasheet	87
APPENDIX C: NodeMCU V3 Datasheet	91
APPENDIX D: MG995 Servo Motor Datasheet	93

CHAPTER 1

INTRODUCTION

1.1 General Introduction

Wireless charging for electric vehicle (EV) was an innovative invention as it did not need a direct connection or contact between vehicle and the charging cable. The owner of the wireless charging electric vehicle just have to park their vehicles just above the transmitter charging pad within the acceptable lateral range between the transmitter and receiver pad beneath the electric vehicle.

1.2 Importance of the Study

This research mainly focus on how to improve the wireless power efficiency by many factors such as alignment of coil, impedance matching, and compensation circuit. Thus, the maximum current or maximum charging rate can be achieved to reduce charging time.

For detailed explanation of impedance matching, impedance matching is important in order to have maximum power transfer. Impedance matching is a scenario where the impedance of load side and source side is equivalent to each other, producing maximum power transfer. There are three major components that carrying the impedance which are source impedance, transmission line impedance, and load impedance.

When the mismatching of impedance happens between source and load side, reflection of wave energy will happen. The equation of the reflection coefficient is shown in equation (1.1), where Z_S refers to source impedance and Z_L refers to load impedance. (Hanqiao, 2015)

$$\Gamma = \frac{Z_L - Z_S}{Z_L + Z_S} \quad (1.1)$$

Based on equation (1.1), when Z_L is equal to Z_S , the reflection coefficient will become “0” which means no reflection at all or perfect impedance matching.

Meanwhile, when Z_L is infinite (open circuit), the reflection coefficient will be infinite also which means it causes full reflection of wave energy. Moreover, when the Z_L is zero (short circuit), the reflection coefficient will equal to “1” which means complete discontinuity and cannot absorb any of the incident wave energy.

Besides that, the impedance matching also applies the Thevenin Equivalent Circuit theory. Thevenin’s Theorem is an analytic method to simplify the circuit at source side into one source (E_{Thevenin}) and one source impedance (Z_{Thevenin}). Thus, the load impedance can be adjusted easily to match the source impedance to produce maximum power transfer. The illustration of circuit is shown below. The further details of study will be discussed in the following parts.

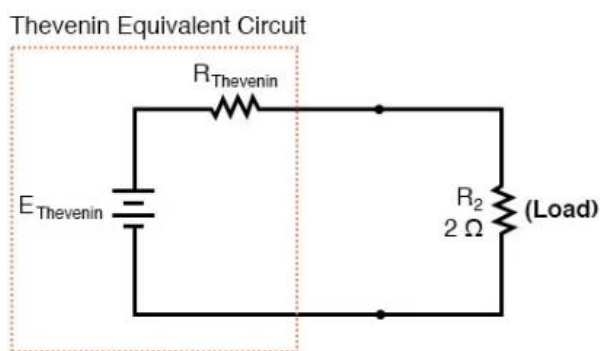


Figure 1.2.1 Thevenin’s Equivalent Circuit

1.3 Problem Statement

Nowadays, the application of electric car is a huge invention that brings the automotive industry to a new era. In old time, cars produce a lot of pollutants such as carbon monoxide that pollutes the air and affecting human’s health.

The main advantage of electric car is it can replace the demand of fuel by electrical system such as battery. Thus, the electric car no longer relies on the fuel as power source so the air pollution is reduced. Moreover, there is one more type of car that uses both electricity and fuel gas as power source called “Hybrid Vehicles”. The implementation of hybrid vehicle is due to the unsatisfied issues of electric car as pure electric car will bring some negative effects.

For the negative effect of using electric car, the recharge station is now under development. In another words, the quantity and availability of recharge point is a major issue to satisfy all electric car users as the battery capacity of some electric

cars are low. In simple word, the user needs to recharge their electric car frequently when having a long journey of driving which is not desirable.

Last but not least, the electricity consumption and recharge time which are the main concerns in this project, in some cases, the user of the recharge station is not satisfy with the high cost of the electricity bill and the long recharge time. There are two major reasons that cause this problem which are the low charging rate and the power loss due to some errors of parameters such as distance, lateral alignment, and tilting angle between transmitting coil and receiving coil when charging the electric vehicle.

1.4 Aim and Objectives

This project mainly focuses on the study of wireless charging system of electric vehicle, design and optimize the system to solve the issues of power loss and improving charging rate when charging the electric car.

Besides, this project will study on the micro-controller system to control the alignment of the transmitter pad and receiver pad automatically so the driver not necessary to achieve the perfect alignment manually by using their vehicle steering.

1.5 Scope and Limitation of the Study

This study mainly focuses on the parameter and physical alignment optimization so that the high efficiency of wireless charging system for vehicles can be achieved in terms of charging time by using micro-controller system. The implementation of Internet of Things (IoT) is also applied into the system which makes the application more convenient to the user.

1.6 Contribution of the Study

The contribution of this study is to make driver able to have maximum power transfer between the transmitter pad and receiver pad of electric vehicle without having a problem of misalignment due to poor parking skill.

Besides, it is a potential project that able to reduce the power supplied from the transmitter pad while having the same charging rate. For example, the standard of 3.3 kW is the lowest power needed for wireless power transfer for electrical vehicle, however, this project needed around 1 kW from transmitter pad to achieve the same

charging rate because the auto-alignment system able to minimize power needed from source.

This project will be a reference for researcher who interested in this kind of project also. Instead of increasing the power draw from source to achieve high charging rate, there is a better solution which is the auto-alignment system. Thus, electric bill is not an big deal when applying this product.

CHAPTER 2

LITERATURE REVIEW

2.1 Introduction

Electric motor is used to drive the electric car (EV) instead of using petrol or diesel engine. It contains a rechargeable battery that can be also used for many purposes such as household, street light, EV charge station etc.

There are various types of electric car which are battery electric vehicles (BEVs), plug-in electric hybrid vehicle (PHEV), and range extender electric vehicles (REEVs). Plug-in electric hybrid car is a combination of electric and petrol that used as the power source of vehicles, the main advantage of PHEV is PHEV not only rely on one power source in case one of the power source is not available, another power source will be the backup. The disadvantage of PHEV is PHEV applies the petrol as one of the power source which is not environmental friendly. Next is the range extender electric vehicles (REEVs), REEVs have a internal combustion engine, electric motor, and plug-in battery pack. The major difference between REEVs compared to PHEV is that the wheels always driven by the electric motor, the battery is recharged by the internal combustion engine. Last but not least, the battery electric vehicles (BEVs) is a most environment friendly vehicles due to the zero emission of pollutant and it is fully electrically powered. With these types of vehicles, the most preferable vehicles in future must be the battery electric vehicles (BEVs) because it is the most environment friendly.

With the most preferable vehicle in future, BEVs, recharging of battery is the major issue that encountered by most of the BEVs users. There are some factors that must be considered are the recharge station availability, recharge time, capability to move the car when charging. In order to achieve the situation whereby the vehicle is able to be charged while in motion, wireless charging was proposed.

Wireless charging vehicle in high power applications are now dominating the application of the plug in electric vehicles. It consists two ways of charging vehicle without using wire such as dynamic and static. In past, the wireless charging vehicle was in motionless state when charging, which leads

to the undesired issue such as unable to charged up when vehicle is in motion. Thus, dynamic wireless charging vehicle was implemented. This is to ensure the car able to be charged while in motion. However, there was an issue regarding the capability of charging the vehicle while the vehicle is moving in very fast speed. (Junwei, 2018)

2.2 Literature Review

2.2.1 Battery Chargers

When designing the battery chargers, there are three main considerations which are charging state, stabilizing state, and terminating state.

There are many types of charging methods which are constant voltage (CV), constant current (CC), IUI, taper current, trickle, float, pulsed, and burp charging.

For the CV and CC charging methods, the CC/CV method is the common way of charging the lithium batteries. At the beginning, the battery is empty, CC mode is triggered to charge up the battery rapidly. At the same time, the charging voltage increased. When the maximum charging voltage is achieved, CV mode will be triggered to slow down the charging rate, which means that the charging current will start to decrease until the battery is fully charged. At this point, CV mode will be ended. The main purpose of CV mode is to slow down the charging rate by decreasing the charging current because the current will generate heat and decrease the lifespan of the battery.

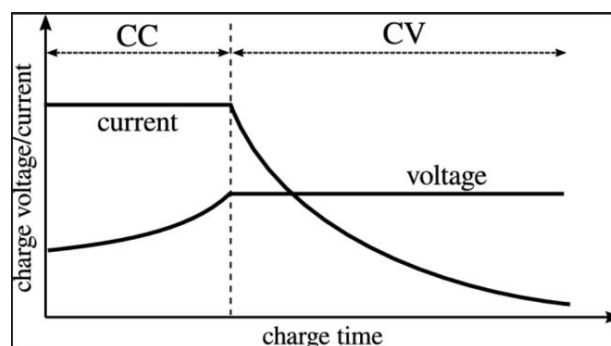


Figure 2.2.1.1 Graph of CC/CV Charging Method

For the IUI charging method, the concept is similar to the CC/CV charging, the only difference of IUI compared to CC/CV is IUI has an additional phase at last which is constant current phase again. In this third

phase, the charging current will be constant and the charging voltage will be increased again to a higher preset value. Thus, the charge in the battery will be equalized to increase battery life.

For the taper current charging method, when the battery is in low charge condition, the charger delivers high-rate charging current. Charging current is tapered to lower charging rate as the battery becomes more charges or almost fully charged.

Next, the trickle charging method, trickle charging able to compensate the discharging of battery. This charging method often used to maintain battery fully charged at no load condition by supplying continuous current charging. In addition, NiMH and Lithium battery are not suitable for this charging method because these types of battery will undergo overcharging and get damaged. Moreover, is the float charging method, the DC charging source, battery and the load are connected in parallel to each other permanently. The DC source held at a constant voltage below the battery's upper voltage limit. Emergency power back up system often use this kind of charging method.

Last but not least, pulsed charging method, there are three phases for pulsed charging method which are positive charging, discharge pulse (burp), and rest period (no charging). For the positive charging phase, the pulsed charger delivers the current as pulse to the battery. By controlling the pulses width, the rate of charging can be controlled precisely. During the discharge period, this negative pulse dislodge any gas bubbles that attached on the electrodes during positive charging phase. This is to prevent the oxidation process happen on the electrodes, prolong the battery life span and capacity. During rest period, the charging current is zero and the cooling and settling of electrolyte occurs before next pulse cycle starts. (Electropaedia, n.d.)

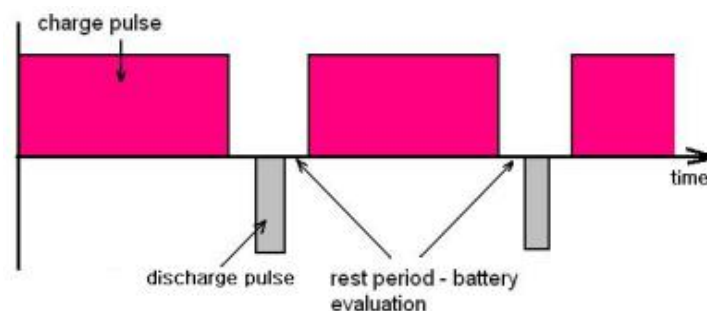


Figure 2.2.1.2 Waveform of Pulsed Charging Method

2.2.2 Basics of Wireless Power Transmission

Wireless power transmission is a technology where the energy can be transferred through an air distance without any conductor in between the two terminals. There are many types of coupling methods, compensation circuit, coil design etc. in order to achieve maximum power transfer.

2.2.2.1 Coupling Methods

There are two major categories of wireless coupling methods which are non-radiative method for near distance and radiative method for long distance. For the non-radiative coupling method, there are two coupling methods which are inductive coupling and capacitive coupling. For radiative coupling method, there are two coupling methods which are microwaves and lasers.

Inductive coupling is a scenario where the current is changed in one wire induces potential difference to another wire, and the power is transmitted wirelessly. In detailed explanation, the change of current in one coil will generate the magnetic field around it. The electromotive force (EMF) will be induced by magnetic field in the second wire according to Faraday's Law shown below. (Nave, n.d.)

$$\varepsilon = -N \frac{\Delta\phi_M}{\Delta t} \quad (2.1)$$

N = number of loops

$\Delta\phi_M$ = change in
magnetic flux

Δt = change in time

ε = induced voltage

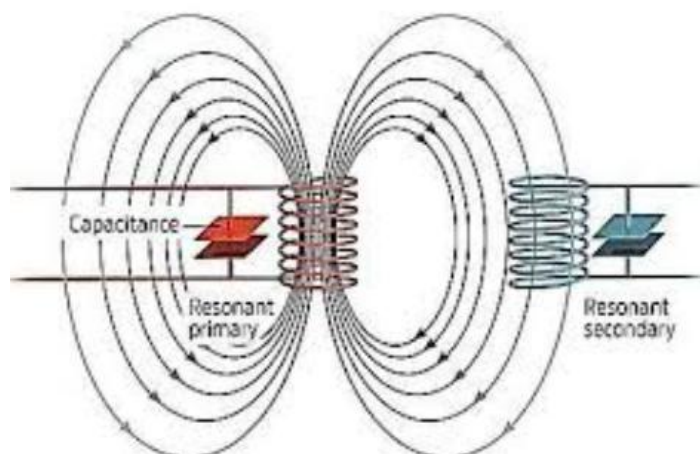


Figure 2.2.2.1.1 Resonant Inductive Coupling

Capacitive coupling is a transfer of energy from one wire to another wire through electric field thus power is transferred wirelessly. In detailed explanation, the electric field allows the transmission of power between electrodes which are anode and cathode.

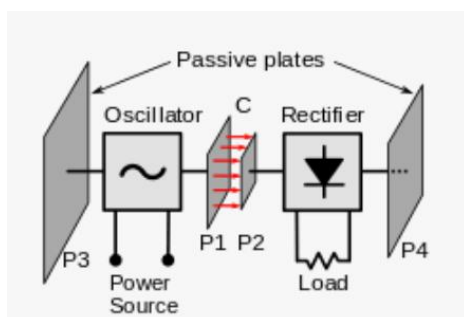


Figure 2.2.2.1.2 Capacitive Coupling

Microwaves power transmission is a technique that the energy able to be transferred in long distance. There are three essential components in microwaves technique which are conversion of electrical power into microwave power, the waves are captured by absorption antenna, and lastly microwave is re-converted back to electrical power. In order to generate the microwaves, a component named magnetron is used. By definition, magnetron is a high-powered vacuum tube that generates microwaves applying the interaction of magnetic field with stream of electrons and it is operated using direct current (DC).

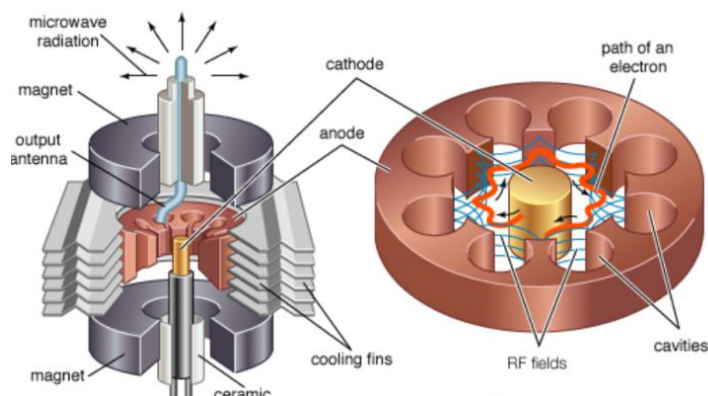


Figure 2.2.2.1.3 Structure of Conventional Magnetron

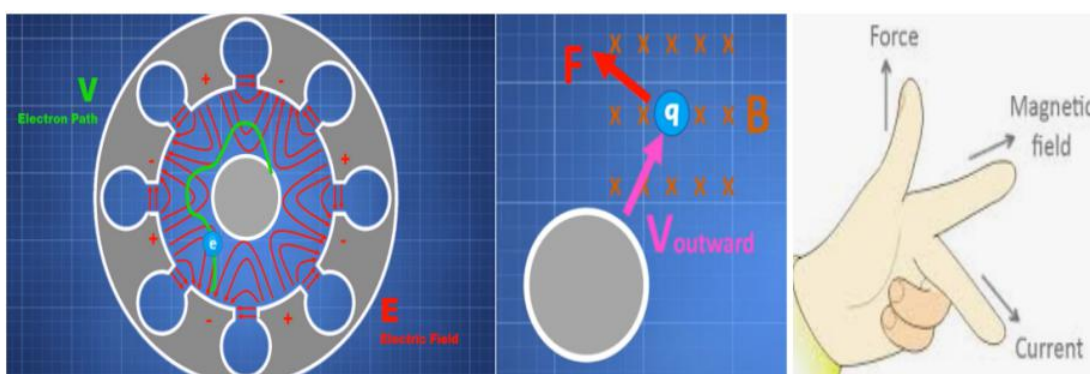


Figure 2.2.2.1.4 Flow of Electrons in Interact Space using Left Hand Rule

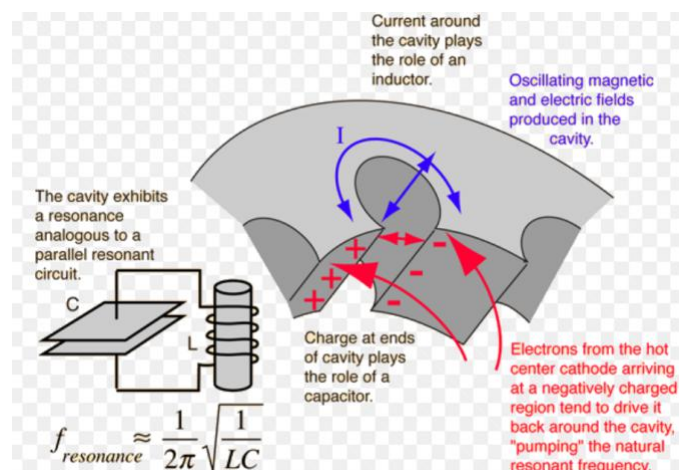


Figure 2.2.2.1.5 Resonant Cavity of Magnetron

Based on Figure 2.2.2.1.4, the electrons flow from cathode (internal rode) to the anode (outer ring). Assuming the magnetic field flows in direction of into the paper, based on “Left Hand Rule”, the force will be generated and applied to the flowing electrons and cause the electron move in a direction shown in Figure 2.2.2.1.4. Based on Figure 2.2.2.1.5, the electron from the cathode will reach the negatively charge region and drive it back around the

cavity, “pumping” the natural resonant frequency. The cavity is equivalent to the combination of capacitor with inductor and resonant frequency formula are shown in Figure 2.2.2.1.5. Thus, microwaves will be generated in the cavity of magnetron.

Last but not least, the laser wireless power transmission is highly directional and coherent. However, its magnitude will be attenuated when propagating through atmosphere. The receiver of the laser technique is photovoltaic cell. (Dave, 2019)

2.2.2.2 Coil Designs with Power Efficiency

There are many ways of designing the inductive coils in terms of type of wire used, diameter of wire, coiling methods, alignment, distance between two coils etc. There are several types of metal that can be used to conduct electricity such as silver, copper, gold, aluminium, rhodium etc. However, for the applications nowadays, copper is commonly used as the conductor because the price of copper wire is cheaper than silver with acceptable electrical conductivity that has not much difference from silver. The comparison of the electrical resistivity of metals and its formula are shown below.

(Metal 100)	Electrical Resistivity at 293 K, $\mu\Omega\text{cm}$	Thermal Conductivity $\text{Wm}^{-1}\text{k}^{-1}$	Relative Electrical Conductivity (Copper = 100)	Relative Thermal Conductivity (Copper = 100)
Silver	1.63	419	104	106
Copper	1.694	397	100	100
Gold	2.2	316	77	80
Aluminum	2.67	238	63	60
Beryllium	3.3	194	51	49
Magnesium	4.2	155	40	39
Tungsten	5.4	174	31	44
Zinc	5.96	120	28	30
Nickel	6.9	89	24	22
Iron	10.1	78	17	20
Platinum	10.58	73	16	18
Tin	12.6	73	13	18
Lead	20.6	35	8.2	8.8
Titanium	54	22	3.1	5.5
Bismuth	117	9	1.4	2.2

Table 2.2.2.2.1 Electrical Resistivity, Thermal Conductivity, Relative Electrical Conductivity and Relative Thermal Conductivity of Metals

$$R = \frac{\rho L}{A} \quad (2.2)$$

ρ = resistivity
 L = length
 A = cross sectional area

There are various shapes of coils such as single-coil circular rectangular pad (CRP), multiple-coil bipolar polarized pad (BPP), single-coil non-polarized pad (CP), etc. The comparison of different coil methods are shown below. (Azuwa, 2019)

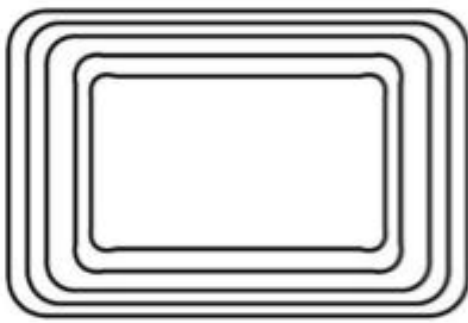


Figure 2.2.2.2.1 single-coil circular
Rectangular pad (CRP)



Figure 2.2.2.2.2 single-coil circular non-
polarized pad (CP)

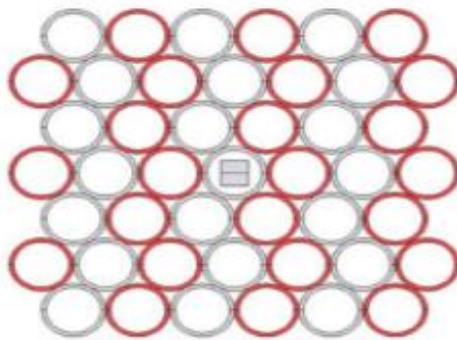


Figure 2.2.2.2.3 multiple-coil
Homogeneous pad (HP)

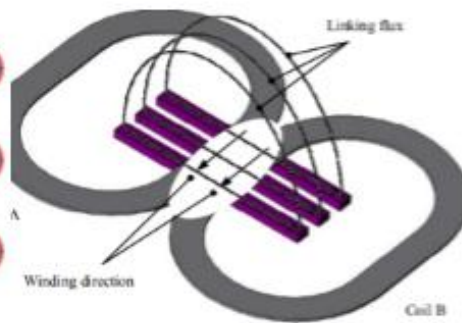


Figure 2.2.2.2.4 double-D polarized pad
(DDP)

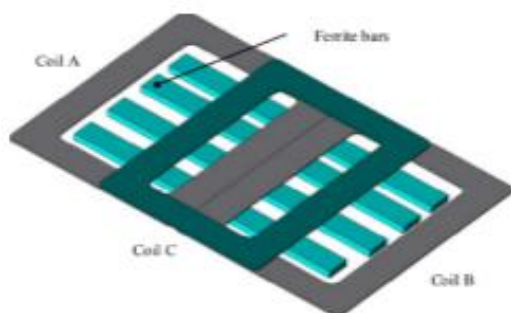


Figure 2.2.2.2.5 multiple-coil double-D

Quadrature polarized pad (DDQP)

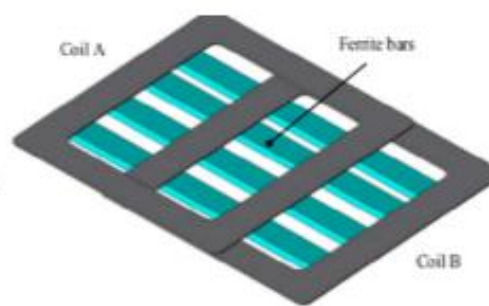


Figure 2.2.2.2.6 multiple-coil bipolar

polarized pad (BPP)

	CRP	CP	HP	DDP	DDQP	BPP
Transferrable power	Medium	Medium	Low	High	High	High
Pad design size	Medium	Medium	Large	Small	Small	Small
Pad weight	Low	Low	High	Low	Medium	Medium
System material cost	Low	Low	High	Medium	High	Medium
Transmission distance	Low	Low	Medium	Medium	High	High
Charging zone	Small	Small	Large	Medium	Large	Large

Table 2.2.2.2.2 Comparisons of Different Shape of Coils

2.2.2.3 Efficiency versus Misalignment of Coils of Wireless Power Transmission

Efficiency of wireless charging for electric car is the main consideration as it can save users' time consumption with high charging rate. There are various positioning factors of charging pad that will decrease the efficiency which are the distance, misalignment, etc between transmitter coil and receiver coil.

Based on Figure 2.2.2.3.2, maximum mutual inductance can be achieved between the coils when the lateral misalignment equals to zero. Whenever the lateral misalignment occur, the mutual inductance between two coils will decrease accordingly. Based on Figure 2.2.2.3.3, when the distance between transmitting and receiving coils increases, the mutual inductance decreases. This is because the magnetic field from the transmitter side is

getting harder to transmit the power to another side of coil in longer distance. Based on Figure 2.2.2.3.4, the mutual inductance is highest when the angular misalignment equals to zero and decreasing with the increasing of angular misalignment.

With all the positioning methods, it can be concluded that in order to achieve highest mutual inductance between coils, the coils must be placed closely, zero lateral misalignment and zero angular misalignment. (Sakir, 2017)

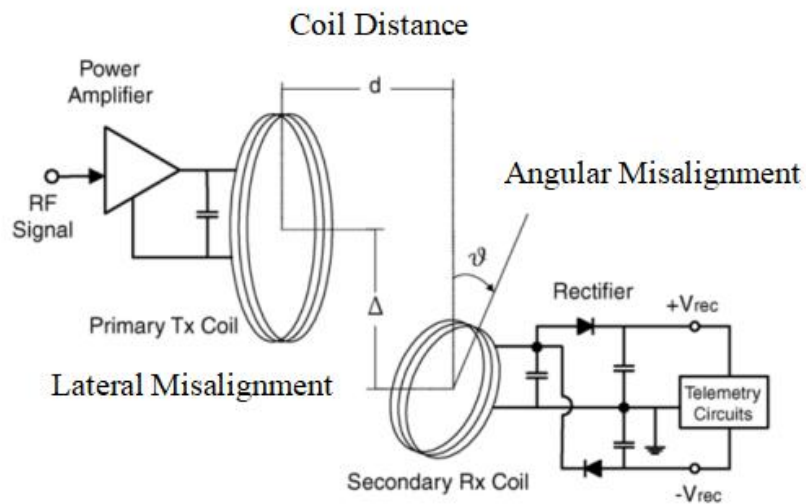


Figure 2.2.2.3.1 Lateral, Angular Misalignment and Coil Distance

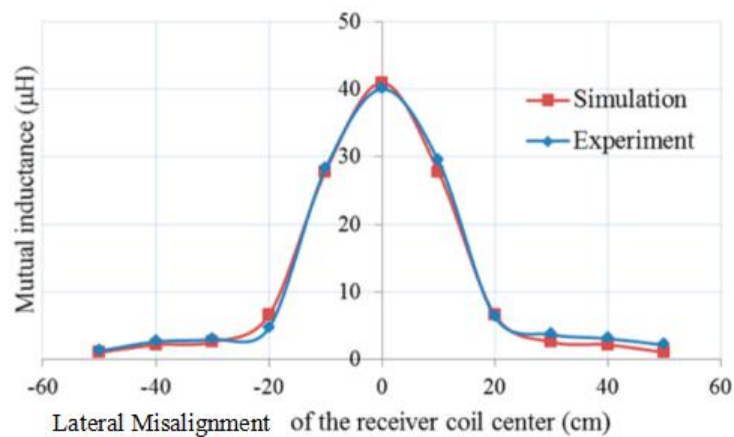


Figure 2.2.2.3.2 Graph of Mutual Inductance versus Lateral Misalignment of coils

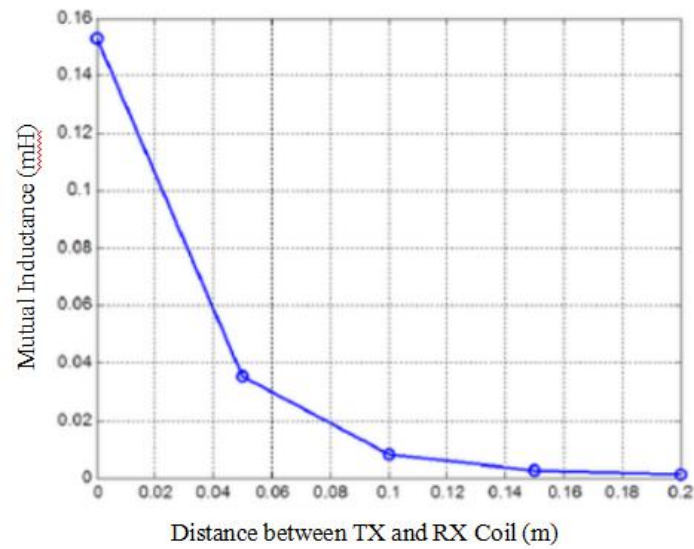


Figure 2.2.2.3.3 Graph of Mutual Inductance versus Distance of Coils

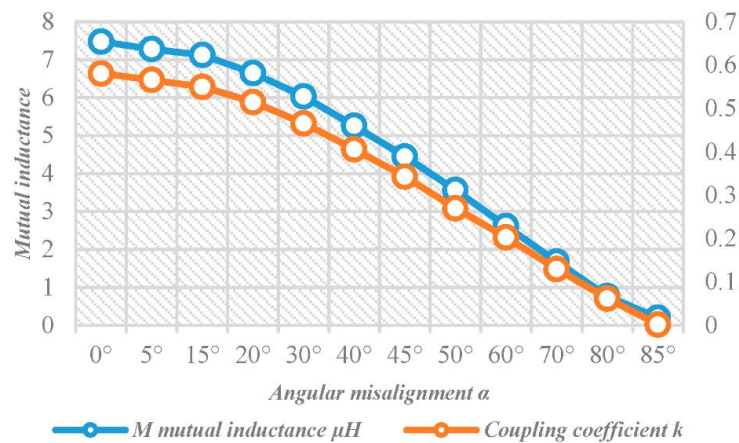


Figure 2.2.2.3.4 Graph of Mutual Inductance versus Angular Misalignment of Coils

2.2.3 Basics of Electronics Circuit Designs

For the circuit design of inductive wireless charging, basically there are five major elements to be studied which are high frequency inverter, current gain and compensation network, inductive wireless power transfer, voltage gain and compensation network, and lastly high frequency rectifier.

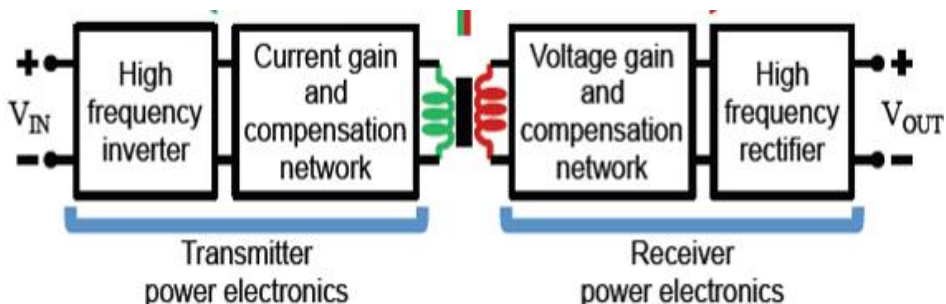


Figure 2.2.3.1 Block Diagram of Inductive Wireless Vehicle Charging

2.2.3.1 Inverter

Direct current (DC) can be converted into alternating current (AC) by inverter. The technique of building up the inverter is either using half-bridge or full-bridge method. The output voltage of the the half-bridge inverter is half of full-bridge inverter, which means that the power produced from half-bridge inverter is 1/4 times of the full-bridge inverter since the power is proportional to square of output voltage. Thus, most of the applications preferred full-bridge inverter. (David, 2016)

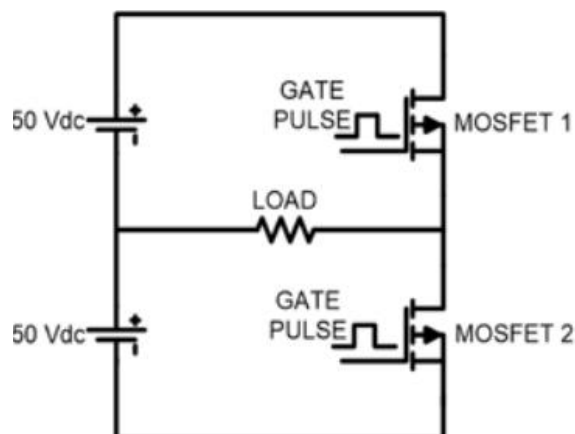


Figure 2.2.3.1.1 Half-Bridge Inverter

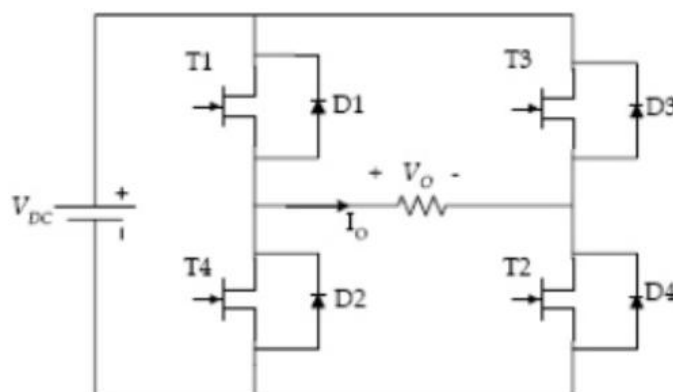


Figure 2.2.3.1.2 Full-Bridge Inverter

The MOSFET behaves like a switch. An ideal switch will be used to replace the MOSFET for explaining the inverting technique from DC to AC waveform. Based on the circuit diagram below, assuming the current flow at load is from left to right shown as arrow, when MOSFET S1 and S2 are on, then current will flow through V_{DC} , S1, load, and S2, the current flow direction at load is same with the arrow, thus V_0 is equal to V_{DC} . When MOSFET S1 and S3 are on, the circuit is incomplete referred to the V_{DC} , thus V_0 equal to zero. When MOSFET S3 and S4 are on, the current will flow through V_{DC} , S3, load, and S4, the current flow direction is opposing the arrow, thus V_0 is equal to $-V_{DC}$. When MOSFET S2 and S4 are on, the circuit is incomplete referred to V_{DC} , thus no current flow and V_0 is equal to zero. The processes are repeated to get the next cycle of same output waveform.

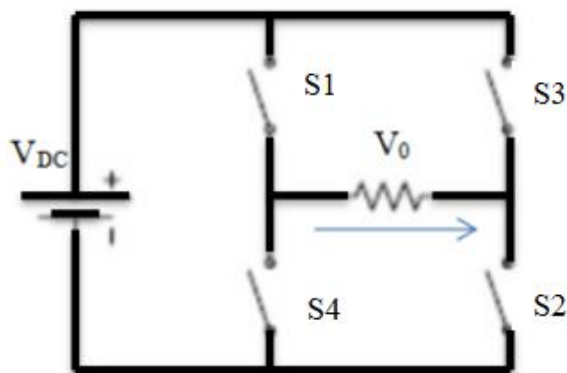


Figure 2.2.3.1.3 Full-Bridge Inverter (Ideal Switch)

S1	S2	S3	S4	V_0
1	1	0	0	V_{DC}
1	0	1	0	0
0	0	1	1	$-V_{DC}$
0	1	0	1	0

Table 2.2.3.1.1 Truth Table of Full-Bridge Inverter

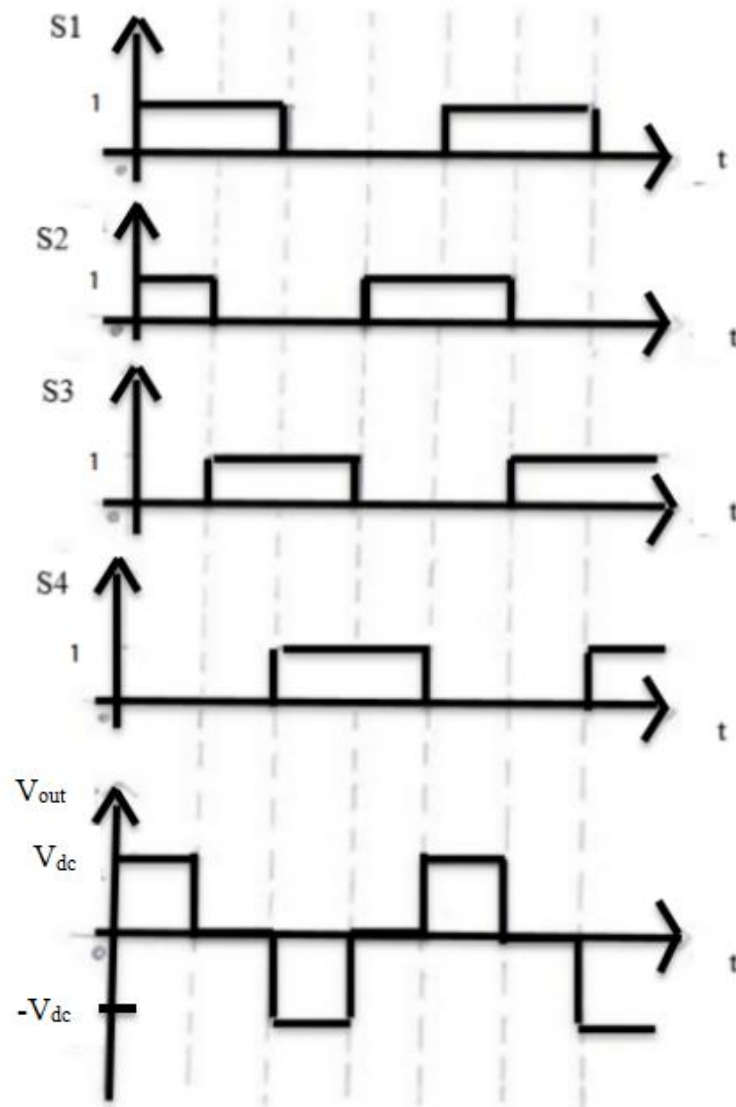


Figure 2.2.3.1.4 Waveform of Four MOSFET and Output Voltage

There are two frequency levels of inverter which are low frequency and high frequency. High frequency inverter operates at around 50 kHz or higher; low frequency inverter operates below 50 kHz. The advantages of high frequency inverter are it has smaller footprint and cheaper; the disadvantage is it does not operate well with high surge loads and high torque tools. The advantage of low frequency inverter is it operates well with high surge loads and operates cooler; the disadvantages are heavier and more expensive.

2.2.3.2 Compensation Network

In order to achieve maximum power transfer, compensation network is necessary to eliminate the imaginary part or reactance. There are four basic topologies of compensation network which are series-series circuit (SS), series-parallel circuit (SP), parallel-series circuit (PS), and parallel-parallel circuit (PP). L_1 and L_2 is the self-inductance, M is the mutual inductance. Resonance frequency is the frequency that allows maximum wireless power transfer. (Viktor, 2019)

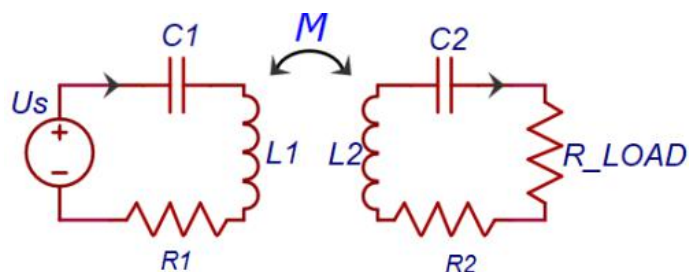


Figure 2.2.3.2.1 Series-Series Circuit (SS)

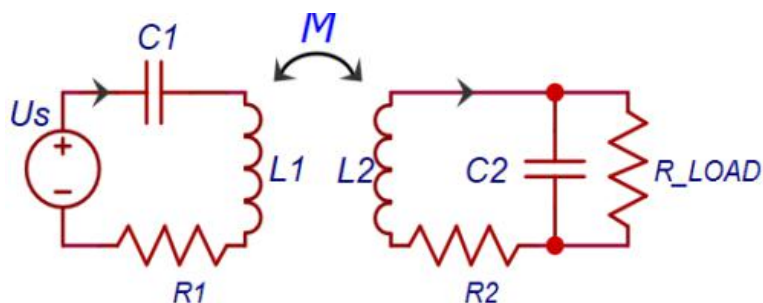


Figure 2.2.3.2.2 Series-Parallel Circuit (SP)

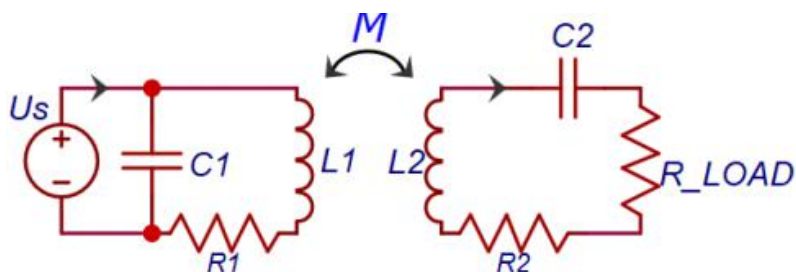


Figure 2.2.3.2.3 Parallel-Series Circuit (PS)

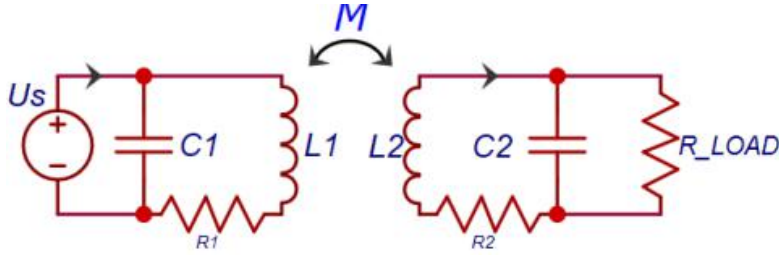


Figure 2.2.3.2.4 Parallel-Parallel Circuit (PP)

For SS topology, the equivalent impedance at secondary side and the resonant frequency (ω_s) are shown in equation (2.3). For SP topology, the equivalent impedance at secondary side and the resonant frequency (ω_p) are shown in equation (2.4). By comparing equation (2.3) and (2.4), when the load resistance, R_L is larger than $(L_2 / C_{p2})^{0.5}$, Z_{e2} will be larger than Z_{e1} , which means that the power transfer efficiency will be higher in the SP topology. This is because when the equivalent impedance at the secondary side is greater than the primary side, the efficiency of power transfer will be greater. Thus, SP topology is more suitable for high impedance load application.

$$Z_{e1} = \frac{(\omega_s M)^2}{R_2 + R_L}, \quad \omega_s^2 = \frac{1}{L_2 C_{s2}} \quad (2.3)$$

$$Z_{e2} = \frac{(\omega_p M)^2}{R_2 + \frac{L_2}{C_{p2} R_L}}, \quad \omega_p^2 = \frac{1}{L_2 C_{p2}} - \frac{1}{C_{p2}^2 R_L^2} \quad (2.4)$$

For the PP topology, the equivalent input impedance is shown in equation (2.5). The imaginary part of the input impedance can be expressed as equation (2.6) with $L=L_1=L_2$, $C=C_1=C_2$. The resonance frequency can be expressed as equation (2.7) by substituting the imaginary part in equation (2.5) to zero. “k” is the mutual inductance coefficient.

$$Z_{in} = \frac{(1 - \omega^2 L_1 C_1)[R_L(1 - \omega^2 L_2 C_2) + j\omega L_2] - \omega^2 M C_1 (\omega^2 M C_2 R_L - j\omega M)}{(j\omega L_1)[R_L(1 - \omega^2 L_2 C_2) + j\omega L_2] + (j\omega M)(\omega^2 M C_2 R_L - j\omega M)} \quad (2.5)$$

$$\text{Im}(Z_{in}) = \frac{\omega L [1 - \omega^2(L^2 - M^2)C/L] [(1 - \omega^2 LC)^2 R_L^2 - \omega^4 M^2 C^2 R_L^2 + \omega^2 L^2 - \omega^2 M^2]}{[\omega^2 L^2 - \omega^2 M^2]^2 + R_L^2 [\omega L(1 - \omega^2 LC) + \omega^3 M^2 C]^2} \quad (2.6)$$

$$f = \frac{1}{2\pi} \sqrt{\frac{L}{(L^2 - M^2)C}} = \frac{1}{2\pi} \sqrt{\frac{1}{(1 - k^2)LC}} \quad (2.7)$$

Moreover, for SS topology, there is an issue which is the frequency splitting phenomena. Frequency splitting phenomena is a situation where there are multiple peak values of efficiency which is not desirable because all of these peak value never reach the desired maximum power transfer efficiency. This phenomena only happens when the small resistance of load is used as shown in Table 2.2.3.2.1.

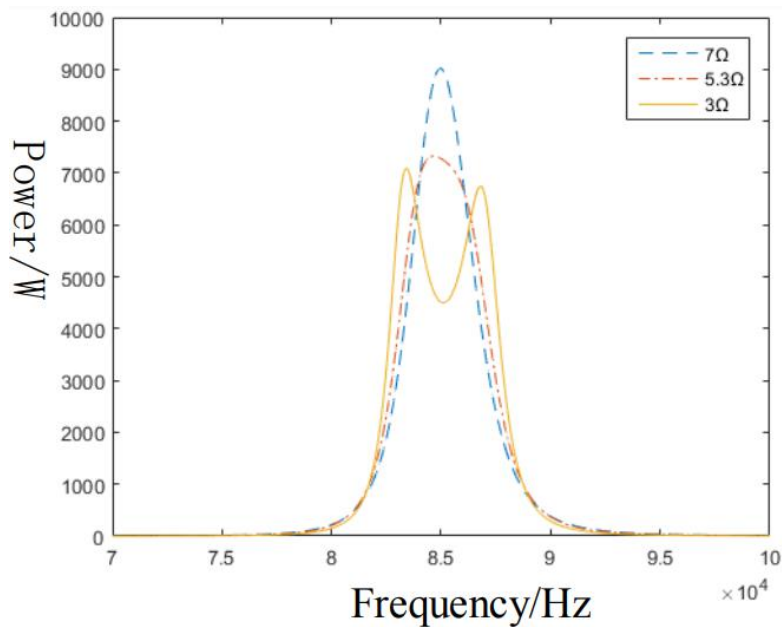


Figure 2.2.3.2.5 Frequency Splitting (Yellow Solid Line)

Conditions	Resonance Frequencies
$(R_2 + R_L)^2 - \frac{2L}{C} \geq 0$	$f_1 = \frac{1}{2\pi\sqrt{LC}}$
$(R_2 + R_L)^2 - \frac{2L}{C} < 0$	$\Delta < 0$ $f_1 = \frac{1}{2\pi\sqrt{LC}}$
	$\Delta = 0$ $f_1 = \frac{1}{2\pi\sqrt{LC}}$
	$f_2 = \frac{1}{2\pi} \sqrt{\frac{-(R_2 + R_L)^2 - \frac{2L}{C}}{2(L^2 - M^2)}}$
	$\Delta > 0$ $f_1 = \frac{1}{2\pi\sqrt{LC}}$ $f_{2,3} = \frac{1}{2\pi} \sqrt{\frac{-(R_2 + R_L)^2 - \frac{2L}{C} \pm \sqrt{\left[(R_2 + R_L)^2 - \frac{2L}{C} \right]^2 - \frac{4(L^2 - M^2)}{C^2}}}{2(L^2 - M^2)}}$
Where:	$\Delta = \left[(R_2 + R_L)^2 - \frac{2L}{C} \right]^2 - \frac{4(L^2 - M^2)}{C^2}$

Table 2.2.3.2.1 Resonance Frequencies with Different Conditions in SS Topology

Topologies	Features
SS	<ol style="list-style-type: none"> 1. Equal to short circuit at resonance frequency 2. Suitable for load impedance less than $(L_2/C_2)^{0.5}$ 3. Large current in the circuits 4. The phenomenon of frequency splitting
SP	<ol style="list-style-type: none"> 1. Equal to open circuit at resonance frequency 2. Suitable for load impedance larger than $(L_2/C_2)^{0.5}$ 3. Large voltage in the secondary circuit 4. The compensated capacitance is related to load
PS	<ol style="list-style-type: none"> 1. Equal to open circuit at resonance frequency 2. Suitable for load impedance less than $(L_2/C_2)^{0.5}$ <p>Tiny current in the circuits</p> <ol style="list-style-type: none"> 2. Tiny load power 3. The resonance frequency is affected by mutual inductance
PP	<ol style="list-style-type: none"> 1. Equal to open circuit at resonance frequency 2. Suitable for load impedance larger than $(L_2/C_2)^{0.5}$ 3. Tiny current in the circuits 4. Tiny load power 5. The resonance frequency is affected by mutual inductance 6. The compensated capacitance is related to load and mutual inductance

Table 2.2.3.2.2 Qualitative Comparisons of Four Topologies

2.2.3.3 Converter

Alternating current (AC) is converted into direct current (DC) by converter or rectifier. Basically there are two types of rectifier which are half-wave and full-wave. Center tapped rectifier and bridge rectifier are categorized as full-wave rectifier. The circuits are shown below.

For the half-wave rectifier, when the current flows in the direction shown as arrow, the current is allowed to pass through the diode due to forward bias and pass through resistor; meanwhile charging the smoothing capacitor, when output voltage reach its peak value, the smoothing capacitor starts to discharge. Normally before the smoothing capacitor is completely discharged, another new cycle of input voltage will start and charge up the smoothing capacitor again. Thus, the value of capacitance of the smoothing capacitor is the main concern for its charging rate and discharging rate to determine how well is the smoothing property of output voltage. The formulas of time constant, capacitor voltage at specific time when charging and discharging are shown in equations (2.8), (2.9), and (2.10). The disadvantage of half-wave rectifier is when the current flows in the direction that opposing the direction of arrow shown in Figure 2.2.3.3.1, the current is blocked by the diode due to reverse bias property of the diode. To further improve the circuit, the full-wave rectifier is used. (Sourav, 2019)

Full-wave converter allows reverse current flows due to forward bias of the diodes and mirrors the negative side of the voltage waveform to the positive side as shown in Figure 2.2.3.3.4. The ripple voltage is smoothed by the smoothing capacitor. As a small conclusion, most of the applications apply full-wave rectifier because the smoothing capacitor can be recharged up in a shorter time so it has smoother output voltage compared to half-wave rectifier. (Keith, 2016)

$$T = RC \quad (2.8)$$

$$v_c = V_1 \left(1 - e^{-t/\tau}\right) \text{ (Charging)} \quad (2.9)$$

$$v_c = V_1 e^{-t/\tau} \text{ (Discharging)} \quad (2.10)$$

Where:

v_C = voltage across capacitor during transient

V_1 = applied voltage

t = time in seconds from change in applied voltage

τ = time constant

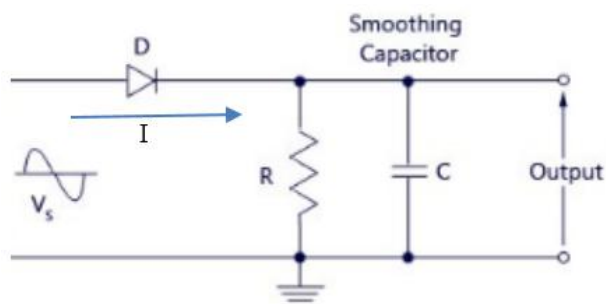


Figure 2.2.3.3.1 Half-Wave Rectifier

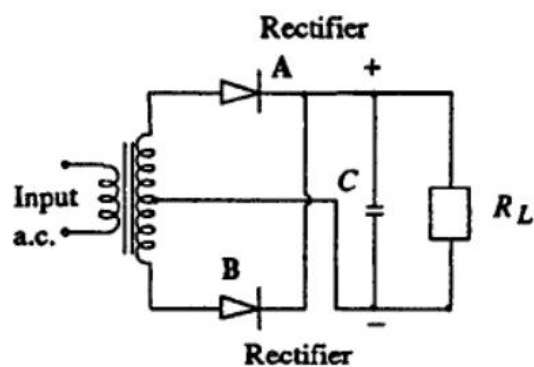


Figure 2.2.3.3.2 Full-Wave Rectifier (Center Tapped Rectifier)

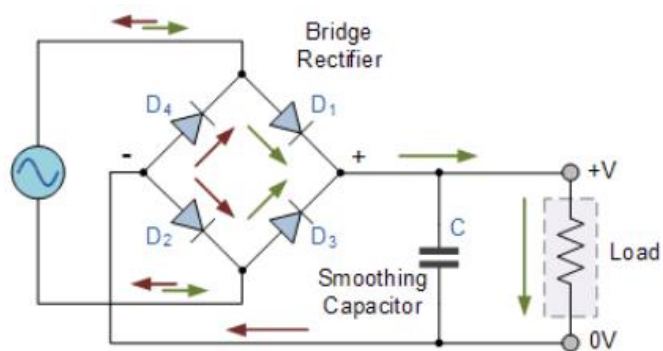


Figure 2.2.3.3.3 Full-Wave Rectifier (Bridge Rectifier)

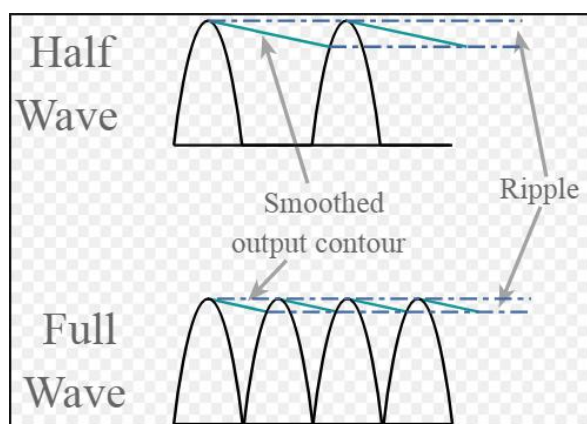


Figure 2.2.3.3.4 Output Waveform of Half-Wave and Full-Wave Rectifier

2.2.3.4 Internet of Things (IoT)

In recent years, the Internet of Things (IoT) has been one of the emerging technologies that gained a huge amount of attention from most companies in various sectors as it contains the potential to revolutionize the way we do things. IoT is basically a concept of connecting any device that are integrated with sensors to connect and exchange data with other devices through the Internet. For example, the ability to control all of the electrical appliances in a house through a smart phone is one usage of IoT as all the devices are connected to the Internet, and data is transferred through a smart phone. Some examples of large-scale implementation of IoT are smart cities, smart manufacturing, smart power grids and etc.

The usage and development of IoT has been increasing tremendously throughout recent years due to factors like the development of the 4th Industrial Revolution in most countries and the demand to automate processes. In 2014, the Ministry of Science, Technology and Innovation (MOSTI) in Malaysia has developed a National IoT Strategic Roadmap which serves as a guide to produce a national eco-system in order to utilise IoT as a source of economic growth.

Besides that, the development of Low-Power Wide Area Network (LPWAN) wireless communication also facilitates the development of IOT since an Internet connection that is able to cover a wide range with low power consumption and low cost is vital to the implementation of IoT. LPWAN is a wireless communication network that permits the transmission of data over long distances at a lower speed. The battery lifespan of LPWAN are able to

last for years, and it is suitable for applications that requires a low bandwidth and low transmission frequency at long distances under varying environments.

The arrival of 5G telecommunication also helps to provide connectivity to IoT sensors, and Malaysia is now in the process of implementing it. The three main pillars of 5G connectivity are the Enhanced Mobile Broadband which transmits data 10 times faster than 4G connectivity, the Ultra Reliable Low Latency Communications for applications that cannot afford delays in signal transmission, and the Massive Machine Type Communication which allows telecommunication companies to provide a platform to support IoT applications. These properties of 5G connectivity are all able to expedite the implementation and development of IoT. (Steve, 2020)

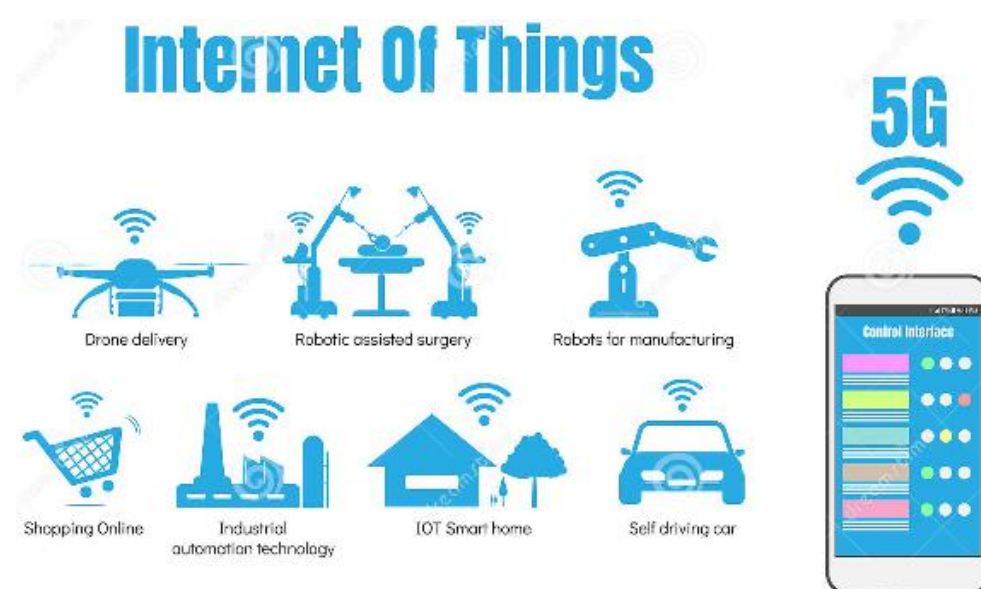


Figure 2.2.3.4.1 Internet of Things

2.3 Summary

As the summary of the literature review, there are many types of charging methods for battery which are constant voltage (CV), constant current (CC), IUI, taper current, trickle, float, pulsed, and burp.

Besides, there are four methods of wireless power transmission which are inductive coupling, capacitive coupling, microwave and laser technique.

For the coil designs, copper wire is the material that is used in most applications because it has lower price than silver. Although copper has lower

electrical conductivity than silver, copper is still the choice for most of the applications due to the high cost-effectiveness of copper. Moreover, there are various shapes of coils such as single-coil circular rectangular pad (CRP), single-coil circular non-polarized pad (CP), multiple-coil homogeneous pad (HP), double-D polarized pad (DDP), multiple-coil double-D quadrature polarized pad (DDQP), and multiple-coil bipolar polarized pad (BPP).

For the positioning of coils and efficiency of power transfer, there are three positioning factors for circular coil which are gap between transmitter coil and receiver coil, lateral misalignment, and angular misalignment. The maximum efficiency of wireless power transfer can be achieved when the gap between transmitter coil and receiver coil is close enough with a limited minimum distance, zero lateral misalignment, and zero angular misalignment. By comparing the circular pad and rectangular pad, circular pad is preferred because it has the advantage in term of less misalignment angles compared to rectangular pad. The extra one positioning factor in rectangular pad is the parallel angular misalignment.



Figure 2.3.1 Parallel Angular Misalignment of Rectangular Pad

Last but not least, for the overall circuit design of wireless power transfer, there are three parts needed to be considered which are inverter circuit, compensation circuit, and converter circuit. Direct current (DC) is converted into alternating current (AC) by inverter; compensation circuit used to compensate the imaginary part of the circuit to maximize the power transfer; alternating current (AC) is converted into direct current (DC) by converter.

CHAPTER 3

METHODOLOGY AND WORK PLAN

3.1 Introduction

Since there were a space of improvement for this wireless power transfer system. There are two objectives to be achieved in this project. The first one is to optimize the power electronic circuit design and coil design to achieve maximum power transfer between transmitter and receiver, and the second one is to achieve the optimum alignment between transmitter and receiver.

In order to achieve the maximum power transfer in term of circuit design, the compensation circuit plays the very important role to eliminate the reactance parts, in other words, it able to minimize the total impedance which allowing maximum current pass through the circuit.

Besides, in order to achieve maximum power transfer in term of alignment of transmitter and receiver pads, the auto-alignment system was implemented using Internet of Things (IoT) including the mobile apps called “Blynk”. The following diagram is the overall block diagram of the entire system in this project.

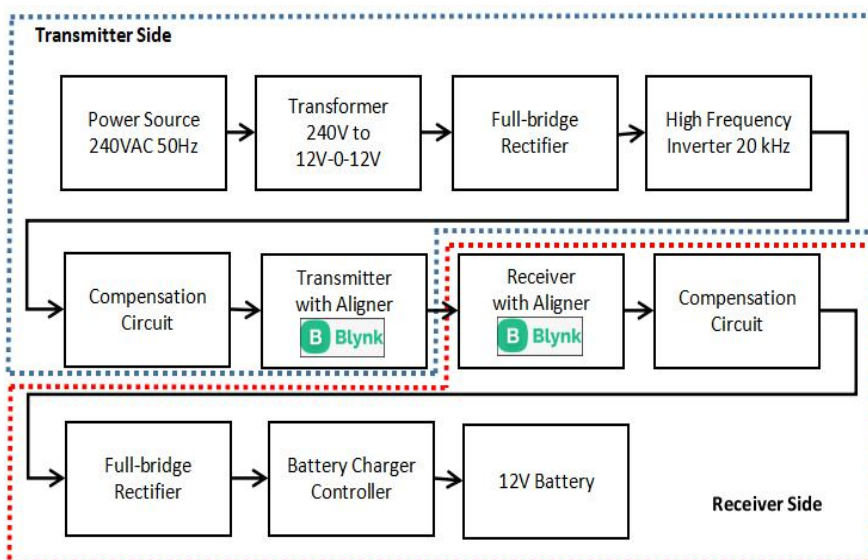


Figure 3.1.1 Overall Block Diagram of the Project

3.2 System Design

3.2.1 Electrical Circuit Design

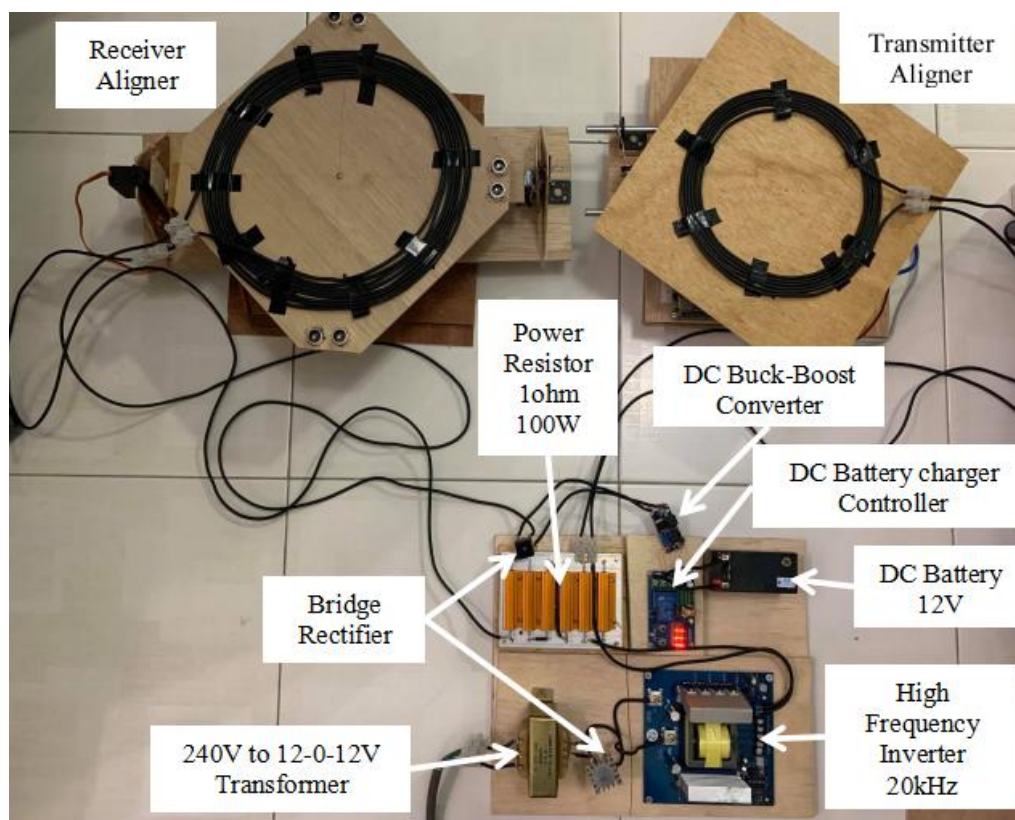


Figure 3.2.1.1 Overall Connection of the Hardware

First of all, the system was powered by the 240 VAC 50 Hz from the wall socket. Then the voltage was stepped down to 12 VAC by the step down transformer. After that, the 12 VAC was rectified by the full-bridge converter to produce 12 VDC and then to the 20 kHz high frequency inverter to produce back 12VAC. The main reason of doing all these steps were to increase the frequency of the AC voltage from 50 Hz to 20 kHz because it would be very difficult if directly increase the frequency of AC voltage. The reason of having high frequency AC voltage (20 kHz) instead of 50 Hz was to allow the power to be transmitted from transmitter to receiver within a considerable range. If 50 Hz AC source was used, the power can't being transmitted although the transmitter was attached directly to the surface of receiver pad. This

experiment was conducted in the process of making this project become successful. Moreover, the value of 20 kHz from inverter was verified by multimeter.



Figure 3.2.1.2 Six-pin Center-tapped Transformer
(0-115-230V to 12-0-12V, 4A/50VA)

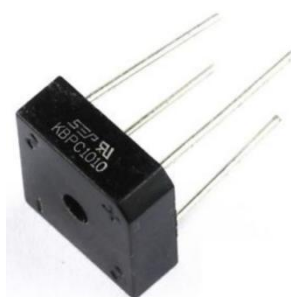


Figure 3.2.1.3 Bridge Rectifier (1000V, 10A)

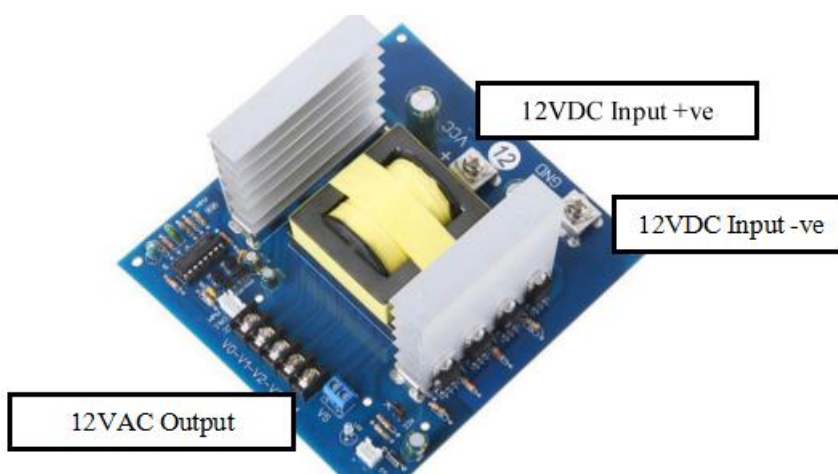


Figure 3.2.1.4 High Frequency Inverter (20 kHz)



Figure 3.2.1.5 Power Resistor (100W, 1 Ω)

After increasing AC voltage, the compensation circuit took part in order to eliminate the reactance part and allow maximum current flowed through the circuit. Based on the literature review, series-parallel (SP) compensation circuit has the best efficiency comparing to series-series circuit (SS), parallel-series circuit (PS), and parallel-parallel circuit (PP). Thus, SP compensation circuit was applied in this project to deliver the best efficiency of wireless power transfer.

In order to compute the value of capacitance for compensation circuit without using LCR meter, the inductance value of coils must be calculated first. Firstly, an inductive coil with unknown inductance value and a resistor with 100 Ω was connected in series with the function generator as power source. The frequency of the function generator was varied until the voltage drop of the inductive coil and resistor were the same, in other words at this time the reactance of inductive coil was equal to resistance of resistor ($X_L = R$). This is because the value of reactance of inductive coil was changing with the frequency of function generator. Next, the inductance was calculated by using equation (3.1). Lastly, the capacitance value was computed by applying the resonance equation (3.2).

A set of the data in this project as example, with transmitter coil with 8 turns, outer diameter of 165mm, inner diameter of 125mm, zero distance between adjacent core; receiver coil with 8 turns, outer diameter of 300mm, inner diameter of 260mm, zero distance between adjacent core, the measured

inductance of transmitting and receiving coils were 15.01 μH and 32.05 μH respectively. Thus, the value of capacitors for transmitter side and receiver side were 4.22 μF and 1.98 μF respectively. These parameters were verified using LCR meter. Multiple capacitors with value of 1 μF were connected in parallel to add up and suit the compensation value needed as close as possible because there was no capacitor with exactly value of 4.22 μF and 1.98 μF in market.

$$X_L = 2\pi fL$$

$$L = X_L / (2\pi f) \quad (3.1)$$

$$X_L = X_C$$

$$2\pi fL = 1 / (2\pi fC)$$

$$C = 1 / ((L) (2\pi f)^2) \quad (3.2)$$

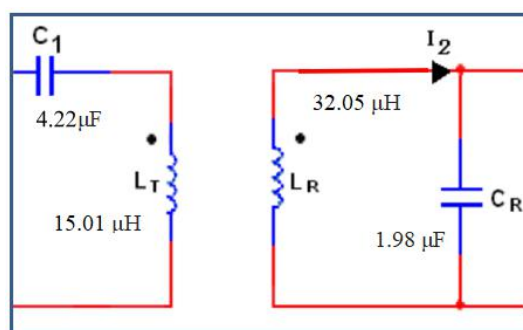


Figure 3.2.1.6 Illustration of SP Topology with Calculated Value of Resonance Capacitance and Inductance in 20 kHz



Figure 3.2.1.7 Verifying Inductance Value with LCR Meter

After the compensation circuit at receiver side, the AC current and voltage would pass through the full-bridge converter and smoothen by 2.2 μF capacitor producing 12 VDC. Then the DC buck-boost converter was used to step up the DC voltage from 12 VDC to around 15 VDC. This is to ensure the high charging rate of battery. However, more charging voltage may have drawbacks too, excessive charging voltage such as more than 24 VDC may damage the 12V DC battery. After that, the battery charging controller was connected between the output of DC buck-boost converter and 12V DC battery to trigger or cut off the charging of battery with a DC voltage range set by the controller. In this project, the capacity of 12V DC battery is 1.2 Ah (GPP 1212) for prototype experiment purpose only.

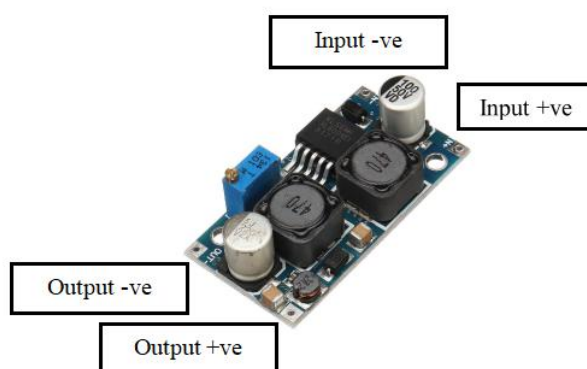


Figure 3.2.1.8 DC Buck-Boost Converter

(Input: 5-30V, Output: 1.5-35V, Max Current: 4A)

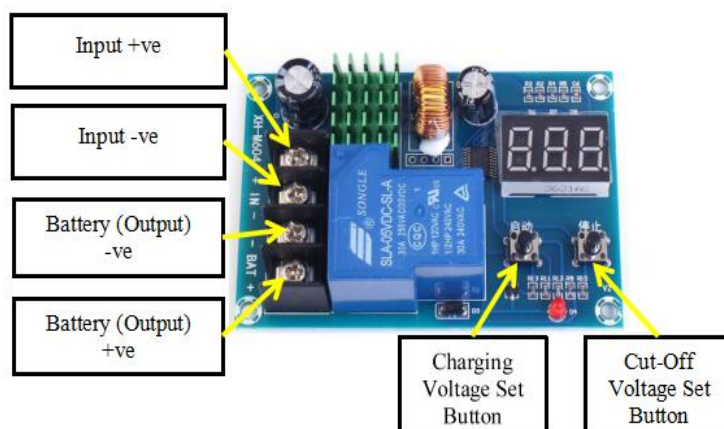


Figure 3.2.1.9 DC Battery Charging Controller (6-60 VDC)



Figure 3.2.1.10 DC 12V, 1.2Ah Battery (GPP1212)

Last but not least, the conducting wire used was 2.5mm copper cable. Based on Table 3.2.1.1, the maximum current capacity of 2.5mm copper cable is around 27A.

Conductor CSA	Reference Method A (enclosed in conduit in thermally insulating wall etc)		Reference Method B (enclosed in conduit on a wall or in trunking etc)		Reference Method C (clipped direct)		Reference method F (in free air or on a perforated cable tray horizontal or vertical)					
	Touching		Spaced by one diameter		Touching		Touching		Spaced by one diameter		Horizontal	Vertical
	2 cables, 1ph ac or dc	3 or 4 cables, 3ph ac	2 cables, 1ph ac or dc	3 or 4 cables, 3ph ac	2 cables, 1ph ac or dc	3 or 4 cables, 3ph ac	2 cables, 1ph ac or dc flat	3 cables, 3ph ac flat	3 cables, 3ph ac trefoil			
1mm ²	11	10.5	13.5	12	15.5	14						
1.5mm ²	14.5	13.5	17.5	15.5	20	18						
2.5mm ²	20	18	24	21	27	25						
4mm ²	26	24	32	28	37	33						
6mm ²	34	31	41	36	47	43						
10mm ²	46	42	57	50	65	59						
16mm ²	61	56	76	68	87	79						
25mm ²	80	73	101	89	114	104	131	114	110	146	130	
35mm ²	99	89	125	110	141	129	162	143	137	181	162	

Table 3.2.1.1 Current Carrying Capacity of Copper Cable

3.2.2 Mechanical Aligner Design

There were three parameters to be study in this aligner which were distance, d , lateral misalignment, L , and tilting angle difference, θ between transmitter and receiver pad. There were two aligners in this project consisting transmitter aligner and receiver aligner. The transmitter aligner was mainly used for minimizing the lateral misalignment, L and distance, d between transmitter and receiver pad. On the other hand, the receiver aligner was used to minimize the tilting angle difference, θ between the transmitter and receiver pad.

3.2.2.1 Transmitter Side

In general, the function of transmitter aligner was to adjust its alignment to fit the receiver pad in terms of distance (d) and the lateral distance (L) between the receiver and transmitter.

Based on Figure 3.2.2.1.2, the transmitter aligner has 4 levels consisting level 1, level 2, level 3, and top level. Basically, level 1 consisted only a servo motor (MG995) as the foundation to rotate the whole aligner 360 degrees continuously shown in Figure 3.2.2.1.5. For level 2, it consisted a servo motor and a infrared sensor, the servo motor moved continuously in the direction shown in Figure 3.2.2.1.6, the infrared sensor was used to stop the servo motor when moving back to default position. With the combination of movement of servo motors at level 1 and level 2, it produced a horizontal spiral movement shown in Figure 3.2.2.1.7 to reduce the lateral misalignment, L to approximately zero between the center of transmitter and receiver pad by using the infrared sensor at top level shown in Figure 3.2.2.1.1. The concept behind was the infrared sensor will trigger signal when its receiver sensed the wave refracted form its emitter, it will not refract any wave if it encountered the black surface. The illustration of infrared sensor behaviour is shown in Figure 3.2.2.1.8.

Next, level 3 was basically dealing with the distance adjustment, d between the transmitter and receiver pad. The mechanical technique used was the scissor lift method to lift up the transmitter pad vertically. It consisted only a servo motor and a ultrasonic sensor. The servo motor will rotate 180

clockwise and anti-clockwise repeatedly to lift up or lower down the transmitter pad and finally stop when the ultrasonic sensor at the top level shown in Figure 3.2.2.1.1 reads the desire distance between transmitter and receiver pad. The movement of mechanical parts in level 3 and behaviour of ultrasonic sensor are shown below.

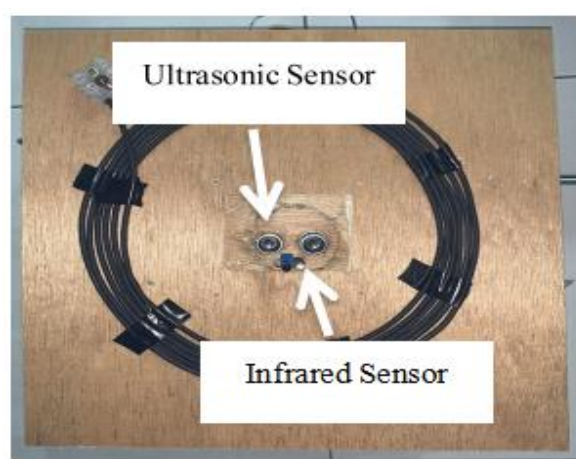


Figure 3.2.2.1.1 Transmitter Aligner (Top Level, Top View)



Figure 3.2.2.1.2 Transmitter Aligner (Front View)

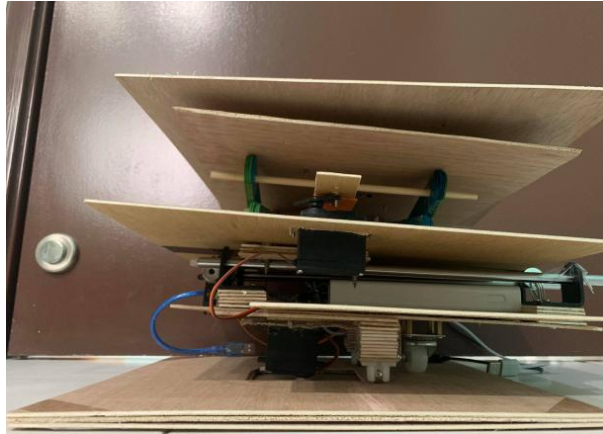


Figure 3.2.2.1.3 Transmitter Aligner (Side View)

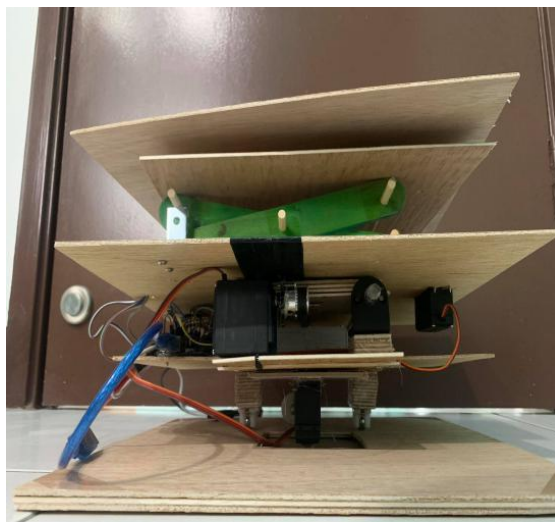


Figure 3.2.2.1.4 Transmitter Aligner (Rear View)

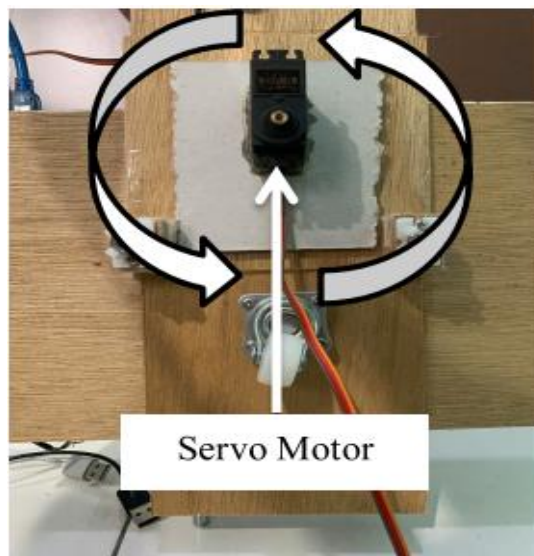


Figure 3.2.2.1.5 Transmitter Aligner (Level 1, Bottom View)

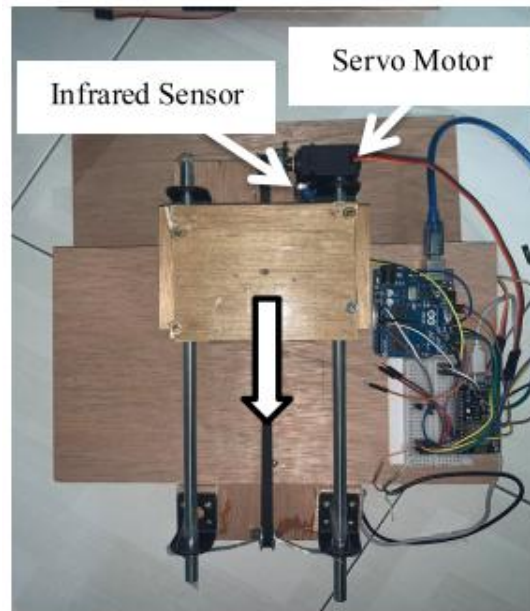


Figure 3.2.2.1.6 Transmitter Aligner (Level 2, Top View)



Figure 3.2.2.1.7 Combination of Movement of Servo Motor (level 1) and Servo Motor (level 2) (Top View)

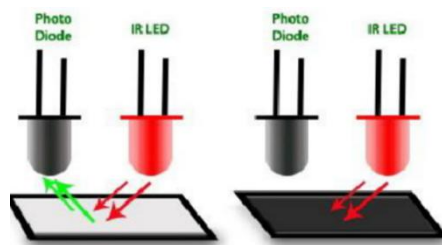


Figure 3.2.2.1.8 Illustration of Infrared Sensor Behaviour when Encounter White and Black Surface

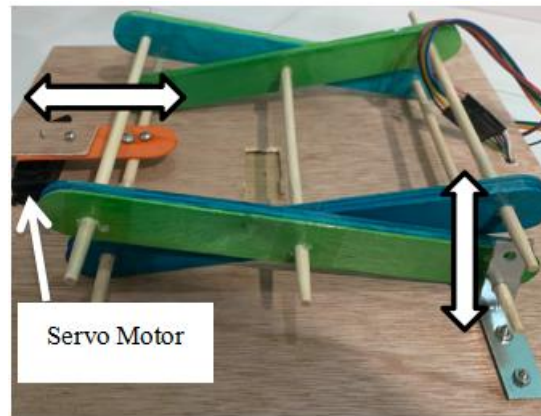


Figure 3.2.2.1.9 Transmitter pad (Level 3, Side View)

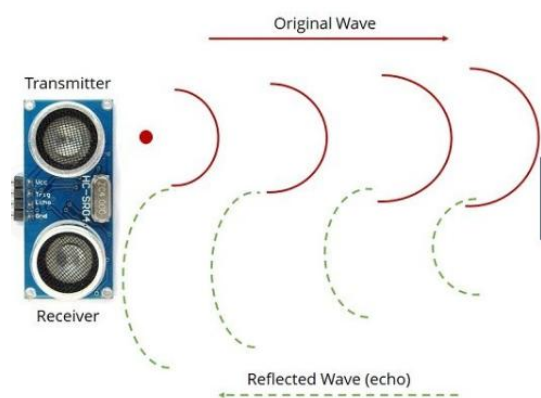


Figure 3.2.2.1.10 Behaviour of Ultrasonic Sensor

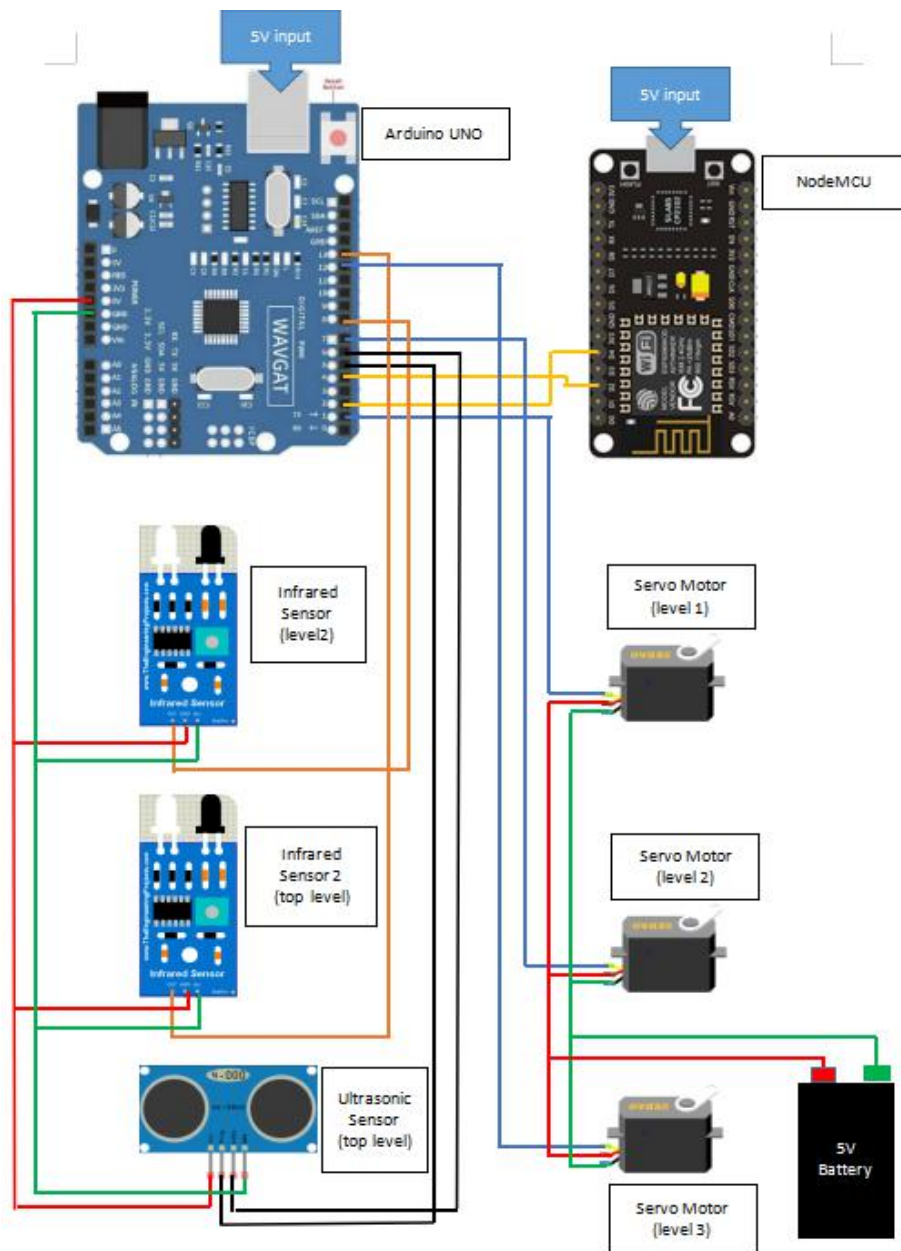


Figure 3.2.2.1.11 Circuit Diagram of Transmitter Aligner

3.2.2.2 Receiver Side

In general, receiver aligner was used to minimize the tilting angle difference, θ between transmitter and receiver pad. In this case, there were only two level which were level 1 and level 2. In addition, the receiver aligner was placed upside down to demonstrate the real situation for wireless charging of electric vehicle.

In level 1, it consisted only a servo motor which turned 180 degrees clockwise and then anti-clockwise repeatedly. In level 2, it consisted a servo motor too which turned 50 degrees (maximum) clockwise and then anti-clockwise repeatedly. These two servo motors will stop moving when the three ultrasonic sensors at the top level having a exactly same distance value (tilting angle difference between receiver and transmitter approximate equal to zero).

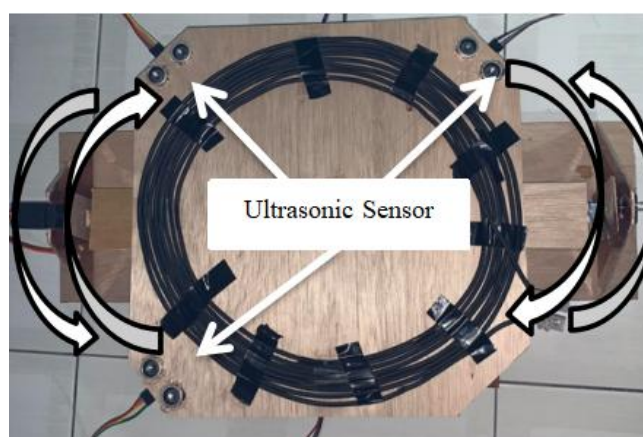


Figure 3.2.2.2.1 Receiver Aligner (Top View)

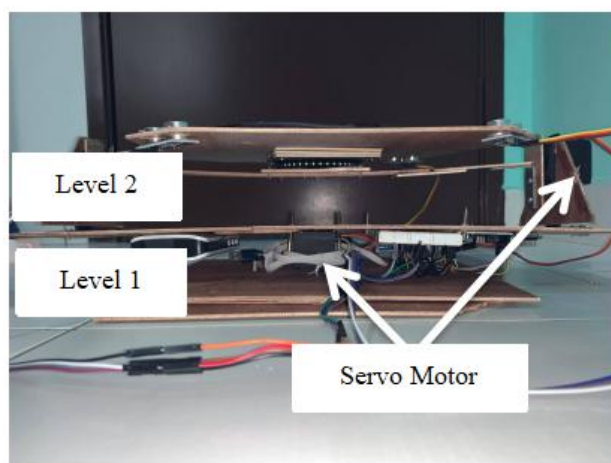


Figure 3.2.2.2.2 Receiver Aligner (Front View)

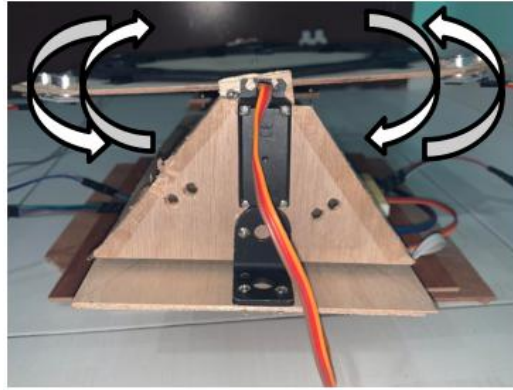


Figure 3.2.2.2.3 Receiver Aligner (Side View)

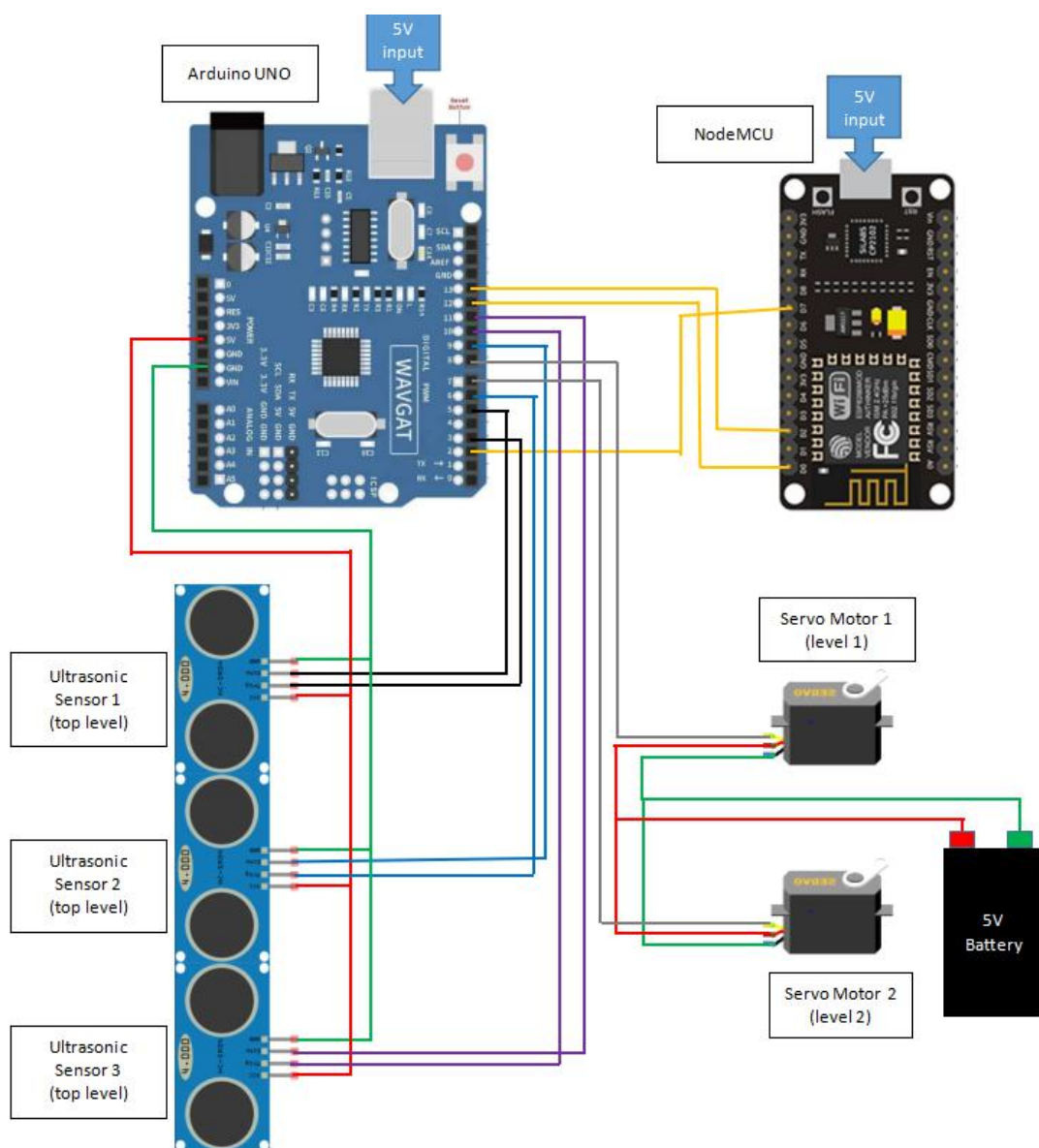


Figure 3.2.2.2.4 Circuit Diagram of Receiver Aligner

3.2.2.3 Internet of Things (IoT)

Nowadays, Internet of Thing (IOT) was widely used around the world especially industry field. Form the word itself, it means almost all electronic and electrical devices able to connect with each other to transfer data, monitoring data etc.

In this project, IoT plays an important role where it allowed the transmitter and receiver aligner able to “communicate” with the users. In detailed explanation, the user only need download the mobile apps called “Blynk”, what “Blynk” did was it can either turn the auto-alignment system on or off. The communication between the “Blynk” apps and the aligners were done through Wi-Fi, the NodeMCU contain the Wi-Fi module to communicate with “Blynk” in mobile apps. The user manual or the program flow was presented in the flowchart below.

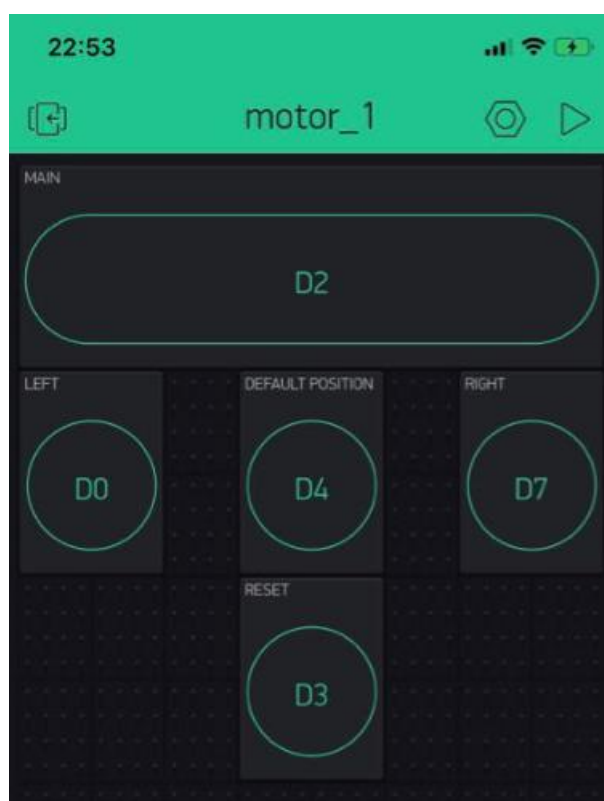


Figure 3.2.2.3.1 Layout of “Blynk” Mobile Application

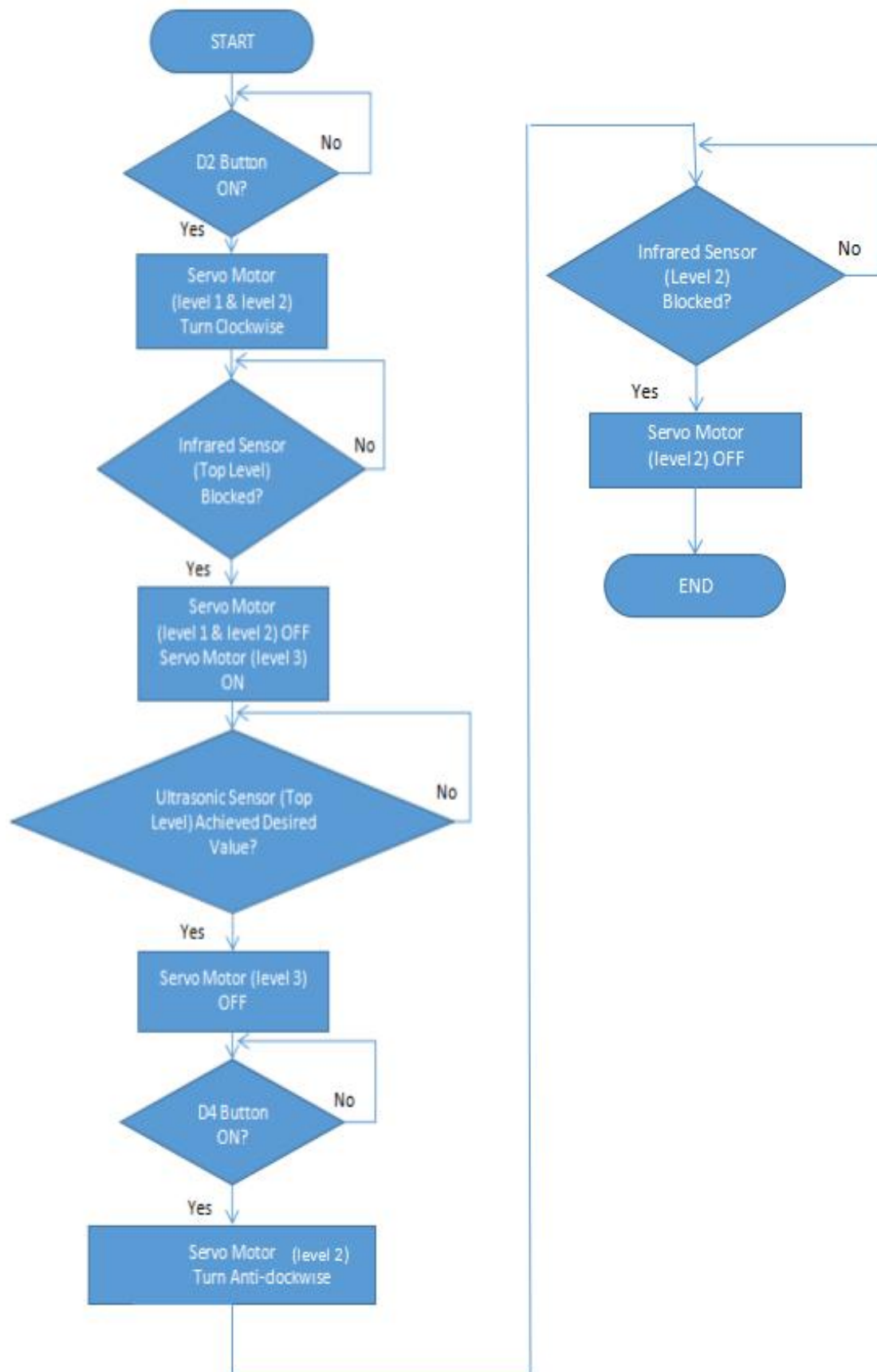


Figure 3.2.2.3.2 Flow Chart for Program Flow (Transmitter Aligner)

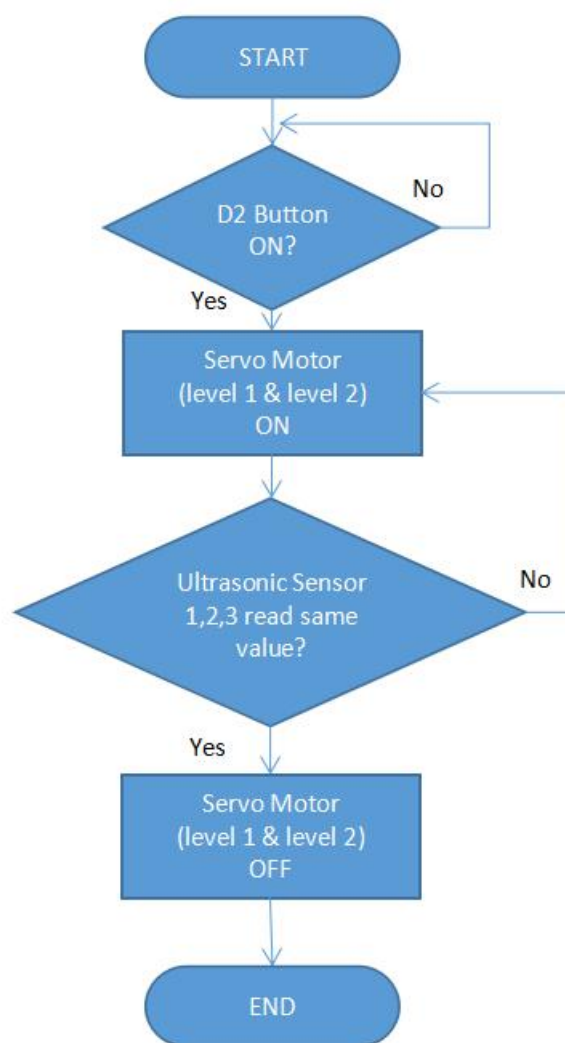


Figure 3.2.2.3.3 Flow Chart for Program Flow (Receiver Aligner)

In addition, there were some extra inputs button which were D0, D3, and D7. Button D0 and D7 were for backup purpose in case the receiver aligner took so much time to reach optimum tilting angle difference, they were push button to manually adjust the turning angle of the servo motor (level 2) in receiver aligner (D0 for clockwise; D7 for anti-clockwise). Besides, Button D3 was for resetting all the servo motor in transmitter aligner into default position.

3.3 Hardware Requirements, Costs, and Work Schedule

System	Component	Specification	Unit	Cost per Unit (RM)	Total Cost (RM)
Electrical	Center-Tapped Transformer	240V to 12-0-12V, 4A	1	90.00	90.00
	Bridge Rectifier	1000V, 10A	2	1.90	3.80
	Inverter Module Board	1000W, 20kHz	1	110.00	110.00
	Power Resistor	1ohm, 100W	6	4.00	24.00
	Monolithic Ceramic Capacitor	1 μ F, 50V	1 pack (100 pieces)	6.00	6.00
	Copper PVC Cable	2.5mm	1 roll (80m)	36.50	36.50
	DC Buck-boost Converter	3.8V-32V to 1.25V-35V, 3A	1	3.80	3.80
	Battery Charger Controller	6-60V	1	22.80	22.80
	Lead Acid Battery	12V, 1.2Ah	1	44.00	44.00
Total					340.90
Aligner (Transmitter)	Arduino UNO	5V	1	24.50	24.50
	NodeMCU	5V	1	19.00	19.00
	Infrared Sensor	3.3V	2	9.00	18.00
	Ultrasonic Sensor	3.3V	1	3.90	3.90
	Servo Motor (MG995)	5V	3	11.50	34.50
	Plywood	30cm x 30cm, 3mm	10	1.90	19.00
	L-Shape Bracket	25mmx25mmx25mm	4	1.00	4.00
	Stainless Steel Rod	8mm diameter, L=300mm	2	16.00	32.00
	Caster Wheel	50mmx50mm	3	4.50	13.50
Total					168.40

Mechanical (Receiver)	Arduino UNO	5V	1	24.50	24.50
	NodeMCU	5V	1	19.00	19.00
	Ultrasonic Sensor	3.3V	3	3.90	11.70
	Servo Motor (MG995)	5V	2	11.50	23.00
	Plywood	30cm x 30cm, 3mm	10	1.90	19.00
	L-Shape Bracket	25mmx25mmx25mm	2	1.00	2.00
				Total	99.20
				GRAND TOTAL	608.50

Table 3.3.1 Cost of Hardware for Project

No	Project Activities	W 1	W 2	W 3	W 4	W 5	W 6	W 7	W 8	W 9	W 10	W 11	W 12	W 13	W 14
1	Project Planning, Budgeting	■													
2	Acquiring Material		■	■	■										
3	Electrical Circuit Design and Optimization					■	■	■	■	■	■				
4	Mechanical Aligner Design and Optimization							■	■	■	■	■	■		
5	Overall System Testing and Collect Data												■	■	■
6	Report Writing												■	■	■

Table 3.3.2 Gantt Chart of Project Work Schedule

3.4 Summary

The compensation circuit, coil design, and alignment are the main concerns in this project. The capacitor value for compensation circuit can be calculated using resonance equation where $X_L = X_C$. The inductance value of coil can be obtained using manual calculation shown above and verified by LCR meter.

For the coil design, the circular spiral flat coil is chosen because it can distribute the magnetic field evenly. The effects of inner diameter, outer diameter, core diameter, distance between neighbour core, and turns of coil towards power efficiency of wireless power transfer will be discussed in the

discussion part. The parameter for compensation circuit will be changed also depending to the coil design.

Last but not least, the alignment of the transmitter and receiver pad can be done automatically using knowledge from IoT so user no need to park or align their vehicle manually to achieve optimum alignment between transmitter and receiver pad.

CHAPTER 4

RESULTS AND DISCUSSION

4.1 Introduction

This section will study on the behaviour of power efficiency between the transmitter coil and receiver coil against the distance, d , lateral misalignment, L , and tilting angle difference, θ . The compensation circuit and coil design to achieve maximum current will be investigated also and verified using LCR meter and manual calculation. Besides, the charging behaviour of battery will be discussed also.

4.2 Results

4.2.1 Effect of Coil Distance, Lateral Misalignment, and Angle Difference (Experimental)

The parameter of coils are set to $N=11$, fixed outer radius = 150mm, inner radius = 122.5mm, adjacent core distance = 0mm, core diameter = 2.5mm. This parameter was selected because this coil design delivered maximum power efficiency more than 80%.

Distance, d (mm)	Transmitter Current (A)	Transmitter Voltage (V)	Transmitter Power (W)	Receiver Current (A)	Receiver Voltage (V)	Receiver Power (W)	Power Efficiency (%)
3	2.30	24.00	55.20	2.00	23.12	46.24	83.76
10	2.30	24.00	55.20	1.90	21.48	40.81	73.94
20	2.30	24.00	55.20	1.90	20.46	38.87	70.42
30	2.30	24.00	55.20	1.80	19.44	34.99	63.38
40	2.30	24.00	55.20	1.70	17.39	29.56	53.55
50	2.30	24.00	55.20	1.50	15.14	22.71	41.14
60	2.30	24.00	55.20	1.30	13.09	17.02	30.83

70	2.30	24.00	55.20	1.00	10.23	10.23	18.53
80	2.30	24.00	55.20	0.50	6.74	3.37	6.11
90	2.30	24.00	55.20	0.30	6.13	1.84	3.33
100	2.30	24.00	55.20	0.10	4.10	0.41	0.74

Table 4.2.1.1 Results of Power Efficiency against Distance between
Transmitter Coil and Receiver Coil

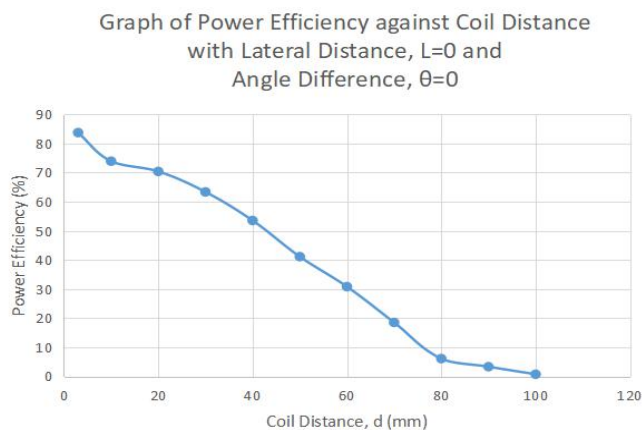


Figure 4.2.1.1 Graph of Power Efficiency against Coil Distance between
Transmitter Coil and Receiver Coil

Lateral Distance, L(mm)	Transmitter Current (A)	Transmitter Voltage (V)	Transmitter Power (W)	Receiver Current (A)	Receiver Voltage (V)	Receiver Power (W)	Power Efficiency (%)
0	2.30	24.00	55.20	2.10	22.91	48.12	87.17
10	2.30	24.00	55.20	2.10	22.91	48.12	87.17
20	2.30	24.00	55.20	2.10	22.91	48.12	87.17
30	2.30	24.00	55.20	2.10	22.91	48.12	87.17
40	2.30	24.00	55.20	2.10	22.91	48.12	87.17
50	2.30	24.00	55.20	2.00	22.10	44.19	80.05
60	2.30	24.00	55.20	1.90	20.87	39.65	71.83
70	2.30	24.00	55.20	1.80	19.03	34.25	62.04
80	2.30	24.00	55.20	1.70	17.39	29.56	53.55
90	2.30	24.00	55.20	1.60	15.55	24.88	45.07
100	2.30	24.00	55.20	1.30	12.48	16.23	29.39
110	2.30	24.00	55.20	0.60	7.37	4.42	8.00

120	2.30	24.00	55.20	0.30	5.10	1.53	2.77
130	2.30	24.00	55.20	0.10	3.50	0.35	0.63
140	2.30	24.00	55.20	0.05	2.20	0.11	0.20
150	2.30	24.00	55.20	0.01	1.00	0.01	0.02

Table 4.2.1.2 Results of Power Efficiency against Lateral Misalignment
between Transmitter Coil and Receiver Coil

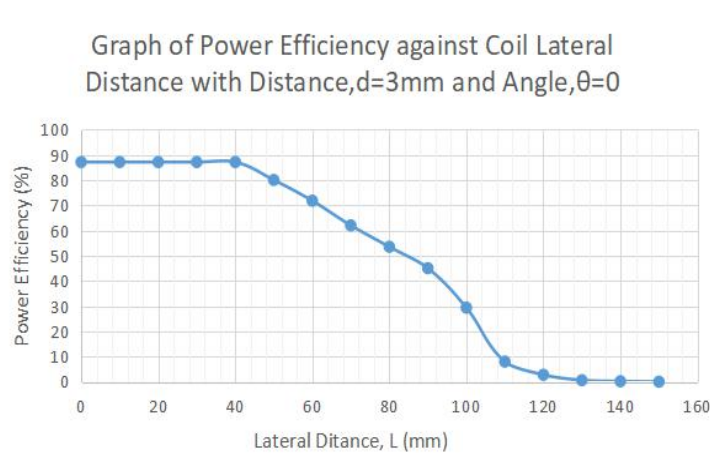


Figure 4.2.1.2 Graph of Power Efficiency against Lateral Misalignment
between Transmitter Coil and Receiver Coil

Tilting Angle, θ	Transmitter Current (A)	Transmitter Voltage (V)	Transmitter Power (W)	Receiver Current (A)	Receiver Voltage (V)	Receiver Power (W)	Power Efficiency (%)
0	2.30	24.00	55.20	2.00	22.92	45.83	83.02
10	2.30	24.00	55.20	1.90	19.64	37.32	67.60
20	2.30	24.00	55.20	1.50	14.11	21.17	38.36
30	2.30	24.00	55.20	1.10	12.27	13.50	24.46
40	2.30	24.00	55.20	0.20	4.50	0.90	1.63
50	2.30	24.00	55.20	0.10	3.90	0.39	0.70
60	2.30	24.00	55.20	0.06	2.17	0.13	0.24
70	2.30	24.00	55.20	0.04	1.50	0.06	0.11
80	2.30	24.00	55.20	0.03	1.00	0.03	0.05
90	2.30	24.00	55.20	0.01	0.60	0.006	0.01

Table 4.2.1.3 Results of Power Efficiency against Tilting Angle Difference
between Transmitter Coil and Receiver Coil

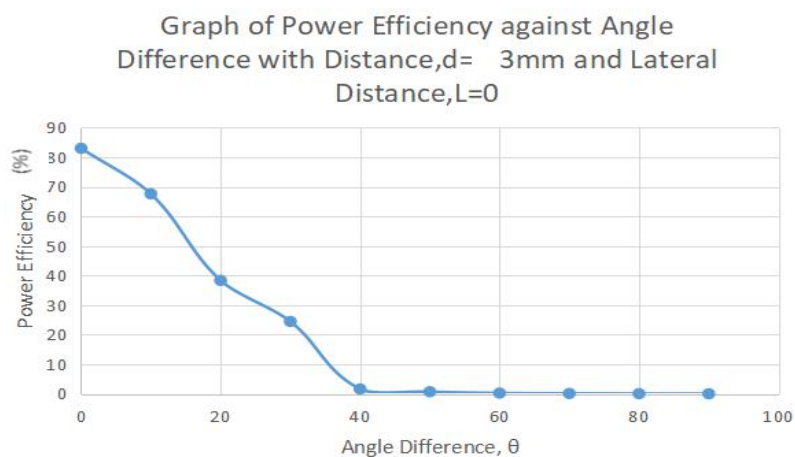


Figure 4.2.1.3 Graph of Power Efficiency against Tilting Angle Difference between Transmitter Coil and Receiver Coil

4.2.2 Effect of Coil Turns and Inner Radius (Experimental)

The parameter of coils were remained constant with outer radius, $r = 150\text{mm}$; adjacent core distance = 0mm . The manipulated variable was the coil turns and the inner radius changed from 5 turns to 14 turns and 137.5mm to 115.0mm respectively.

Coil Turns (N)	Outer Radius (mm)	Inner Radius (mm)	Calculated Self-Inductance (μH)	Measured Self-Inductance (μH)	Compensate Capacitance Based on Measured Self-Inductance (μF)
5	150	137.5	15.80	10.89	5.82
6	150	135.0	22.05	17.20	3.68
7	150	132.5	29.10	24.35	2.18
8	150	130.0	36.86	32.05	1.98
9	150	127.5	45.22	40.43	1.57
10	150	125.0	54.13	49.45	1.28
11	150	122.5	63.51	58.66	1.08
12	150	120.0	73.28	68.49	0.92
13	150	117.5	83.38	78.60	0.81
14	150	115.0	93.75	88.90	0.71

Table 4.2.2.1 Compensation Capacitance needed for Different Number of Coil Turns with Fixed Outer Radius

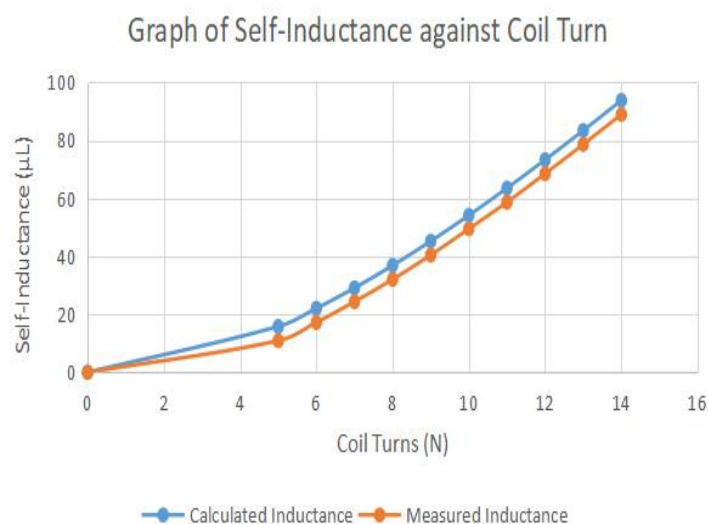


Figure 4.2.2.1 Graph of Self-Inductance against Coil Turns with Fixed Outer Radius

Coil Turns	Transmitter Current (A)	Transmitter Voltage (V)	Transmitter Power (W)	Receiver Current (A)	Receiver Voltage (V)	Receiver Power (W)	Power Efficiency (%)
5	2.71	16.80	45.53	2.41	11.43	27.55	60.52
6	2.70	18.60	50.22	2.40	13.51	32.43	64.57
7	2.65	19.40	51.41	2.35	15.69	36.88	71.74
8	2.60	20.30	52.78	2.30	17.09	39.30	74.46
9	2.55	21.30	54.32	2.25	19.29	43.40	79.90
10	2.40	22.50	54.00	2.10	21.20	44.52	82.45
11	2.30	24.00	55.20	2.00	23.12	46.24	83.76
12	2.25	24.40	54.90	1.64	24.81	40.57	73.90
13	2.15	25.60	55.04	1.33	25.78	34.28	62.28
14	2.10	27.80	58.38	1.11	26.86	29.72	50.90

Table 4.2.2.2 Power Efficiency against Coil Turns with Fixed Outer Radius

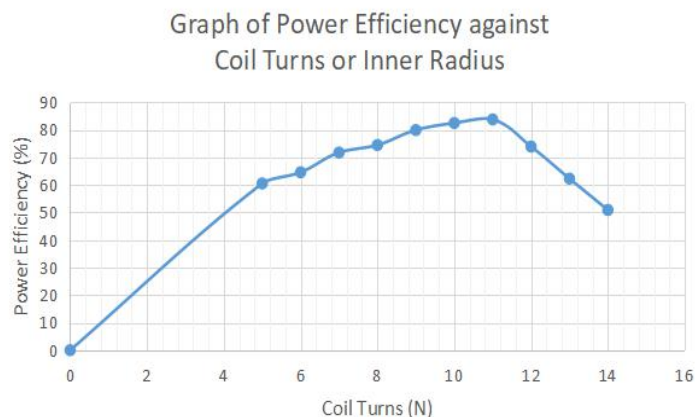


Figure 4.2.2.2 Graph of Power Efficiency against Coil Turns with Fixed Outer Radius

4.2.3 Effect of Coil Turns and Outer Radius (Experimental)

The parameter of coils were remained constant with inner radius, $r = 62.5\text{mm}$; adjacent core distance = 0mm . The manipulated variable was the coil turns and the outer radius changed from 5 turns to 14 turns and 75mm to 97.5mm respectively.

Coil Turns (N)	Outer Radius (mm)	Inner Radius (mm)	Calculated Self-Inductance (μH)	Measured Self-Inductance (μH)	Compensate Capacitance Based on Measured Self-Inductance (μF)
5	75.0	62.5	6.77	5.25	12.06
6	77.5	62.5	9.58	8.09	7.83
7	80.0	62.5	12.84	11.30	5.60
8	82.5	62.5	16.56	15.01	4.22
9	85.0	62.5	20.71	19.20	3.30
10	87.5	62.5	25.31	23.80	2.66
11	90.0	62.5	30.35	28.12	2.25
12	92.5	62.5	35.84	34.23	1.85
13	95.0	62.5	41.78	40.63	1.56
14	97.5	62.5	48.18	46.70	1.36

Table 4.2.3.1 Compensation Capacitance needed for Different Number of Coil Turns with Fixed Inner Radius

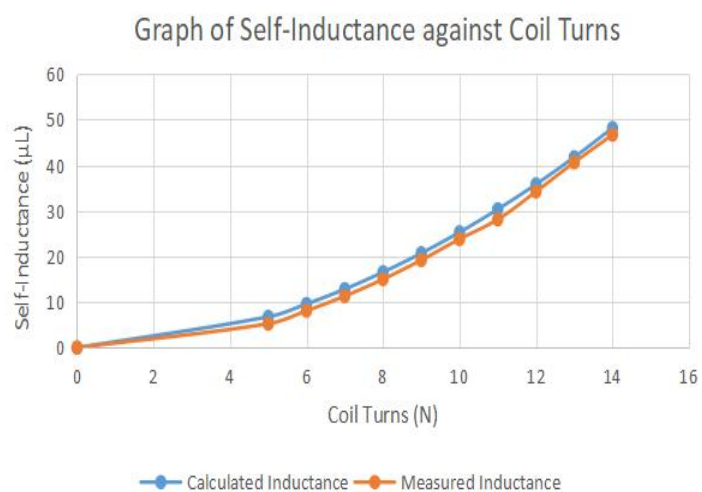


Figure 4.2.3.1 Graph of Self-Inductance against Coil Turns with Fixed Inner Radius

Coil Turns	Transmitter Current (A)	Transmitter Voltage (V)	Transmitter Power (W)	Receiver Current (A)	Receiver Voltage (V)	Receiver Power (W)	Power Efficiency (%)
5	2.57	15.63	40.17	2.23	12.51	27.98	69.67
6	2.45	17.42	42.70	2.13	14.46	30.83	72.21
7	2.31	19.13	44.20	2.00	17.20	34.58	78.25
8	2.25	20.00	45.00	1.95	18.74	36.68	81.52
9	1.99	20.13	39.97	1.57	18.86	29.53	73.90
10	1.65	21.45	35.34	1.10	20.10	22.00	62.28
11	1.32	24.95	32.90	0.72	23.38	16.74	50.90
12	0.94	27.45	25.76	0.46	25.72	11.76	45.67
13	0.85	28.20	23.90	0.38	26.42	10.06	42.10
14	0.62	30.83	19.20	0.26	28.89	7.44	38.78

Table 4.2.3.2 Power Efficiency against Coil Turns with Fixed Inner Radius

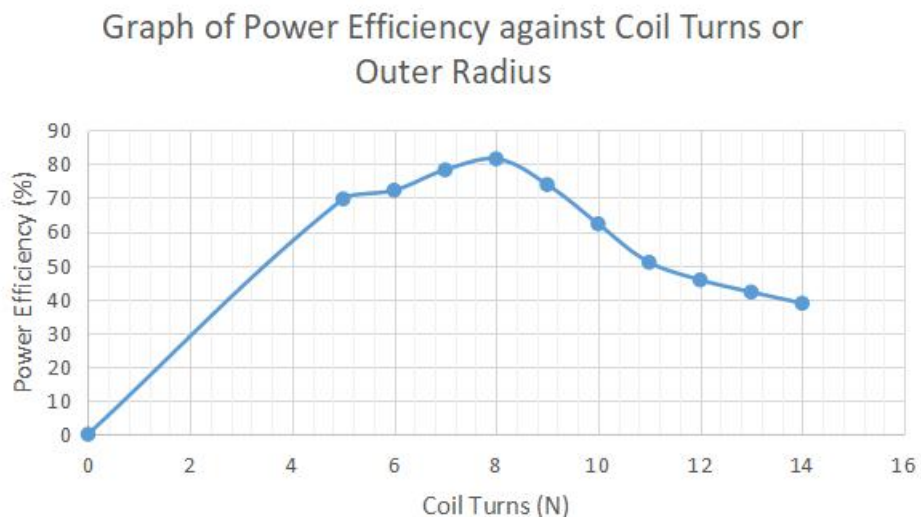


Figure 4.2.3.2 Graph of Power Efficiency against Coil Turns with Fixed Inner Radius

4.2.4 Battery Charging Behaviour (Experimental)

Time Taken (hour)	Manual Alignment (optimum)		Auto Alignment	
	Battery Voltage (V)	Charging Current (A)	Battery Voltage (V)	Charging Current (A)
1	10.1	0.43	8.5	0.36
2	11.2	0.43	9.3	0.36
3	12.1	0.43	10.5	0.36
4	12.1	0.30	11.3	0.36
5	12.1	0.21	12.1	0.36
6	12.1	0.14	12.1	0.22
7	12.1	0.13	12.1	0.15
8	12.4	0.12	12.1	0.12
9	12.6	0.10	12.1	0.11

Table 4.2.4.1 Charging Current and Voltage of Battery (1.2Ah, 12V Lead Acid DEAD Battery with Initial Voltage 3.35V)

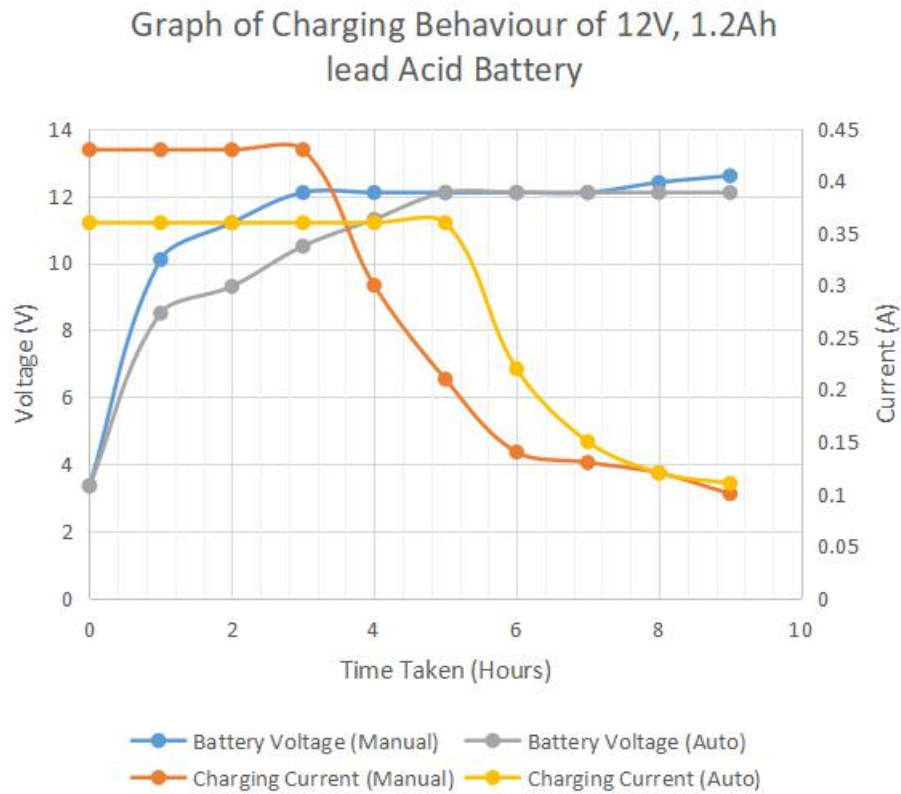


Figure 4.2.4.1 Graph of Charging Behaviour for Lead Acid Battery

4.2.5 Simulation using MATLAB (SIMULINK)

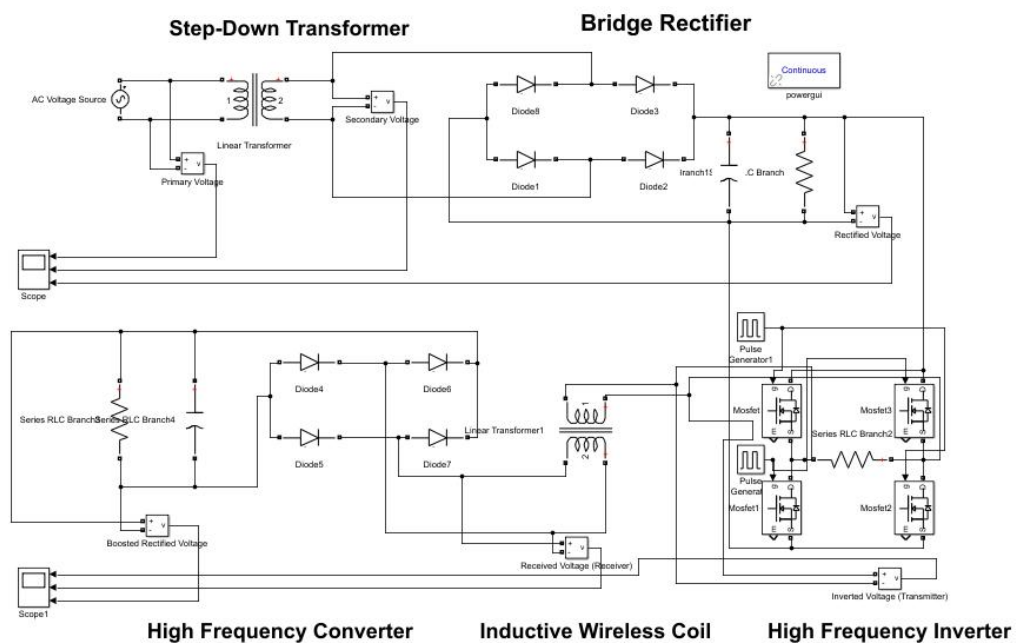


Figure 4.2.5.1 Simulation Circuit of Wireless Power Transfer Circuit
(SIMULINK)

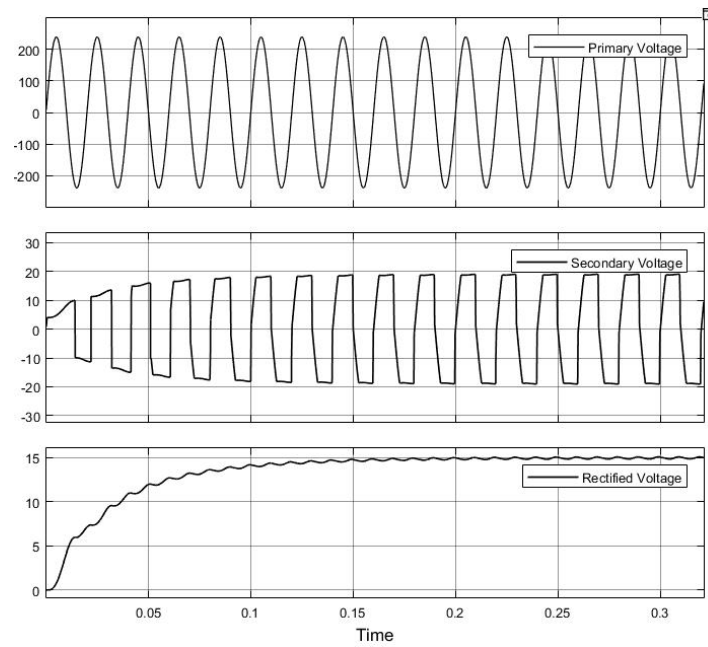


Figure 4.2.5.2 Simulation Results at Step Down Transformer (1)Primary Voltage, (2)Secondary Voltage, (3)Rectified Voltage

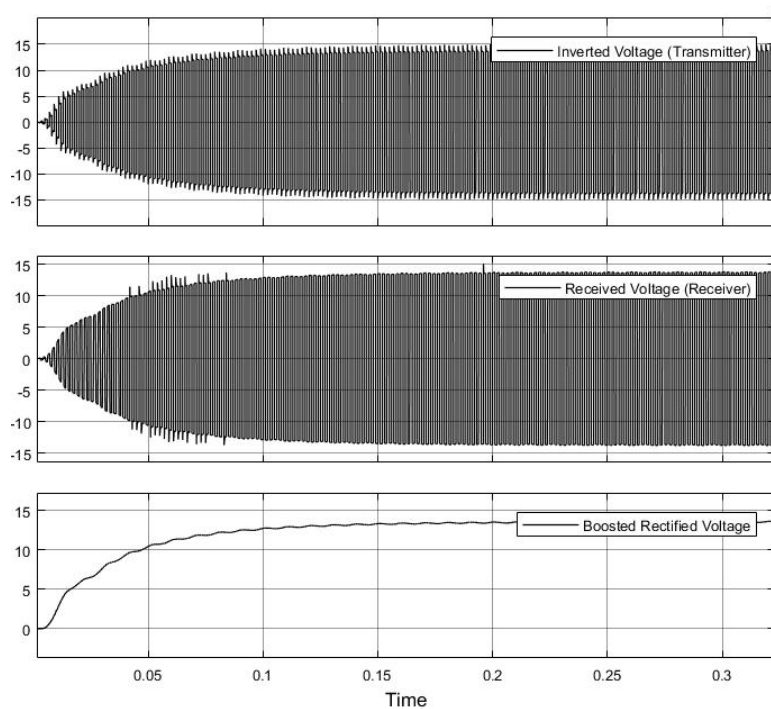


Figure 4.2.5.3 Simulation Results of (4)High Frequency Inverted Voltage (Transmitter), (5)Received Voltage (Receiver), (6)Rectified Voltage

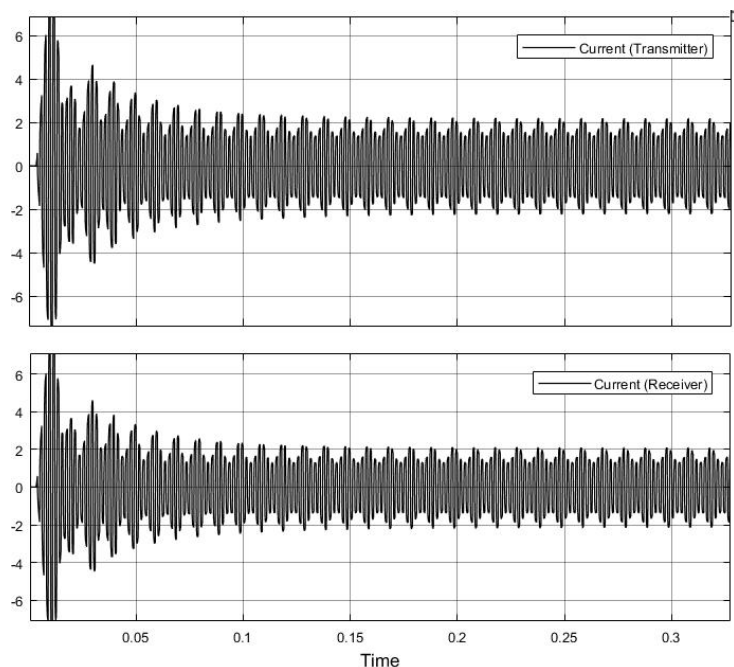


Figure 4.2.5.4 Simulation Results of (7)Transmitter Current, (8)Receiver Current

4.2.6 Simulation using Ansys Maxwell

Coil Turns (N)	Outer Radius (mm)	Inner Radius (mm)	Simulated Self-Inductance (μH)
5	150	137.5	12.63
6	150	135.0	17.14
7	150	132.5	22.14
8	150	130.0	27.65
9	150	127.5	33.49
10	150	125.0	39.66
11	150	122.5	46.16
12	150	120.0	52.99
13	150	117.5	60.15
14	150	115.0	67.64

Table 4.2.6.1 Simulation of Self-inductance against Coil Turns with Fixed Outer Radius

Coil Turns (N)	Outer Radius (mm)	Inner Radius (mm)	Simulated Self-Inductance (μH)
5	75.0	62.5	5.92
6	77.5	62.5	8.32
7	80.0	62.5	10.75
8	82.5	62.5	13.39
9	85.0	62.5	16.29
10	87.5	62.5	19.29
11	90.0	62.5	22.61
12	92.5	62.5	25.71
13	95.0	62.5	28.86
14	97.5	62.5	32.23

Table 4.2.6.2 Simulation of Self-inductance against Coil Turns with Fixed Inner Radius

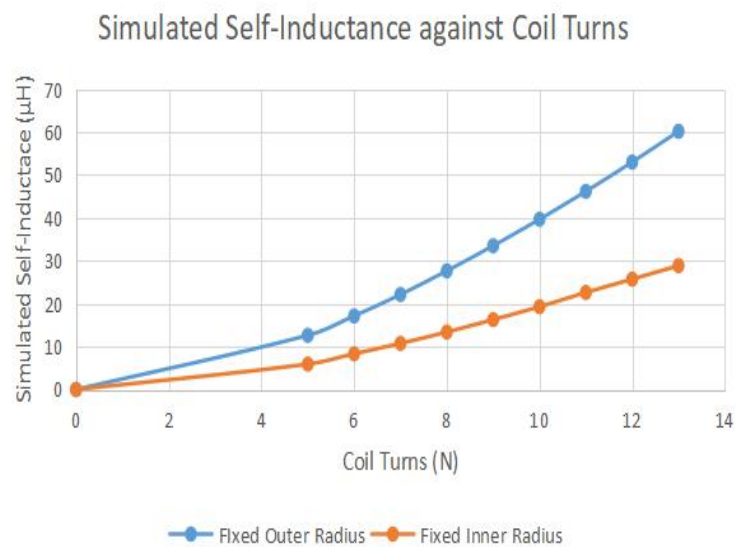


Figure 4.2.6.1 Simulated Self-Inductance against Coil Turns

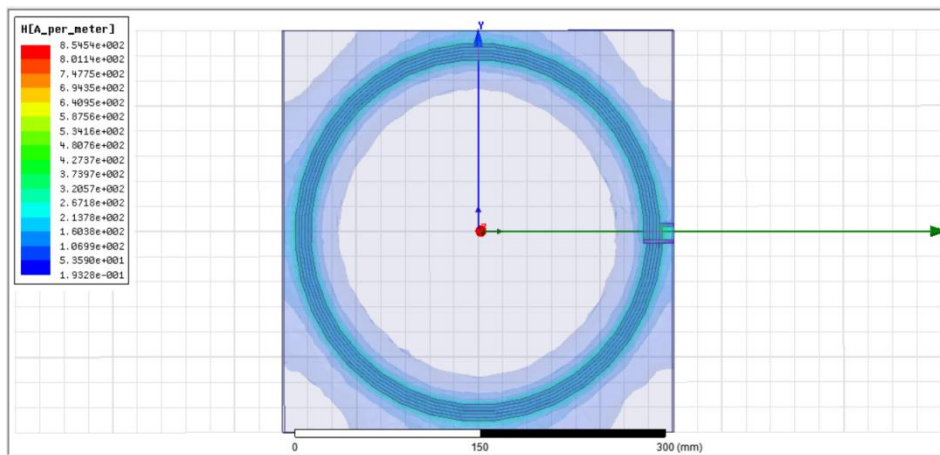


Figure 4.2.6.2 Magnetic Field Intensity of Coil
(N=5, Fixed Outer Radius=150mm)

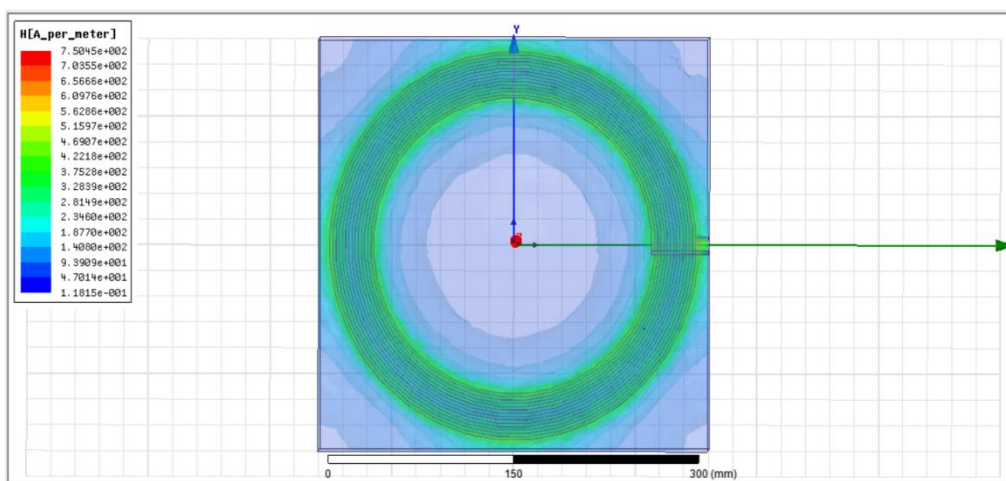


Figure 4.2.6.3 Magnetic Field Intensity of Coil
(N=14, Fixed Outer Radius=150mm)

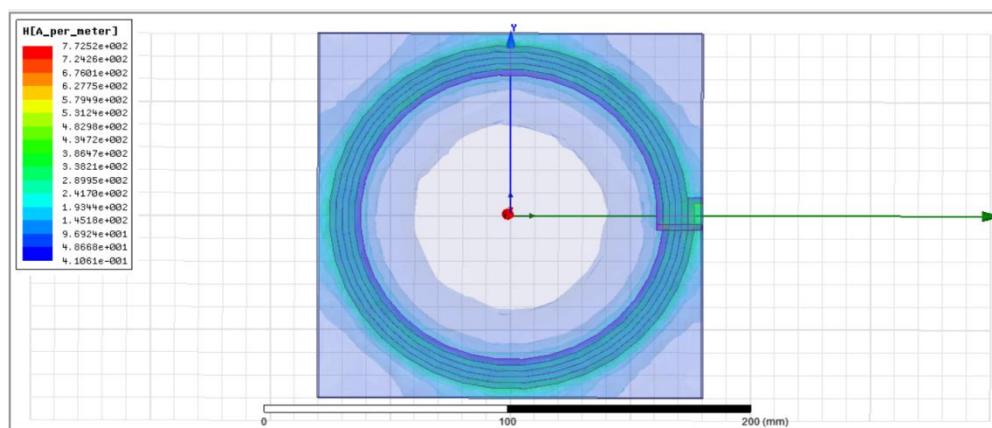


Figure 4.2.6.4 Magnetic Field Intensity of Coil
(N=5, Fixed Inner Radius=62.5mm)

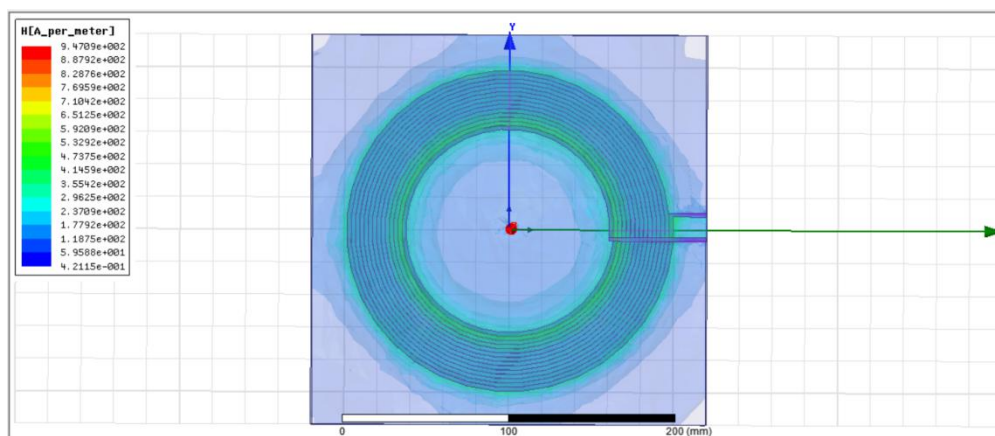


Figure 4.2.6.5 Magnetic Field Intensity of Coil
(N=14, Fixed Inner Radius=62.5mm)

Name	Value	Unit	Evaluated Value	Description
DLL Location	syslib			
DLL Version	1.0			
RectHeight	2.5	mm	2.5mm	Cross-section rectangle..
RectWidth	2.5	mm	2.5mm	Cross-section rectangle ..
StartHelixRadius	122.5	mm	122.5mm	Start radius from rectan...
RadiusChange	2.6	mm	2.6mm	Radius change per tum
Pitch	0	mm	0mm	Helix pitch
Tums	11		11	Number of turns
SegmentsPerT...	36		36	Number of segments p...
RightHanded	1		1	Helix direction, non-zer...

Figure 4.2.6.6 Setting of Coils in Simulation

Misalignment Coordinate of Receiver relative to Origin of Transmitter, d (mm)	Simulated Coupling Coefficient	Simulated Mutual Inductance (μH)
(0, 0, 10)	0.68	30.63
(0, 0, 20)	0.48	21.56
(0, 0, 30)	0.35	15.73
(0, 0, 40)	0.26	11.72
(0, 0, 50)	0.20	8.84
(0, 0, 60)	0.15	6.71

(0, 0, 70)	0.11	5.06
(0, 0, 80)	0.09	3.71
(0, 0, 90)	0.06	2.63
(0, 0, 100)	0.04	1.68

Table 4.2.6.3 Simulated Coupling Coefficient and Mutual Inductance against Misalignment Coordinate relative to Origin of Transmitter Coil (distance,d)

Misalignment Coordinate of Receiver relative to Origin of Transmitter, L (mm)	Simulated Coupling Coefficient	Simulated Mutual Inductance (μH)
(0, 0, 10)	0.68	30.63
(0, 10, 10)	0.65	29.21
(0, 20, 10)	0.60	28.93
(0, 30, 10)	0.52	25.16
(0, 40, 10)	0.45	21.55
(0, 50, 10)	0.38	18.43
(0, 60, 10)	0.33	15.77
(0, 70, 10)	0.28	13.49
(0, 80, 10)	0.24	11.51
(0, 90, 10)	0.20	9.77
(0, 100, 10)	0.17	8.22

Table 4.2.6.4 Simulated Coupling Coefficient and Mutual Inductance against Misalignment Coordinate relative to Origin of Transmitter Coil (lateral distance, L)

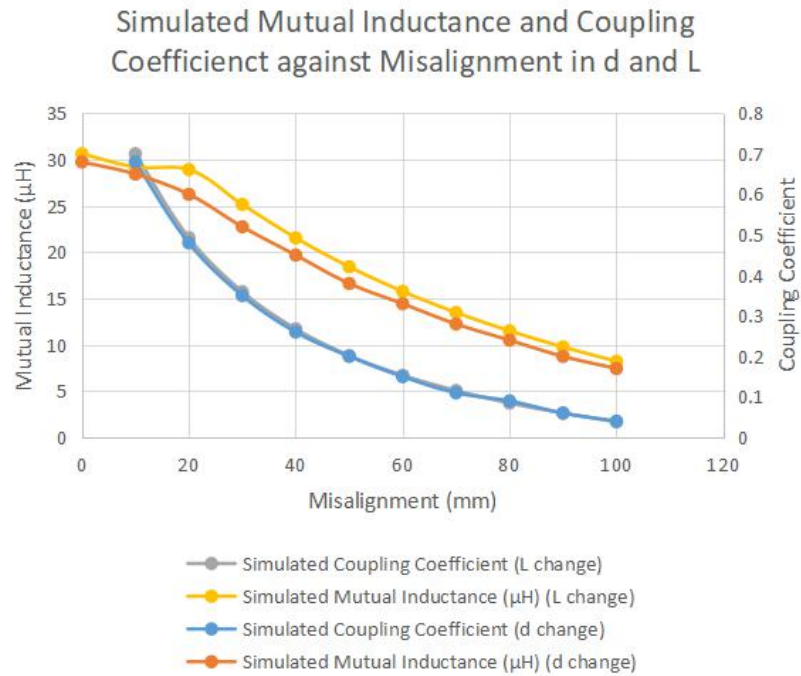


Figure 4.2.6.7 Simulated Mutual Inductance and Coupling Coefficient against Misalignment in Distance, d and Lateral Distance, L

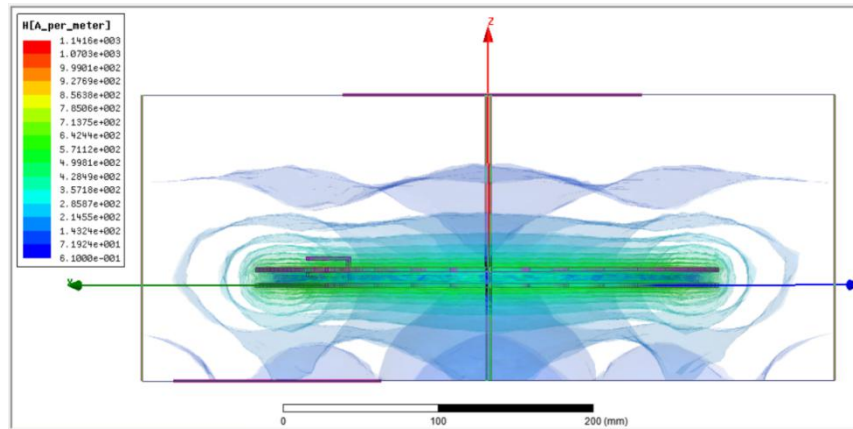


Figure 4.2.6.8 Magnetic Field Intensity of Coils with Misalignment Coordinate (0, 0, 10)

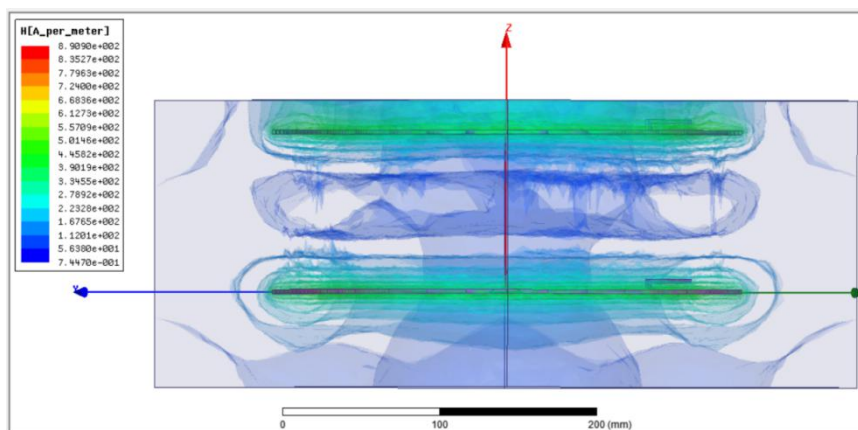


Figure 4.2.6.9 Magnetic Field Intensity of Coils with Misalignment
Coordinate (0, 0, 100)

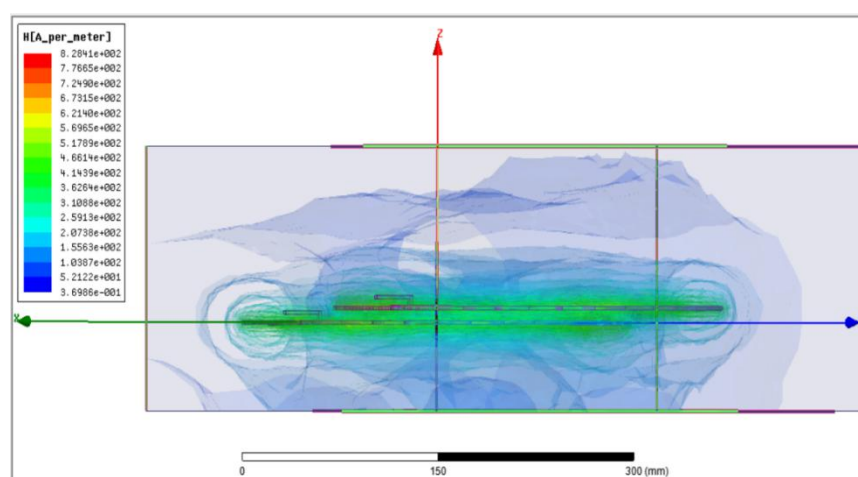


Figure 4.2.6.10 Magnetic Field Intensity of Coils with Misalignment
Coordinate (0, 100, 10)

4.3 Discussion

4.3.1 Effect of Coil Distance, Lateral Misalignment, and Angle Difference (Experimental)

Based on the compiled results including coil distance, lateral misalignment and angle difference shown below, the power efficiency apparently was decreasing with the increasing of coil distance, lateral misalignment, and angle difference.

Focusing on the angle difference of coils, the critical angle where the power efficiency dropped to approximate zero in this case was 40 degrees. For

the coil distance, it dropped to approximate zero when $d=100\text{mm}$. For lateral misalignment, it dropped approximate to zero when $L=130\text{mm}$.

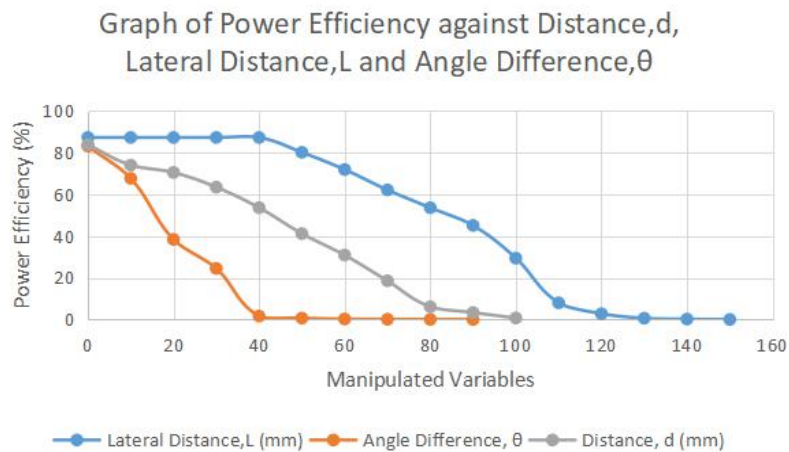


Figure 4.3.1.1 Graph of Power Efficiency against Distance, Lateral Misalignment, and Angle Difference

So, the keyword for coil alignment issue is the mutual inductance. Mutual Inductance is the interaction of one coils magnetic field on another coil as it induces a voltage in the adjacent coil. For the method of calculating the mutual inductance, first, the two inductive coils have to be connected in series, then the self-inductance of the combination is measured and using this value, the mutual inductance is calculated. The formulas are shown below.

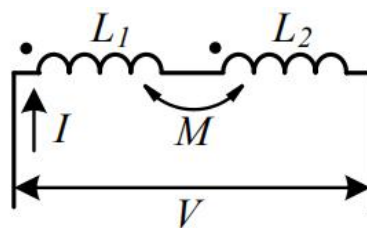


Figure 4.3.1.2 Two coils connected in series with magnetic fields in one direction.

$$V = V_1 + V_{M,1} + V_2 + V_{M,2} \quad (4.1)$$

Where V is total induced voltage of the series combination, V_1 and V_2 are the voltages induced by L_1 and L_2 , $V_{M,1}$ and $V_{M,2}$ are voltages induced by M in these two coils. Then, by applying the Lenz's Law with $V = -L(dI/dt)$, the equation (4.1) is derived into equation (4.2) below. Thus, the total inductance, L is shown in equation (4.3) where L_1 and L_2 are self inductance of each coil, and M is the mutual inductance, and finally mutual inductance M is obtained. The greater the misalignment or distance between coils, the lower the mutual inductance, this statement can be proven using simulation shown in following section. With the known mutual inductance, the value of coupling coefficient, k can be calculated using formula (4.4), the value of k ranged from 0 to 1, ideally 1 means 100% coupling efficiency. In addition, the quality factor of and inductor coil can be obtain also using formula (4.5) or (4.6). Quality factor is the ratio of the reactance of the inductor to its own resistance, the higher the value of quality factor, the closer it behaves like an ideal inductor. (Electronics, n.d.)

$$\begin{aligned} V &= -L_1 dI/dt + MdI/dt + L_2 dI/dt + MdI/dt \\ &= -(L_1 + L_2 + 2M)dI/dt \end{aligned} \quad (4.2)$$

$$\begin{aligned} L &= L_1 + L_2 + 2M \\ M &= [L - (L_1 + L_2)]/2 \end{aligned} \quad (4.3)$$

$$k = \frac{M}{\sqrt{L_s L_d}} \quad (4.4)$$

$$Q_s = \frac{\omega L_s}{R_s} \quad (4.5)$$

$$Q_d = \frac{\omega L_d}{R_d} \quad (4.6)$$

4.3.2 Effect of Coil Turns, Inner Radius and Outer Radius (Experimental)

The equation below is the formula of self-inductance of the circular flat spiral coil that can be derived from a modified Wheeler's formula for a single-layer helical coil, with conversion from inches to meters (39.37 inch/m) and μH to H (10^{-6}).

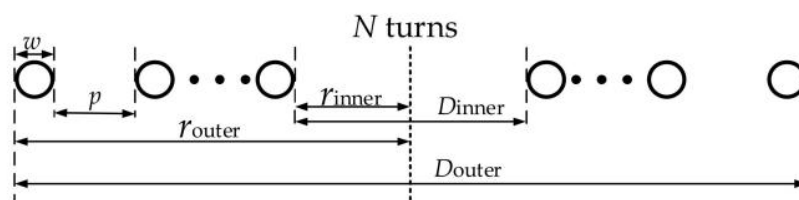


Figure 4.3.2.1 Section View of a Circular Flat Spiral Coil

$$L = \frac{N^2(D_{outer} - N(w + p))^2}{16D_{outer} + 28N(w + p)} \times \frac{39.37}{10^6} (H) \quad (4.7)$$

The measured value of self-inductance for every set of coils with different number of turns are verified using the equation above. Based on the result, the self-inductance of coil increased non-linearly with the increase of coil turns. Taking a set of data from Table 4.2.3.1 with 8 turns of coil as example, the percentage error of measure value and calculated value shown in equation (4.8) is less than 10% which is within the acceptable range. The higher the self-inductance value, the lower the compensate value of capacitor which was verified with equation (4.9).

$$\begin{aligned} \text{Percentage Error} &= |\text{Measured Value} - \text{Exact Value}| / \text{Exact Value} \times 100 \quad (4.8) \\ &= |15.01 - 16.56| / 16.56 \times 100 \\ &= 9.36 \% \end{aligned}$$

$$\begin{aligned}
X_L &= X_C \\
2\pi fL &= 1 / (2\pi fC) \\
C &= 1 / ((L) (2\pi f)^2)
\end{aligned}
\tag{4.9}$$

Based on the pattern of graph of power efficiency against coil turns, it can be concluded that the power efficiency will increase sharply with the increases of turn of coil. However, at a certain amount of turns of coil, the power efficiency started to drop. This is because when the coil turns increase, the more magnetic field will be created and induce more voltage and current to the receiver side. However, excessive turns of coil will lead to excessive self-inductance and AC resistance. Whenever the self-inductance of the coil is too high, relatively, the capacitor value in order to compensate the circuit will be decreased and harder to handle because the very small and precise capacitor value available in the market is very limited. Thus, the slight error in the compensation circuit will make the reactance become more dominant to the resistance $((X_L - X_C) \gg R)$ and eventually increase the impedance significantly and lower the current flow. (NDT, n.d.)

$$Z = \sqrt{R^2 + (X_L - X_C)^2} \tag{4.10}$$

By comparing the power efficiency between fixed outer radius (150mm), and fixed inner radius (62.5mm), the maximum power efficiency that fixed outer radius coil can be achieved is 83.76% with 11 turns while the fixed inner radius coil is 81.52% with 8 turns. With the small difference of 2.24% between these two cases, it can be concluded that the overall size of the coil is not the most important factor in term of power efficiency if amount of overall power drawn is not the concern, the important thing is to compensate the inductive coil with compatible capacitor. However, if the results need a high overall power together with high power efficiency, the size of coil only plays important role as shown in equation below. The terms of overall power (W) and power efficiency (%) carried different meaning.

$$\mathcal{E} = -N \frac{\Delta\Phi}{\Delta t} \quad (4.11)$$

Where:

N = number of turn

$\Phi = BA$ = magnetic flux

B = external magnetic field

A = area of coil

4.3.3 Battery Charging Behaviour (Experimental)

Based on the figure below, the charging curve of the 12V, 1.2Ah, lead acid battery behaves like CC/CV curve where CC is constant current mode and CV is constant voltage mode. The labeled line 1 is the time taken for manual alignment where the CC mode turns to CV mode, which means current start to drop and battery voltage start to be constant at around 3rd hour.

The same thing happen to auto alignment system, the only difference is the initial charging current is lower and the time taken to change from CC mode to CV mode is around 2 hours longer than manual alignment. “t” indicates the time difference between auto alignment and manual alignment system to change from CC to CV mode.

This is mainly because of the auto alignment is not perfectly aligned as manual alignment. In detail explanation, there was a limitation for the sensor used for auto alignment system, the ultrasonic sensor used to detect the distance between transmitter and receiver not able to detect the distance less than 2cm. Meanwhile, the manual alignment had 3mm as transmitting distance where ultrasonic sensor (HC-SR04) not able to achieve it. However, the auto aligner still able to achieve its own optimum alignment for maximum power transfer. (Acme, n.d.)

For the background of charging a lead acid battery, the maximum charging current for lead acid battery in order to protect the battery life is 25% of its rating in term of “Ah”. For example, a 10Ah lead acid battery need no more than 2.5A charging current to ensure battery health. Back to this project, the battery chosen to conduct this project is 1.2Ah, which means the charging current should be no more than 0.3A to avoid shorting its lifespan. After the

adjustment of the current flow to the battery using power resistor, the optimum charging current can be achieved is around 0.4A. The maximum capability of the current draw by this system is around 2.3A as shown in the results above, which means it can charge the lead acid battery with around 9.2Ah without damaging the battery.

In addition, the expected fully charged time in this project with 1.2Ah and 0.4A charging current is around 3 hours only as calculated using equation (4.12). The experimental results showed that it takes more than 3 hours to fully charge the battery. This is because there was a battery charger controller as shown in Figure 3.2.1.9 above connected to the battery to control the charging state of the battery. Whenever the battery is in charging mode or not, the led voltage indicator or display on the charging controller will always light up which means it consumes part of the current either when it is in charging mode or cut-off mode, which make sense to the lower charging rate as expected result. (All, n.d.)

$$\text{Time Taken (Hours)} = \text{Ampere Hour (Ah)} / \text{Ampere (A)} \quad (4.12)$$

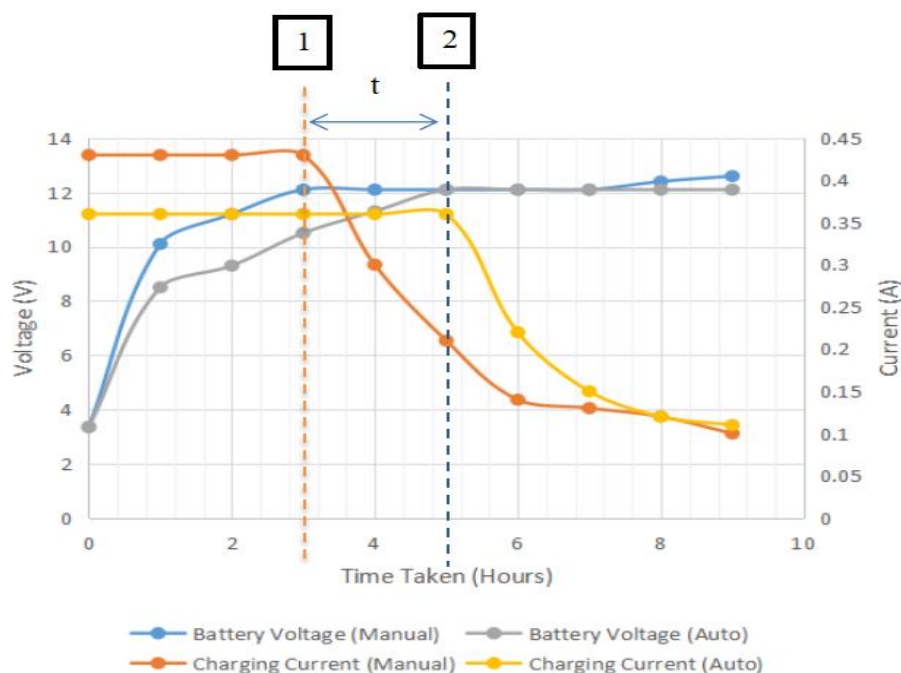


Figure 4.3.3.1 Analysis of CC/CV Curve of Charging Battery

4.3.4 Simulation using MATLAB (SIMULINK)

Based on the simulated results, it can be observed that the AC voltage is stepped down and rectified using step down transformer and full bridge rectifier respectively. Graph (1) and (2) is showing the 50Hz of the AC voltage, $T=0.02s$. Then, the rectified voltage go through high frequency inverter sampled at 20kHz shown in graph (4). The mutual inductive component or called transmitting and receiving coil is assumed having 100% power transfer (perfect alignment and compensation) due to parameter limitation from this simulation software. Thus, only the experimental results with highest power efficiency is chosen to discussed with simulation. Simulated results shows that around 2.1A and 20V with 100% power efficiency while experimental results shows that maximum current of 2.3A and voltage of 24V with 87.17% power efficiency. The percentage error between simulation and experimental result is 12.83% using equation (4.8). The lower power efficiency from experimental result mainly due to the tiny misalignment and the compensation circuit is not 100% ideal.

4.3.5 Simulation using Ansys Maxwell

“Ansys Maxwell” is a software that is widely used for electromagnetic simulation purpose. With this software, the density of magnetic flux, magnetic field etc. can be visualize in detail.

The power efficiency is not defined in this simulation as the magnetic field from transmitter will not induce any voltage or current to receiver side automatically in this simulation. The value of current at receiver is manually defined but not from induction of transmitter. Thus, there are only 3 responding variables to be studied in this simulation are coupling coefficient between coils, self-inductance and their mutual inductance with input AC current set = 2A with 20kHz. Besides, the option of tilting angle is not available in this simulation.

For the coupling coefficient and mutual inductance versus alignment, the parameters of coils are set to $N=11$, fixed outer radius = 150mm, inner radius = 122.5mm, adjacent core distance = 0.1mm. Core diameter = 2.5mm. These

parameters were selected because it delivered maximum power efficiency more than 80% based on experimental results.

For the self-inductance versus coil turns, there are two sets of data which includes fix inner radius with different coil turns and fix outer radius with different coil turns.

Based on the simulated results, the self-inductance is increasing with the coil turns. The coupling coefficient and mutual inductance are decreasing with increasing of misalignment in terms of distance, d and lateral distance, L . For the magnetic field intensity, H of coils, the magnetic field intensity achieves the highest value when the coil turn increased and having best alignment coordinate in “mm” (0, 0, 10).

4.4 Summary

The power efficiency is decreasing with greater misalignment in terms of distance (d) lateral misalignment (L), and tilting angle (θ). The self-inductance of coil is increasing the coil turns and verified using formula and simulation. The power efficiency reach maximum value up to more than 80% with coil parameters of $N=11$, fixed outer radius = 150mm, inner radius = 122.5mm, adjacent core distance = 0mm, core diameter = 2.5mm. With the auto-alignment system, the charging time of battery is delayed 2 hours compared to manual aligned coils. With the simulation from MATLAB, the parameters such as input current, input voltage, transmitted current and voltage etc. successfully verify the experimental results.

CHAPTER 5

CONCLUSIONS AND RECOMMENDATIONS

5.1 Conclusions

In a nutshell, the coil design, power electronic circuit, compensation circuit and simulation of wireless power transfer were studied in this project and the its behaviour from experiment is closely matched with the simulation. The auto-alignment system is the innovation part of the entire project because it applied the knowledge from IoT which is a breakthrough of the project where it makes user easier to use the system.

5.2 Recommendations for future work

For the coil design, the coils are made up by copper wire covered with PVC cable. This PVC cable will potentially affect the efficiency of the power transfer as the PVC cable will affect the permeability of magnetic field from the copper wire into the air. The improvement can be done in future is replacing the PVC copper cable with the bare copper wire with insulation material on its surface. The reason of using PVC cable instead of insulated bare wire is because it is very hard to turn the coil to become perfect flat spiral circular shape if bare wire with insulation is used.

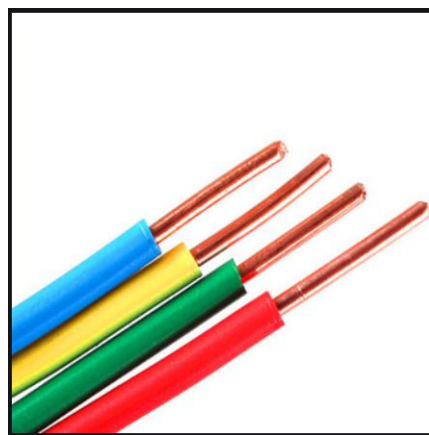


Figure 5.2.1 PVC Covered Copper Wire



Figure 5.2.2 Insulated Bare Copper Wire

Besides, the material used to construct the aligner can be improved using plastic instead of plywood. The reason of using plywood mainly because of its cost is much cheaper than plastic. Most of the cost needed when using plastic is the manufacturing process. However, the benefit of replacing plywood with plastic is water proofing issue.

For the simulation part, there are many limitations in the simulation software such as Ansys Maxwell. The limitations are the tilting angle, induction of voltage and current are not available. In detailed explanation, the straight line can be draw in any angle depending on the initial point and final point of the line in the 3-Dimensional volume, the more the number of straight line to create the curve line, the smoother the curve line created. However, it is not possible to draw the entire coil in certain tilt angle as the new defined origin can not be tilt in any way. This might be limitation of personal technical skills to the software. There are many other simulation software in Ansys series such as Ansys Discovery Aim, Ansys HFSS etc. Before applying the Ansys Maxwell software, Ansys Discovery Aim software was used to simulate the coil design. However, the requirement of graphic was relatively high compared to Ansys Maxwell. This would consume at least almost one hour to simulate one time due to the low performance of device used. Considering the presentation purpose, Ansys Maxwell was chosen as it requires lower graphic performance and short simulation time but the trade off is the graphic and detail issues. Besides, Ansys Maxwell does not have animation function for flow of magnetic field, current etc.



Figure 5.2.3 Ansys logo

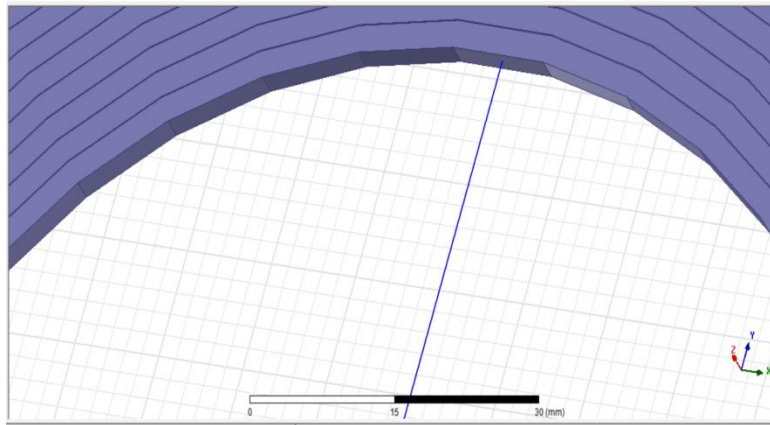


Figure 5.2.4 Detail of Curve Line Built Up with Multiple Straight Line
(Ansys Maxwell)



Figure 5.2.5 Detail of 3-Dimensional View of Simulation
(Ansys Discovery Aim)

CHAPTER 6

ADDITIONAL STUDY FROM THE PROJECT

6.1 Ohmic Loss Analysis

Ohmic loss is a term that define the power loss due to the resistance and current of the conductor. This section studies on how the structure of copper coils affect its ohmic loss. The equation of ohmic loss is shown below. (Hamdi, 2017)

$$\text{Ohmic Loss} = I^2R \quad (6.1)$$

The simulation was carried out using Ansys Maxwell to show that the ohmic loss will increase whenever there is a bending section along the copper wire. Based on the results, whenever there is a bending occurs, the resistance at that section will increase which means the ohmic loss increase linearly with it too. There is an improvement here to get more accurate results, as mentioned in section above, Ansys Maxwell is the software that having lower graphic detail. By default the ohmic loss should be distributed more evenly along the entire coil, lower at outer ring, higher at inner ring as outer ring having smaller bend angle while inner ring having larger bend angle.

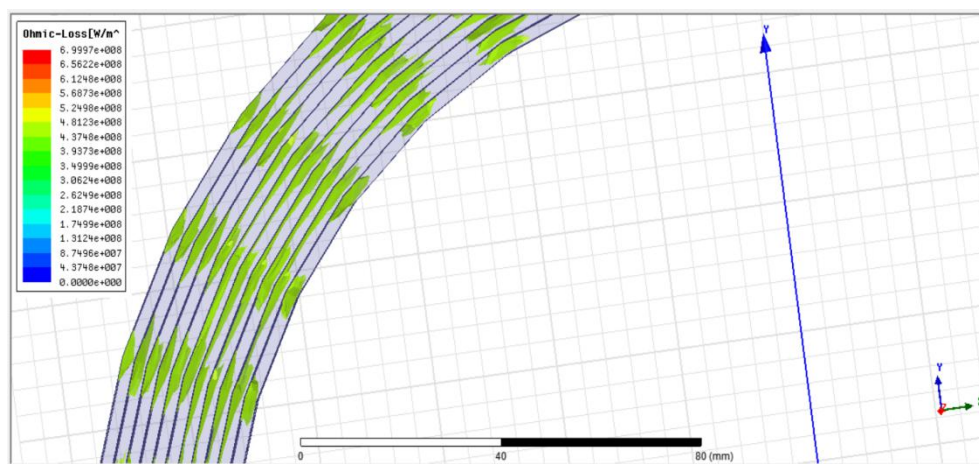


Figure 6.1.1 Simulation of Ohmic Loss of Coil

In more detailed explanation, if bending produces stress in the wire (compression on the inside, tension on the outside), this stress will affect resistivity and hence resistance of the wire. In general, the wire will get slightly longer and thinner when it is bent depending on its material properties. Bending of wire decreases the cross-sectional area and eventually increase the resistance of the wire. Hence, ohmic loss is increased. (ETB, n.d.)

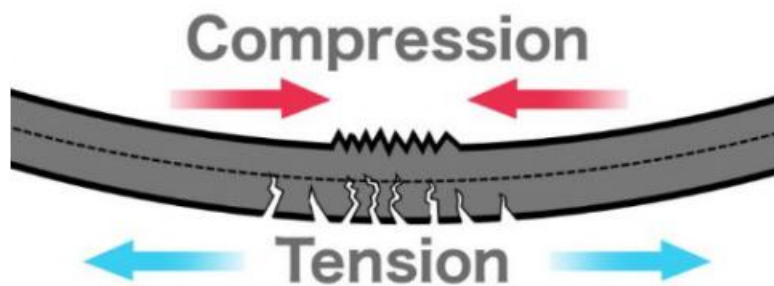


Figure 6.1.2 Compress and Tensile Stress of Bending Conductor



Figure 6.1.3 Stress of Conductor

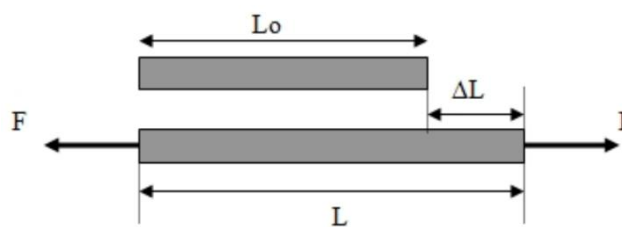


Figure 6.1.4 Strain of Conductor

$$\text{Stress} = F/A_0 \quad (6.2)$$

$$\text{Strain} = \Delta L / L \quad (6.3)$$

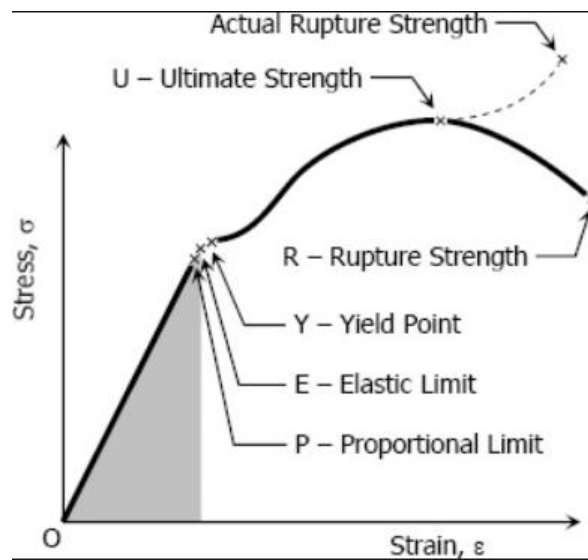


Figure 6.1.5 Relationship of Stress and Strain

$$\text{Young Modulus} = \text{Stress} / \text{Strain} \quad (6.4)$$

6.2 Temperature Analysis

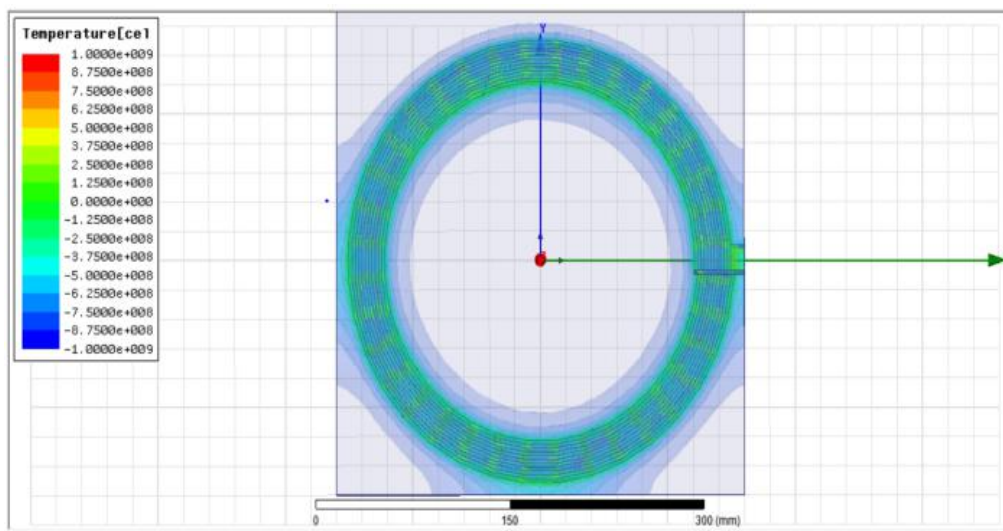


Figure 6.1.6 Simulation of Temperature of Coil

As mentioned in previous section, the ohmic loss will increase at the bending point which means the loss is in the form of heat. Hence, the simulation of temperature of coil shown above verifies the statement.

As the additional heat is generated, this will produce the avalanche effect where the increase of temperature increase the resistance of coil, then

the ohmic loss will be increased again and the avalanche effect will keep repeat. In short, the longer time it operates, the lower the performance it can achieve as temperature is getting higher with time. (All, n.d.)

$$R = R_{\text{ref}}[1 + \alpha(T - T_{\text{ref}})] \quad (6.5)$$

Where,

R or R_t = Conductor resistance at temperature “ T ”

R_{ref} or R_0 = Conductor resistance at reference temperature T_{ref}

α = Temperature coefficient of resistance for the conductor material

T = Conductor temperature ($^{\circ}\text{C}$)

T_{ref} = Reference temperature that α is specified at for the conductor material

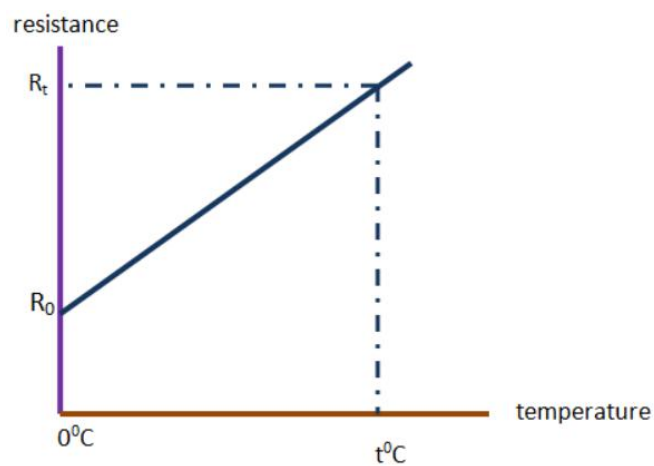


Figure 6.1.7 Graph of Resistance against Temperature

REFERENCES

- Acme, S., 2020. *HC-SR04 Ultrasonic Sensor*. Available through:<<https://www.acmesystems.it/HC-SR04?fbclid=IwAR1q6L6zxSQ056nHEByd-sd4B7pLI6lmMHqb3aTJdyx4s2c7-TJpxtcDcUY>> [Accessed 17 February 2020].
- All, B., n.d.. *Temperature Coefficient of Resistance*. Available through:<https://www.allaboutcircuits.com/textbook/direct-current/chpt-12/temperature-coefficient-resistance/?fbclid=IwAR2hD0882njwKS4eYbaujJcylnpsc7icRpwOSaGSjJx_7dHR9J4CGujH0BA> [Accessed 17 February 2020].
- All, B., n.d.. *Amp-Hour Application to Measure the Battery's Capacity*. Available through:<<https://www.allaboutcircuits.com/textbook/direct-current/chpt-11/battery-ratings/>> [Accessed 17 February 2020].
- Azuwa, A., 2019. *Design and Analysis of 2-coil Wireless Power Transfer (WPT) using Magnetic Coupling Technique*. Available through:<https://www.researchgate.net/publication/333538387_Design_and_analysis_of_2-coil_wireless_power_transfer_WPT_using_magnetic_coupling_technique> [Accessed 17 February 2020].
- Dave, 2019. *Wireless Power Transmission Technology with Applications*. Available through:<<https://www.watelectrical.com/wireless-power-transmission-technology/>> [Accessed 17 February 2020].
- David, G., 2016. *Full-Bridge Inverter*. Available through:<<https://www.sciencedirect.com/topics/engineering/full-bridge-inverter>> [Accessed 17 February 2020].

- Electronics, T., n.d.. *Mutual Inductance*. Available through:<<https://www.electronics-tutorials.ws/inductor/mutual-inductance.html?fbclid=IwAR3aNYrxuGVYXZGzOrfhiuZLJNsjiRmBGg2JECrAWwT7wsjUI3qklyJRQ94>> [Accessed 17 February 2020].
- Electropaedia, n.d.. *Battery Chargers and Charging Methods*. Available through:<<https://www.mpoweruk.com/chargers.htm>> [Accessed 17 February 2020].
- ETB, n.d.. *Stress, Strain and Young's Modulus*. Available through:<https://www.engineeringtoolbox.com/stress-strain-d_950.html?fbclid=IwAR0PuRCvbDi-XgqckhU3nMEGxNk_ymI5dLJE-nRbTOX2gf9PYKtSfLW6Ovw> [Accessed 17 February 2020].
- Hamdi, A., 2017. *Ohmic Loss*. Available through:<<https://www.sciencedirect.com/topics/engineering/ohmic-loss?fbclid=IwAR13URUDsI4zaw2C-sn7TXIKkC3CNRbRe6uNvusQIkhfoiXxO-3fxo35chw>> [Accessed 17 February 2020].
- Hanqiao, Z., 2015. *Reflection Coefficient*. Available through:<<https://www.sciencedirect.com/topics/computer-science/reflection-coefficient>> [Accessed 17 February 2020].
- Junwei, L., 2018. *Review of Static and Dynamic Wireless Electric Vehicle Charging System*. Available through:<<https://www.sciencedirect.com/science/article/pii/S221509861830154X>> [Accessed 17 February 2020].

Keith, G., 2016. *The Charge and Discharge of a Capacitor*. Available through:<http://www.schoolphysics.co.uk/age16-19/Electricity%20and%20magnetism/Electrostatics/text/Capacitor_charge_and_discharge/index.html> [Accessed 17 February 2020].

Nave, R., n.d.. *Faraday's Law*. Available through:<<http://hyperphysics.phy-astr.gsu.edu/hbase/electric/farlaw.html>> [Accessed 17 February 2020].

NDT, n.d..*Eddy Current Inspection Formula-Impedance*. Available through:<https://www.nde-ed.org/GeneralResources/Formula/ECFormula/Impedance/ECImpedance.htm?fbclid=IwAR3Pivt5ZoxtJBtcLi5IuqIm7ssl18OyIILWuz1jdMQ_Qd5fsrI-IAwvz9U> [Accessed 17 February 2020].

Sakir, K., 2017. *Design and Analysis of a Wireless Power Transfer System with Alignment Errors for Electrical Vehicle Applications*. Available through:<https://www.researchgate.net/publication/316041726_Design_and_analysis_of_a_wireless_power_transfer_system_with_alignment_errors_for_electrical_vehicle_applications> [Accessed 17 February 2020].

Sourav, G., 2019. *AC to DC Converter Circuit*. Available through:<<https://circuitdigest.com/electronic-circuits/ac-to-dc-converter-circuit-diagram>> [Accessed 17 February 2020].


Steve, R., 2020. *What is IoT? Everything You Need to Know about the Internet of Things Right Now*. Available through:<<https://www.zdnet.com/article/what-is-the-internet-of-things-everything-you-need-to-know-about-the-iot-right-now/>> [Accessed 17 February 2020].

Viktor, S., 2019. *Compensation Topologies in IPT Systems: Standards, Requirements, Classification, Analysis, Comparison and Application*. Available through: <https://www.researchgate.net/publication/335437296_Compensation_Topologies_in_IPT_Systems_Standards_Requirements_Classification_Analysis_Comparison_and_Application> [Accessed 17 February 2020].

APPENDICES

APPENDIX A: KBPC 1010 Datasheet


KBPC1000 THRU KBPC1010
SINGLE PHASE 10 AMPS SILICON BRIDGE RECTIFIERS

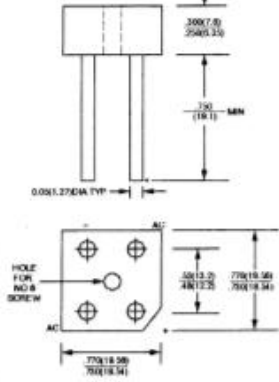


FEATURES

- Surge overload rating 60 amperes peak
- Low forward voltage drop
- Small size, simple installation
- Leads solderable per MIL – STD – 202, method 208

VOLTAGE RANGE
50 to 1000 Volts
CURRENT
10.0 Amperes

KBPC-8/10



Dimensions in inches and (millimeters)

MAXIMUM RATINGS AND ELECTRICAL CHARACTERISTICS

Rating at 25°C ambient temperature unless otherwise specified.
Single phase, half wave, 60 Hz, resistive or inductive load.
For capacitive load, derate current by 20%.

TYPE NUMBER	SYMBOLS	KBPC 1000	KBPC 1001	KBPC 1002	KBPC 1004	KBPC 1006	KBPC 1008	KBPC 1010	UNITS
Maximum Recurrent Peak Reverse Voltage	V_{RRM}	50	100	200	400	600	800	1000	V
Maximum RMS Bridge Input Voltage	V_{RMS}	35	70	140	280	420	560	700	V
Maximum D. C. Blocking Voltage	V_{DC}	50	100	200	400	600	800	1000	V
Maximum Average Forward Rectified Current @ $T_C = 50^\circ C^{(1,2)}$	$I_{F(AV)}$	10							A
Peak Forward Surge Current, 8.3 ms single half sine-wave superimposed on rated load (JEDEC method)	I_{FSM}	250							A
Maximum Forward Voltage Drop per element @ 5A	V_F	1.10							V
Maximum Reverse Current at Rated @ $T_A = 25^\circ C$ D. C. Blocking Voltage per element @ $T_A = 100^\circ C$	I_R	10 500							μA μA
Operating Temperature Range	T_J	- 55 to + 125							$^\circ C$
Storage Temperature Range	T_{STG}	- 55 to + 150							$^\circ C$

NOTE: (1) Bolt down on heat – sink with silicone thermal compound between bridge and mounting surface for maximum heat transfer with #
6 screw
(2) Unit mounted on 5.5 x 6.0 x 0.11" thick (14 x 15 x 0.3cm) Al. Plate



RATINGS AND CHARACTERISTIC CURVES (KBPC1000 THRU KBPC1010)

FIG. 1 - MAXIMUM NON-REPETITIVE FORWARD SURGE CURRENT - PER ELEMENT

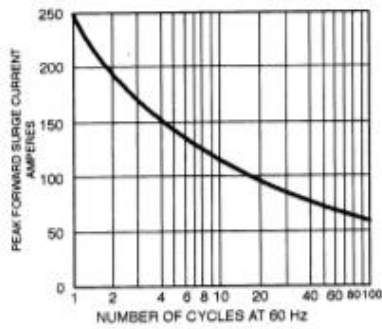


FIG. 2 - TYPICAL FORWARD OUTPUT CURRENT DERATING CURVE

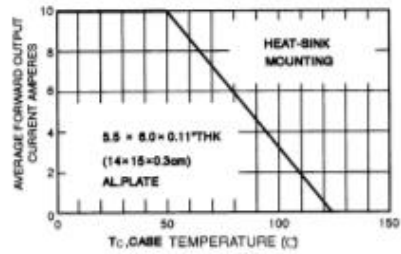


FIG. 3 - TYPICAL FORWARD CHARACTERISTICS PER ELEMENT

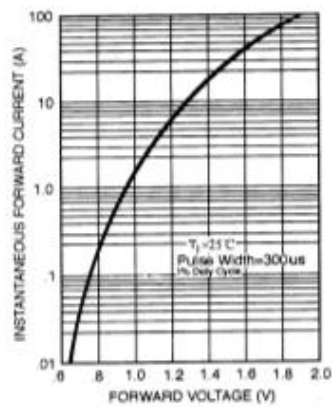
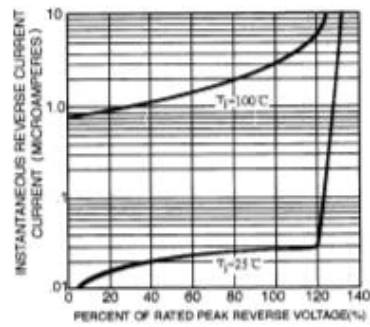


FIG. 4 - TYPICAL REVERSE CHARACTERISTICS - PER ELEMENT



APPENDIX B: Arduino UNO R3 Datasheet

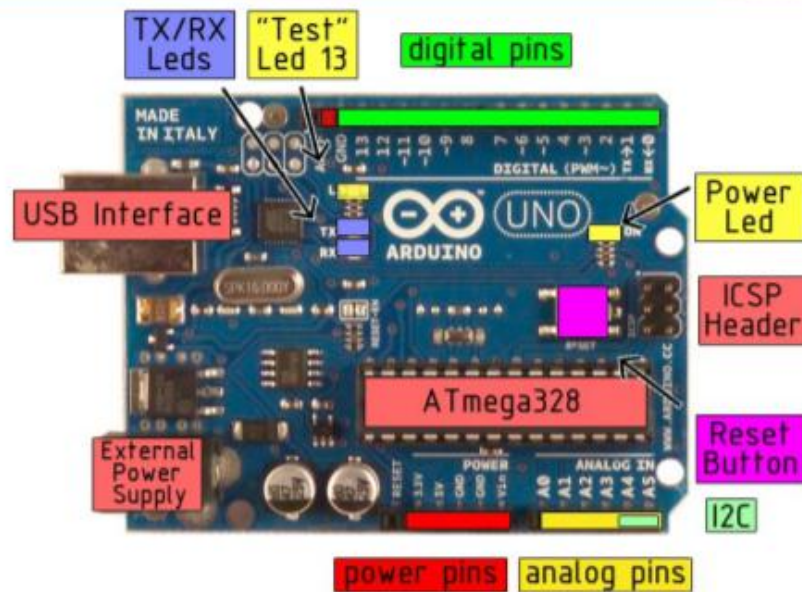
Technical Specification

EAGLE files: [arduino-duemilanove-uno-design.zip](#) Schematic: [arduino-uno-schematic.pdf](#)

Summary

Microcontroller	ATmega328
Operating Voltage	5V
Input Voltage (recommended)	7-12V
Input Voltage (limits)	6-20V
Digital I/O Pins	14 (of which 6 provide PWM output)
Analog Input Pins	6
DC Current per I/O Pin	40 mA
DC Current for 3.3V Pin	50 mA
Flash Memory	32 KB of which 0.5 KB used by bootloader
SRAM	2 KB
EEPROM	1 KB
Clock Speed	16 MHz

the board



radiospares **RADIONICS**



Power

The Arduino Uno can be powered via the USB connection or with an external power supply. The power source is selected automatically.

External (non-USB) power can come either from an AC-to-DC adapter (wall-wart) or battery. The adapter can be connected by plugging a 2.1mm center-positive plug into the board's power jack. Leads from a battery can be inserted in the Gnd and Vin pin headers of the POWER connector.

The board can operate on an external supply of 6 to 20 volts. If supplied with less than 7V, however, the 5V pin may supply less than five volts and the board may be unstable. If using more than 12V, the voltage regulator may overheat and damage the board. The recommended range is 7 to 12 volts.

The power pins are as follows:

- **VIN.** The input voltage to the Arduino board when it's using an external power source (as opposed to 5 volts from the USB connection or other regulated power source). You can supply voltage through this pin, or, if supplying voltage via the power jack, access it through this pin.
- **5V.** The regulated power supply used to power the microcontroller and other components on the board. This can come either from VIN via an on-board regulator, or be supplied by USB or another regulated 5V supply.
- **3V3.** A 3.3 volt supply generated by the on-board regulator. Maximum current draw is 50 mA.
- **GND.** Ground pins.

Memory

The Atmega328 has 32 KB of flash memory for storing code (of which 0,5 KB is used for the bootloader); it has also 2 KB of SRAM and 1 KB of EEPROM (which can be read and written with the [EEPROM library](#)).

Input and Output

Each of the 14 digital pins on the Uno can be used as an input or output, using [pinMode\(\)](#), [digitalWrite\(\)](#), and [digitalRead\(\)](#) functions. They operate at 5 volts. Each pin can provide or receive a maximum of 40 mA and has an internal pull-up resistor (disconnected by default) of 20-50 kOhms. In addition, some pins have specialized functions:

- **Serial: 0 (RX) and 1 (TX).** Used to receive (RX) and transmit (TX) TTL serial data. These pins are connected to the corresponding pins of the ATmega8U2 USB-to-TTL Serial chip.
- **External Interrupts: 2 and 3.** These pins can be configured to trigger an interrupt on a low value, a rising or falling edge, or a change in value. See the [attachInterrupt\(\)](#) function for details.
- **PWM: 3, 5, 6, 9, 10, and 11.** Provide 8-bit PWM output with the [analogWrite\(\)](#) function.
- **SPI: 10 (SS), 11 (MOSI), 12 (MISO), 13 (SCK).** These pins support SPI communication, which, although provided by the underlying hardware, is not currently included in the Arduino language.
- **LED: 13.** There is a built-in LED connected to digital pin 13. When the pin is HIGH value, the LED is on, when the pin is LOW, it's off.



radiospares

RADIONICS



The Uno has 6 analog inputs, each of which provide 10 bits of resolution (i.e. 1024 different values). By default they measure from ground to 5 volts, though it is possible to change the upper end of their range using the AREF pin and the [analogReference\(\)](#) function. Additionally, some pins have specialized functionality:

- **I²C: 4 (SDA) and 5 (SCL).** Support I²C (TWI) communication using the [Wire library](#).

There are a couple of other pins on the board:

- **AREF.** Reference voltage for the analog inputs. Used with [analogReference\(\)](#).
- **Reset.** Bring this line LOW to reset the microcontroller. Typically used to add a reset button to shields which block the one on the board.

See also the [mapping between Arduino pins and Atmega328 ports](#).

Communication

The Arduino Uno has a number of facilities for communicating with a computer, another Arduino, or other microcontrollers. The ATmega328 provides UART TTL (5V) serial communication, which is available on digital pins 0 (RX) and 1 (TX). An ATmega8U2 on the board channels this serial communication over USB and appears as a virtual com port to software on the computer. The '8U2 firmware uses the standard USB COM drivers, and no external driver is needed. However, on Windows, an *.inf file is required..

The Arduino software includes a serial monitor which allows simple textual data to be sent to and from the Arduino board. The RX and TX LEDs on the board will flash when data is being transmitted via the USB-to-serial chip and USB connection to the computer (but not for serial communication on pins 0 and 1).

A [SoftwareSerial library](#) allows for serial communication on any of the Uno's digital pins.

The ATmega328 also support I2C (TWI) and SPI communication. The Arduino software includes a Wire library to simplify use of the I2C bus; see the [documentation](#) for details. To use the SPI communication, please see the ATmega328 datasheet.

Programming

The Arduino Uno can be programmed with the Arduino software ([download](#)). Select "Arduino Uno w/ ATmega328" from the **Tools > Board** menu (according to the microcontroller on your board). For details, see the [reference](#) and [tutorials](#).

The ATmega328 on the Arduino Uno comes preburned with a [bootloader](#) that allows you to upload new code to it without the use of an external hardware programmer. It communicates using the original STK500 protocol ([reference](#), [C header files](#)).

You can also bypass the bootloader and program the microcontroller through the ICSP (In-Circuit Serial Programming) header; see [these instructions](#) for details.

The ATmega8U2 firmware source code is available . The ATmega8U2 is loaded with a DFU bootloader, which can be activated by connecting the solder jumper on the back of the board (near the map of Italy) and then resetting the 8U2. You can then use [Atme's FLIP software](#) (Windows) or the [DFU programmer](#) (Mac OS X and Linux) to load a new firmware. Or you can use the ISP header with an external programmer (overwriting the DFU bootloader).



radiospares RADIONICS



Automatic (Software) Reset

Rather than requiring a physical press of the reset button before an upload, the Arduino Uno is designed in a way that allows it to be reset by software running on a connected computer. One of the hardware flow control lines (DTR) of the ATmega8U2 is connected to the reset line of the ATmega328 via a 100 nanofarad capacitor. When this line is asserted (taken low), the reset line drops long enough to reset the chip. The Arduino software uses this capability to allow you to upload code by simply pressing the upload button in the Arduino environment. This means that the bootloader can have a shorter timeout, as the lowering of DTR can be well-coordinated with the start of the upload.

This setup has other implications. When the Uno is connected to either a computer running Mac OS X or Linux, it resets each time a connection is made to it from software (via USB). For the following half-second or so, the bootloader is running on the Uno. While it is programmed to ignore malformed data (i.e. anything besides an upload of new code), it will intercept the first few bytes of data sent to the board after a connection is opened. If a sketch running on the board receives one-time configuration or other data when it first starts, make sure that the software with which it communicates waits a second after opening the connection and before sending this data.

The Uno contains a trace that can be cut to disable the auto-reset. The pads on either side of the trace can be soldered together to re-enable it. It's labeled "RESET-EN". You may also be able to disable the auto-reset by connecting a 110 ohm resistor from 5V to the reset line; see [this forum thread](#) for details.

USB Overcurrent Protection

The Arduino Uno has a resettable polyfuse that protects your computer's USB ports from shorts and overcurrent. Although most computers provide their own internal protection, the fuse provides an extra layer of protection. If more than 500 mA is applied to the USB port, the fuse will automatically break the connection until the short or overload is removed.

Physical Characteristics

The maximum length and width of the Uno PCB are 2.7 and 2.1 inches respectively, with the USB connector and power jack extending beyond the former dimension. Three screw holes allow the board to be attached to a surface or case. Note that the distance between digital pins 7 and 8 is 160 mil (0.16"), not an even multiple of the 100 mil spacing of the other pins.



radiospares **RADIONICS**



APPENDIX C: NodeMCU V3 Datasheet

HTHandson Technology

User Manual V1.2

ESP8266 NodeMCU WiFi Devkit

A photograph of an ESP8266 NodeMCU WiFi Devkit. It is a small, black PCB with a green ESP8266 module in the center. The board has a micro-USB port on the right side, a USB Type-C port on the left, and a 40-pin header at the bottom. Various components like a capacitor and a resistor are visible on the board.

The ESP8266 is the name of a micro controller designed by Espressif Systems. The ESP8266 itself is a self-contained WiFi networking solution offering as a bridge from existing micro controller to WiFi and is also capable of running self-contained applications.

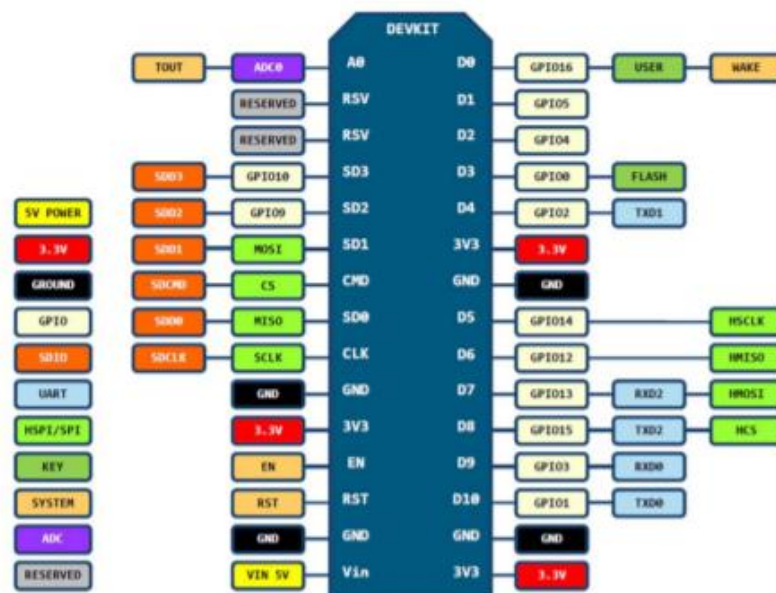
This module comes with a built in USB connector and a rich assortment of pin-outs. With a micro USB cable, you can connect NodeMCU devkit to your laptop and flash it without any trouble, just like Arduino. It is also immediately breadboard friendly.

1 |www.handsontec.com

1. Specification:

- Voltage:3.3V.
- Wi-Fi Direct (P2P), soft-AP.
- Current consumption: 10uA~170mA.
- Flash memory attachable: 16MB max (512K normal).
- Integrated TCP/IP protocol stack.
- Processor: Tensilica L106 32-bit.
- Processor speed: 80~160MHz.
- RAM: 32K + 80K.
- GPIOs: 17 (multiplexed with other functions).
- Analog to Digital: 1 input with 1024 step resolution.
- +19.5dBm output power in 802.11b mode
- 802.11 support: b/g/n.
- Maximum concurrent TCP connections: 5.

2. Pin Definition:

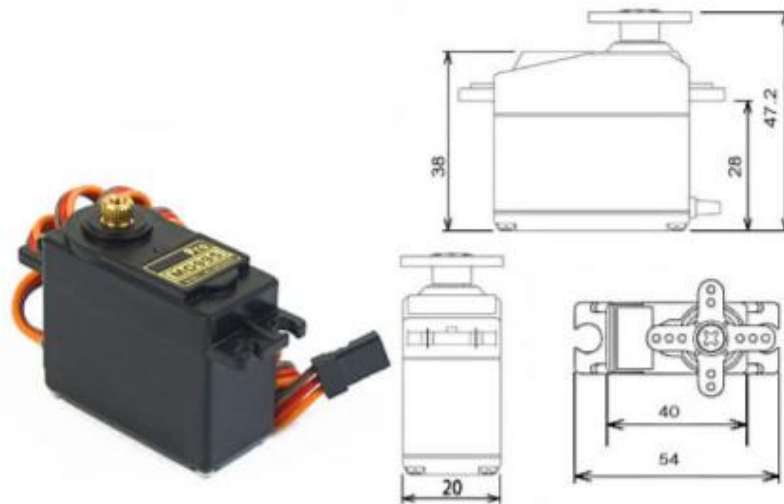


D0(GPIO16) can only be used as gpio read/write, no interrupt supported, no pwm/t2c/ow supported.

3. Using Arduino IDE

APPENDIX D: MG995 Servo Motor Datasheet

MG995 High Speed Metal Gear Dual Ball Bearing Servo



The unit comes complete with 30cm wire and 3 pin 'S' type female header connector that fits most receivers, including Futaba, JR, GWS, Cirrus, Blue Bird, Blue Arrow, Corona, Berg, Spektrum and Hitec.

This high-speed standard servo can rotate approximately 120 degrees (60 in each direction). You can use any servo code, hardware or library to control these servos, so it's great for beginners who want to make stuff move without building a motor controller with feedback & gear box, especially since it will fit in small places. The MG995 Metal Gear Servo also comes with a selection of arms and hardware to get you set up nice and fast!

Specifications

- Weight: 55 g
- Dimension: 40.7 x 19.7 x 42.9 mm approx.
- Stall torque: 8.5 kgf·cm (4.8 V), 10 kgf·cm (6 V)
- Operating speed: 0.2 s/60° (4.8 V), 0.16 s/60° (6 V)
- Operating voltage: 4.8 V a 7.2 V
- Dead band width: 5 μs
- Stable and shock proof double ball bearing design
- Temperature range: 0 °C – 55 °C

PWM=Orange (⏏)
Vcc = Red (+)
Ground=Brown (-)

